Cape Peninsula University of Technology

Warming trends of the Agulhas Current from 1982 to 2019.

By

Mr Bubele Rasmeni

216019400

Research thesis in fulfilment of the requirements of the degree:

Master of Marine Sciences

In the Department of Conservation and Marine Sciences,

Faculty of Applied Science at the Cape Peninsula University of Technology

Supervisor: Dr David Walker

Co-supervisors: Dr Issufo Halo and Dr Tarron Lamont

PLAGIARISM DECLARATION

I, Bubele Rasmeni, declare that the content of this dissertation submitted in partial fulfilment of the requirements for the degree of Master of Science in Marine Science, represents my unaided work and that the dissertation has not previously been submitted for academic examination towards any other qualification in the Cape Peninsula University of Technology or any other university. Furthermore, it represents my own opinions and not necessarily those of the Cape Peninsula University of Technology.

Signed _____ Date 06/10/2023

1. ACKNOWLEDGEMENTS

I would like to thank the following people and organizations for their assistance, support, invaluable contributions, and advice in making this thesis possible.

- I am grateful to my supervisors, Dr Tarron Lamont, Dr Issufo Halo, and Dr David Walker, for their wisdom, rigorous critical input, creative insight, and belief in this project. Their unwavering support has far exceeded my expectations. Thank you for your trust in my abilities and for sharing your knowledge.
- Thank you to my family for their enduring and active support. I never felt I couldn't rely on you for anything. Mama, I will forever appreciate your prayers and your constant support and words of encouragement.
- The financial assistance of the National Research Foundation (NRF) and Cape Peninsula University of Technology (CPUT) towards this research is acknowledged. Opinions expressed in this thesis and the conclusions arrived at, are those of the author, and are not necessarily to be attributed to the National Research Foundation or Cape peninsula University of Technology.
- Thank you to the Copernicus program for making the ocean currents dataset used in this study freely available.
- NOAA is also highly appreciated for making the SST data freely available.

2. ABSTRACT

The Agulhas Current system has been reported to be warming significantly since the 1980s, with warming rates as high as 0.7 oC/decade for the highest warming regions, such as the Agulhas Retroflection and the Agulhas Return Current. Due to the different temporal scale and spatial resolution of datasets used to investigate the warming trends of the Agulhas Current system in previous studies, different warming rates have been reported. The poleward shift and intensification of the subtropical Western Boundary Currents (WBCs), including the Agulhas Current, have been linked to their accelerated warming. While prior research has demonstrated distinct and significant warming trends in the Agulhas Current region, more recent datasets with improved spatial resolution and longer time scales have been made available and more easily accessible. As a result, the general purpose of this study was to update earlier studies with more recent Sea Surface Temperature (SST) timeseries and compare the latest trends with previously reported trends. The main aims of this study were fourfold: (1) to investigate the warming trends in the Agulhas Current and determine the strongest warming regions using the National Oceanic and Atmospheric Administration (NOAA) Optimum Interpolation SST (OISST, v.2) product with a higher spatial resolution (1/4o) and longer temporal coverage (1982–2019) compared to datasets used in previous studies. (2) to calculate the linear trends for the satellite-derived geostrophic currents to determine if the Agulhas Current has intensified from 1993 to 2019. (3) To assess the relationship between SST and the geostrophic current speed by calculating Pearson's correlation. (4) Finally, to assess the influence of the Southern Annular Mode (SAM) and El Niño-Southern Oscillation (ENSO) on SST and geostrophic current speed anomalies over the different regions in the Agulhas Current Results from the linear least squares regression revealed significant ($p < 0.05$) linear warming trends that were consistent with other studies; however, the maximum warming rate of up to 0.57 oC/decade was slightly lower than anticipated warming rates that were reported previously. The present study also found that the Agulhas Retroflection and the Agulhas Return Current are still the strongest warming regions in the Agulhas Current system, consistent with previous research findings. In terms of the overall geostrophic current flow, no significant trend of strengthening or weakening was observed between 1993 and 2019, though localised trends were noted both annually and seasonally. However, based on the overall results, while the correlation is statistically significant, SST may not be directly affecting geostrophic current, and other variables may also play important roles in influencing geostrophic current anomalies. Furthermore, SST was significantly correlated to the geostrophic current speed over the Agulhas Current. The correlation was moderate annually and strong seasonally; a significant and positive moderate annual Pearson's correlation coefficient of around 0.63 was found in most regions. Seasonally, the correlation between SST and

geostrophic current anomalies was greater than 0.8 in some regions. The relationship between climate indices (SAM and ONI), SST, and geostrophic anomalies demonstrated a statistically significant influence of the climate indices on environmental parameters in the Agulhas Current, especially SST. However, while statistically significant in some cases, these correlations are negligible, implying that the influence is weak and other local or mesoscale factors may also be at work.

3. TABLE OF CONTENTS

4. LIST OF FIGURES

LIST OF TABLES

LIST OF ACRONYMS

ADT	Absolute Dynamic Topography
AVHRR	Advanced Very High-Resolution Radiometer
CMEMS	Copernicus Marine Environment Monitoring Service
DJF	December-January-February
EKE	Eddy Kinetic Energy
ENSO	El Niño-Southern Oscillation
ERSSTv3b	Extended Reconstructed Sea Surface Temperature version 2
HadISST1	Hadley Centre Sea Ice and Sea Surface Temperature version 1
HadISST1	Hadley Centre Sea Ice and Sea Surface Temperature version 2
HadSST2	Hadley Centre Sea Surface Temperature version 2
JJA	June-July-August
Kaplanv2	Kaplan Extended Sea Surface Temperature version 2
KZN	KwaZulu-Natal
LHF	Latent Heat Fluxes
MAM	March-April-May
MDT	Mean Dynamic Topography
NOAA	National Oceanic and Atmospheric Administration
OISST	Optimum Interpolation Sea Surface Temperature
SLA	Sea Level Anomaly
SODA	Simple Ocean Data Assimilation SST product27
SON	September-October-November
SSH	Sea Surface Height
SST	Sea Surface Temperature
THF	Turbulent Heat Fluxes
WBCs	Western Boundary Currents

1. CHAPTER 1: INTRODUCTION

1.1 Background

Increasing concentrations of atmospheric greenhouse gasses such as carbon dioxide have been the main cause of Earth's surface warming over the twentieth century (Han and Yan, 2018); and such warming is expected to continue in the foreseeable future (Wu et al. 2012). Oceans absorb both heat and Carbon dioxide, which increases this surface warming (Han and Yan, 2018). The recent (twentieth century) ocean heat absorption has resulted in a significant increase of SST in both tropical and high latitude regions, with the most robust warming in the tropical Indian Ocean and weak warming in the high latitudes over the deep-water forming region (Wu et al. 2012).

This ocean warming is at an enhanced level in subtropical WBCs worldwide (Wu et al. 2012; Seager and Simpson, 2016; Yang et al. 2016; Yang et al. 2020). However, the reported magnitude of this warming in WBCs differs depending on the datasets used to investigate the warming and the region of the current. Subtropical WBCs, which form in the western region of the ocean basins, are fast-flowing, warm, deep, and narrow ocean currents that transport warm water from the tropics to the poles. Ocean currents such as the Gulf Stream, the Agulhas Current, the East Australian Current, and the Kuroshio Current are examples of WBCs (Yang et al. 2016).

According to Wu et al. (2012), post-1900, the rate of surface warming over the path of subtropical WBCs is within the range of 0.8–1.8 ^{o}C/century, and that warming rate is two to three times faster than the rate of global mean surface ocean warming. Wu et al. (2012) argue that the poleward shift and intensification in the strength of these subtropical WBCs might be the reason for their enhanced warming. Detecting and quantifying the enhanced warming trends remains uncertain due to the lack of long-term observations and varying algorithms used to reconstruct SST among reanalysis products. Wu et al. (2012) also suggested that increased upstream land warming is another possible mechanism that might contribute to increased warming in regions of WBC.

The Agulhas Current (Figure 2.1) is among the subtropical WBCs that are warming (Wu et al. 2012; Yang et al. 2016); in fact, it has been reported that warming has been occurring in the Agulhas Current system since the 1980s (Rouault et al. 2009). According to Rouault et al. (2009), the Agulhas Retroflection and the Agulhas Return Current are the strongest warming regions in the Agulhas Current system with a maximum warming rate of 0.7 ^{o}C/decade. Slightly

lower maximum warming rates greater than 0.5 ºC/decade have been reported in recent studies (e.g., Rouault et al. 2009; Rouault et al. 2010; Han and Yan, 2018; Sweijd and Smit, 2020).

1.2 Rationale

The WBCs, including the Agulhas Current, have widespread and well-documented impacts on weather systems and climate conditions (precipitation, temperature, and extreme climatic events such as storms) in adjacent regions (Rouault et al. 2009). Catastrophic occurrences of large storms linked to the Agulhas Current have been reported on South Africa's east coast. Efforts should therefore be focused on better understanding ongoing changes in ocean currents and sea surface temperature trends in the Agulhas Current system due to its impact on weather and climate conditions in the region. This can be achieved through constant investigation of trends of the Agulhas Current using the latest datasets with higher spatial resolution and longer temporal coverage.

Although several studies have investigated the warming trends of the Agulhas Current (e.g., Han and Yan, 2018 (~0.6 ºC/decade); Rouault et al. 2009 (0.7 ºC/decade); Rouault et al. 2010 (0.5 ºC/decade); Sweijd and Smit, 2020 (0.57 ºC/decade); Wu et al. 2012 (~1.8 ºC/century)) published literature about the warming trends focusing only on the Agulhas Current during the last decade (2010–2019), are few. Previous studies were either published before 2010 (e.g., Rouault et al. 2009), used low spatial resolution datasets (e.g., Rouault et al. 2010), or did not only focus on the Agulhas Current (Sweijd and Smit, 2020). The Rouault et al. (2010) study, which assessed the SST trends around South Africa including the Agulhas Current from 1982 to 2009, used the Reynolds et al. (2002) low spatial resolution datasets, a 1º x 1º spatial resolution Optimum Interpolated SST. According to Rouault et al. (2003), the Reynolds et al. (2002) dataset fails to accurately represent features of coastal areas and the core of the Agulhas Current, making it difficult to pinpoint the finer details of the specific oceanographic processes in the region, especially in coastal areas. Therefore, the main aim of this study was to investigate the warming trends in the Agulhas Current using the National Oceanic and Atmospheric Administration (NOAA) Optimum Interpolation SST (OISST, v.2) product with a higher spatial resolution (1/4º) and longer temporal coverage (1982-2019) compared to datasets used in previous studies (e.g., Rouault et al. 2009 and Rouault et al. 2010).

Wu et al. (2012) and Yang et al. (2016) suggested that the rapid warming in subtropical WBCs including the Agulhas Current is consistent with the intensification (faster speeds) of WBCs. Except for the Gulf Stream, Yang et al. (2016) reported that WBCs are intensifying and shifting poleward thus increasing SST in their path. According to Peng et al. (2022), sea surface

warming influences the upper ocean circulation changes. Through ocean model experiments, Peng et al. (2022) suggest that to some extent, there is a sea surface warming-induced acceleration of surface ocean currents, and the acceleration can reach up to ~500m deep in some WBCs including the Agulhas Current. Peng et al. (2022) argue that during sea surface warming vertical shear develops and strengthens the currents in the upper surface layer due to density stratification between the upper and bottom layers and because the vertical-integrated volume transfer remains constant, the flow in the layers below weakens. Due to the information provided above, another distinct aim of this study was therefore to assess the relationship between SST and current speed in the Agulhas Current.

Based on prior research, this study hypothesized that:

1. The Agulhas Current system is warming significantly.
2. The Agulhas Retroflection and the Agulhas Return Current are still the strongest warming regions within the Agulhas Current system.
3. There is a positive relationship between the geostrophic current speed and the SST in the Agulhas Current system.
4. There is a significant influence of climate indices on the SST anomalies in the Agulhas Current.

1.3 Key Research Questions

The following key research questions were addressed to test the hypotheses:

1. How does the high-resolution NOAA OISST dataset characterize the temporal and spatial warming trends of the Agulhas Current system from 1982 to 2019??
2. Which specific regions within the Agulhas Current exhibit the most accelerated warming according to the high-resolution NOAA OISST dataset?
3. Does the high-resolution NOAA OISST dataset reveal a statistically significant relationship between SST and geostrophic current speeds in the Agulhas Current?
4. Do the climate indices (ENSO and SAM) influence the SST and geostrophic current speed anomalies in the Agulhas Current?

2. CHAPTER 2: LITERATURE REVIEW

2.1 The Agulhas Current System

According to Lutjeharms (2006), the Agulhas Current is defined as a WBC of the Indian Ocean subtropical gyre (Figure 2.1) and the strongest WBC in the Southern Hemisphere. It is a warm fast-flowing narrow current that is driven by the large-scale pattern of wind stress curl between the Southern Hemisphere westerly winds and southeast trade winds with an average transport of about 70 Sv (1 Sv = 10^6 m^3 s^{-1}) (Beal et al. 2011). The Agulhas Current is an extension of waterbodies flowing southwestward from three sources, namely, the Mozambique Channel in the form of eddies, the East Madagascar Current in the form of dipolar eddies, and the South Western Indian Ocean sub-gyre (Lutjeharms and Ansorge, 2001; Backeberg et al. 2008; Beal et al. 2011). It flows in a southwestward direction (Figure 2.1), transporting warm, oligotrophic water along the east coast of South Africa (Hutchinson et al. 2018). The Agulhas Current heads offshore around 34^0S (Figure 2.1) and then retroflects back into the southwest Indian Ocean as the Agulhas Return Current (Beal et al. 2011). According to Lutjeharms (2006) and Han and Yan (2018), the sudden turn of the Agulhas Current at the southwestern most point of the Agulhas Bank produces loops, filaments, and mesoscale eddies; leaking warm and salty water from the Indian Ocean into the Atlantic Ocean, which plays a part in the Atlantic Meridional Overturning Circulation. The Agulhas Current system is noted for its impact on climate, marine ecosystem, and regional weather (Reason, 2001; Lutjeharms, 2006; Rouault et al. 2009), and for driving or enhancing the dynamic coastal upwelling along the south coast of South Africa (Beal et al. 2006; Goschen et al. 2015).

The Agulhas Current, Agulhas Retroflection, and Agulhas Return Current make up the Agulhas Current system (Figure 2.1). The Agulhas Current is also separated into two parts, namely the Northern Agulhas Current and the Southern Agulhas Current since there are distinct continental shelf structures and greatly different kinematics within each Agulhas Current region. This literature review therefore supports the main aim of this study, which is to investigate the warming trends in the Agulhas Current, by describing the oceanography of the Agulhas Current System according to its four different domains (Northern Agulhas Current, Southern Agulhas Current, Agulhas Retroflection, and the Agulhas Return Current), the warming trends, as well as the potential mechanisms that cause such warming in the Agulhas Current.

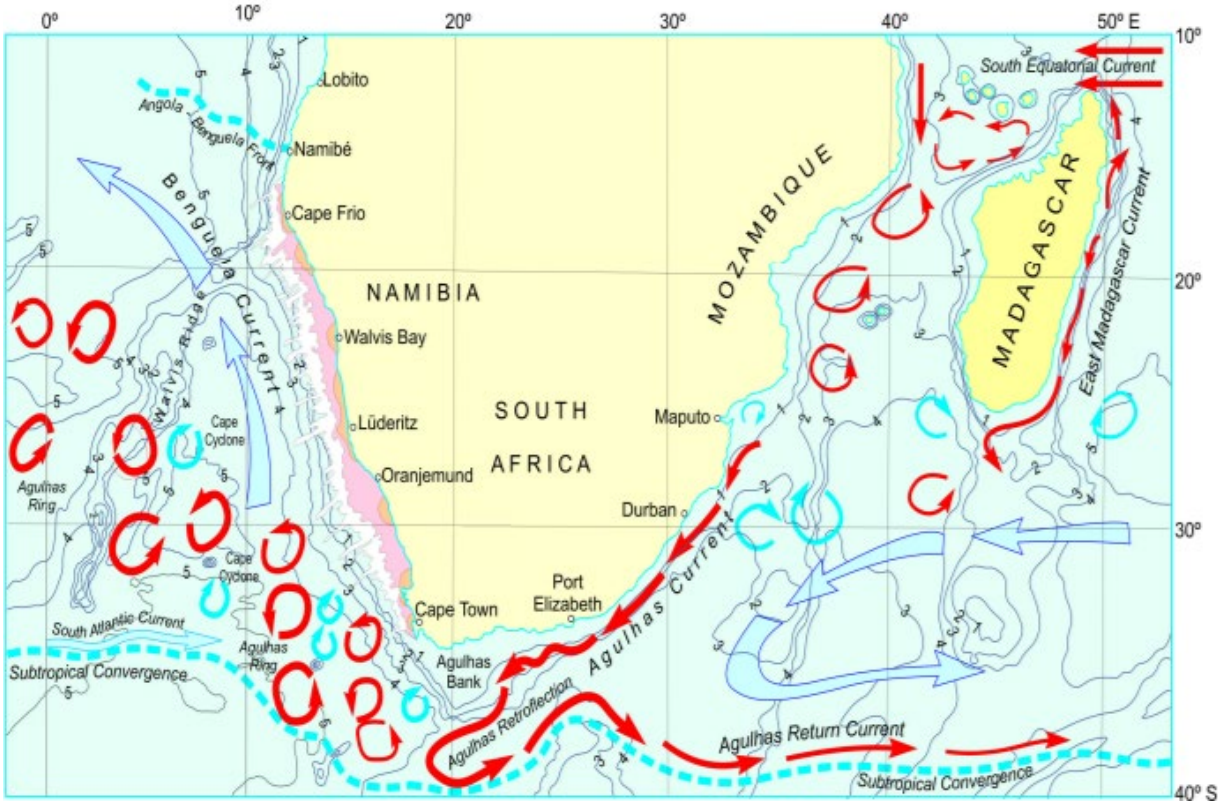

Figure 2.1: A schematic diagram depicting the Agulhas Current system and the general ocean circulation around Southern Africa. The eddies (circular arrows) from the East Madagascar Current and Mozambique Channel, the Agulhas Retroflection as well and the recirculation of the Agulhas Return Current are highlighted. Additionally noted is the leaking of rings and filaments (circular arrows) into the South Atlantic and the location of the Subtropical Convergence in the Southern Ocean. Anticyclonic eddies are depicted by the curved red arrows and cyclonic eddies are indicated by light blue arrows, while the average location of the sub-Tropical Convergence is indicated by a broken light blue line. The Southwest Indian sub gyre's inferred overall motion is indicated by large blue open arrows. The thin contours are showing the depth below the sea surface in kilometres (adapted from Lutjeharms and Ansorge, 2001)

2.1.1 The Northern Agulhas Current

According to Lutjeharms (2006), the Northern Agulhas Current is the northern segment of the Agulhas Current that flows along the steep narrow continental slope and has minor variation in the current trajectory. The latitudinal boundaries of the Northern Agulhas Current are between 27 ºS and 34 ºS (Lutjeharms, 2006). Northern Agulhas Current has a volume flux of 69.7(±4.3) Sv (Lutjeharms, 2007) with a maximum current speed of up to 1.5 m s^{-1} (Van der Vaart and De Ruijter, 2001; Bryden et al. 2005; Rouault et al. 2010; Krug and Tourdre,2012).

The SST in the Northern Agulhas Current can range between a minimum of 21 ºC in August and a maximum of 28 ºC in February (Christensen,1980; Lutjeharms, 2006). Lutjeharms (2006)

suggests a 2 °C downstream drop of sea surface temperature along the entire length of Northern Agulhas Current and such gradient continues throughout the year.

The current core in the northern Agulhas Current flows impressively steadily and with minimal variability (Bryden et al. 2005). The little variability is amongst other processes caused by meandering of the current, and by cyclonic and anticyclonic eddies that originate in the Mozambique Channel and south of Madagascar in this area (Backeberg and Reason, 2010, Braby et al., 2016).

The Northern Agulhas Current can be distinguished from the Southern Agulhas Current by its stable trajectory (Lutjeharms, 2007). This stable trajectory of the current in the region has been associated with the topographic steering caused by the steep continental slope (Lutjeharms, 2007; Roberts et al. 2010; Rouault and Penven, 2011). Although the Northern Agulhas Current is generally stable compared to the Southern Agulhas Current, this stability is occasionally disturbed by the development of meanders such as the Natal Pulses and accompanying eddies at the KwaZulu Natal Bight (Rouault and Penven, 2011).

According to Lutjeharms and Roberts (1988) and Bryden et al. (2005), Natal Pulses are enormous, solitary meanders in the Agulhas Current that are linked to a cold-water core and cyclonic circulation inshore of the Agulhas Current. A barotropic instability causes Natal Pulses to begin in the KwaZulu Natal Bight, where they gradually increase in size as they move downstream at phase velocities of 10 to 20 km d^{-1} (Krug et al. 2014). Krug et al. (2014) suggest that Natal Pulses occur irregularly, with a mean frequency of 4–6 per year, and at intervals of 50–240 days.

There are conflicting results from previous studies that assessed the seasonality of the Agulhas Current. Satellite observations (Krug and Tournadre, 2012) and in-situ data (Beal et al. 2015; Beal and Elipot, 2016) agree that the strongest flows happen during austral summer while results from numerical models (Biastoch et al. 1999; Matano et al. 2002; Hermes et al. 2007; Chang 2009) indicates the strongest transports occur during austral winter and spring. Matano et al. (2002) found the weakest transport to be between the austral autumn and the austral summer. These inconsistent results suggest that seasonality in the Agulhas Current's volume transport and current speed has not been fully clarified (Beal et al. 2015).

2.1.2 The Southern Agulhas Current

The Southern Agulhas Current's northern boundary begins at 34 °S and ends at the Agulhas Retroflection's beginning, which is situated between 16 °E and 20 °E (see Figure 2.1). (Lutjeharms and van Ballegooyen, 1988; Lutjeharms, 2006). With a volume flow of 126 Sv,

which is much larger than that of the Northern Agulhas Current, the Southern Agulhas Current has a surface current speed of over 2 m s^{-1} in the downstream section (Lutjeharms et al. 2003; Lutjeharms, 2007). Similar to the Northern Agulhas Current, there are no observable seasonal variations in the current speeds or volume transport of the Southern Agulhas Current (Lutjeharms, 2006; Beal et al. 2015).

The Southern Agulhas Current's surface temperatures range between 23 and 26 ^{o}C (Schumann and Beekman, 1984; Lutjeharms, 2006). Found in February, the maximum SST ranges from 23 ^{o}C south of Cape Agulhas to 26 ^{o}C near Algoa Bay (Lutjeharms, 2006). The SST of the Southern Agulhas Current drops faster downstream than that of the Northern Agulhas Current over the same distance, owing to higher rates of heat loss to the atmosphere this far south.

According to Bryden et al. (2005) and Lutjeharms (2006), when compared to the Northern Agulhas Current, the Southern Agulhas Current exhibits greater variability. Rouault and Penven (2011), state that from near 34°S to the southern end of the Agulhas Bank, the Southern Agulhas Current resembles other WBC systems, with the regular presence of eddies, plumes, and meanders (Schumann and Beekman, 1984). The presence and passage of increasingly larger meanders known as Natal Pulses can be a cause of increased variability over the Southern Agulhas Current's route (Lutjeharms, 2006; Krug et al. 2014; Leber et al. 2017).

According to Van Leeuwen et al. (2000), Bryden et al. (2005) and Russo et al. (2017) Natal Pulses have a considerable impact on coastal and shelf zones, where they induce localized upwelling. The Natal Pulses are also considered to affect the number of Agulhas Rings that are shed into the Atlantic Ocean during the Agulhas Leakage; which is a transfer of water that is salty and warm from the Indian Ocean to the Atlantic Ocean (Schouten et al. 2002; Yamagami et al. 2019). However, Rouault and Penven (2011) and Elipot and Beal (2015) disagree with Schouten et al. (2002), they argue that the formation of Agulhas rings is not dependent on the presence of Natal Pulses. Furthermore, the Agulhas Current maintains its transport during a meander (Leber and Beal, 2014), and Biastoch et al. (2009), through a numerical model, highlight that the Natal Pulses do not have a strong influence on the Agulhas leakage, casting doubt on the relationship between the Natal Pulses and Agulhas Leakage variability. Lutjeharms (2006) and Rouault et al. (2010) suggest that the Natal Pulses cause the Southern Agulhas Current's path to shift offshore.

Little is known about the Agulhas Current's inter-annual to decadal variability as a result of a lack of in-situ observations and the limitations of numerical models. However, it has been suggested that mesoscale anomalies such as meander events and Agulhas Rings have inter-annual

variability linked to the Indian Ocean Dipole and El Nino Southern Oscillation modes (Beal et al. 2015).

2.13 The Agulhas Retroflection

The Agulhas Retroflection is a section of the Agulhas Current that undergoes a direction change and it stretches between 16 ºE and 20 ºE with a loop diameter of around 300 to 400 km (Lutjeharms and van Ballegooyen, 1988; Lutjeharms, 2007; Beal and Elipot, 2016). In the Agulhas Retroflection area, the Agulhas Current is reversed and redirected into the South Indian Ocean as the Agulhas Return Current (Beal and Elipot, 2016). The Agulhas Retroflection is a unique characteristic for a WBC in that it occurs near the meridional extremities of the surrounding continent (Lutjeharms and Ansorge, 2001; Lutjeharms, 2006). This is contrary to the continental constraints that other WBCs, such as the Kuroshio, the Gulf Stream, and the Brazil Currents face (Lutjeharms, 2006).

The current speed in the Agulhas Retroflection area varies. Current speeds over 0.5 m s^{-1} have been found up to 60% of the time in the retroflection region, although a maximum speed of 2 m s^{-1} has also been recorded (Lutjeharms, 2006; Lutjeharms, 2007). A large leakage from the Indian Ocean to the Atlantic Ocean occurs here, resulting in an inter-ocean exchange of water, energy, and biota (Beal et al. 2011; Elipot and Beal, 2015; Leber et al. 2017). The leakage is a combination of Agulhas filaments as well as the Agulhas Rings (Lutjeharms, 2006; Elipot and Beal, 2015; Beal and Elipot, 2016).

According to Garzoli et al. (1996), Retroflection has some of the highest levels of mesoscale variability in the entire world's oceans and is linked to the development and dissipation of enormous anticyclonic eddies known as Agulhas Rings (Lutjeharms and Van Ballegooyen, 1988, de Ruijter et al., 1999). The average diameter of these Agulhas Rings is 324 ± 94 km, and they move away from the Retroflection at a rate of 5 to 8 km/day (Olson and Evans, 1986). These rings, along with eddies and filaments (Biastoch et al., 2008b; Beal et al., 2011), are the primary contributors of the Agulhas leakage because they transfer warm, salty water from the Indian Ocean into the South Atlantic Ocean (Gordon, 1986). According to Lutjeharms (2006), the Agulhas rings have radial speeds within 0.29 m s^{-1} and 0.90 m s^{-1} with an average of 0.56 m s^{-1}. Imbol Nkwinkwa et al. (2019) state that the leakage water from the Retroflection region to the South Atlantic Ocean in the eddy corridors has a temperature that ranges between 18 ºC and 20 ºC.

2.1.4 The Agulhas Return Current

The Agulhas Return Current comprises the water from the Agulhas Current that flows eastward after passing through the Agulhas Retroflection (Lutjeharms and Ansorge, 2001; Boebel et al., 2003, Lutjeharms, 2006). According to Lutjeharms and Ansorge (2001), the Agulhas Return Current begins between 16 ^{o}E and 20 ^{o}E of the retroflection area and ends between 66 and 70 ^{o}E.

Strong eddy formation and significant solitary meanders are responsible for the Agulhas Return Current region's substantial mesoscale variability (Lutjeharms and Valentine, 1988; Lutjeharms and Ansorge, 2001). The region's uneven seafloor topography is what causes these meanders (Lutjeharms, 2006). The first of these essentially stationary meanders passes over the Agulhas Plateau between 25 and 29 degrees east (Pichevin et al., 1999).

The sea surface current speed of the Agulhas Return Current fluctuates, with a maximum speed of around 2.1 m s^{-1} around the Agulhas Retroflection region and decreasing to 1.1 m s^{-1} around 32 ^{o}E (Boebel et al. 2003). The Agulhas Return Current, which connects the Atlantic, Indian, and Southern Oceans due to its pivotal location between two oceanic gyres, is also regarded as a component of the inter-ocean exchange (Lutjeharms and Ansorge, 2001).

2.2 The warming trends in the Agulhas Current System

Numerous studies have investigated the warming in the Agulhas Current and the possible drivers behind such warming (Rouault et al. 2009; Rouault et al. 2010; Wu et al. 2012; Han and Yan, 2018; Sweijd and Smit, 2020). Han and Yan (2018) state that the region of the Agulhas Current has been one of the fastest-warming areas in the world ocean in the last few decades, and due to heat redistribution, it can be one of the ocean sinks for the excess heat (Chen and Tung, 2014).

According to Rouault et al. (2009), the warming in the Agulhas Current has been occurring since the 1980s, despite the considerable increasing trend in latent and sensible heat fluxes that ought to have cooled the area. The warming in the region increases towards the west (Figure 2.2) until it reaches a peak at the retroflection area and spreads into the Agulhas eddy corridor in the South Atlantic Ocean and the Agulhas Return Current (Rouault et al. 2009). Since the 1980s the retroflection area, Agulhas rings, eddies, and the Agulhas Return Current are estimated to have warmed by up to 0.7 ^{o}C/decade (Figure 2.2), despite increased heat fluxes that were already high due to the air-sea interaction (Rouault et al. 2009).

Rouault et al. (2010) report that there is obvious warming in the Agulhas Current system and note that during all months of the year, most parts of the Agulhas Current system experience a positive trend in SST of up to 0.55 ºC/decade. However, Rouault et al. (2010) state that there is an exception to the region of KZN where most of the warming occurs in the summer. Rouault et al. (2010) emphasize that warming in the Agulhas Current is accompanied by cooling in some inshore regions such as the Port Alfred/Port Elizabeth system and this cooling mechanism might be caused by a combination of Agulhas Current intensification and the increase in upwelling-favourable winds.

Han and Yan (2018) use two major adiabatic physical components namely heave and spice to determine the trends of ocean heat content changes and the excessive heat accumulation rate in the Agulhas Current during two different warming periods (the slowdown period and the acceleration period). The heave component illustrates the temperature changes, which are caused by the upright movement of isopycnals, on the contrary spice determines the changes in temperature along the isopycnals. According to Han and Yan (2018), the slowdown period spans from 1998 to 2013, where the warming rate of mean surface temperature globally increased at a rate much slower (0.05 ºC/decade) compared to the period of accelerated warming (1984 to 1998) where the warming rate was around 0.12 ºC/decade. In addition, Han and Yan (2018) argue that the Agulhas Current region gained more heat during the slowdown period in the global surface warming instead of the accelerated period.

In addition to these findings, a study conducted by Malan et al. (2019) offers a comprehensive analysis of the temperature fluctuations observed in the Agulhas Bank. The study utilises an advanced Ocean General Circulation Model (OGCM) to discern the occurrence of temperature shifts spanning multiple decades on the Agulhas Bank. These shifts are predominantly influenced by the displacement of large-scale wind belts along latitudinal gradients. The observed changes exhibit a robust correlation with the Southern Annular Mode, indicating the possibility of future predictability in the thermal patterns within this geographical area. According to Malan et al. (2019), the spatial arrangement of anomalies in SST indicates that areas with higher temperatures are mainly concentrated in coastal waters with shallower depths. This suggests that the primary drivers of these temperature changes are coastal upwelling and downwelling processes, which are influenced by wind patterns. Malan et al. (2019) highlight the significance of Ekman heat transport in influencing SST. The authors observed that pivotal years, which mark transitions between different thermal regimes, align with peaks and troughs in Ekman heat transport. The study suggests that variations in zonal wind patterns over multiple years and decades have a notable impact on sea surface temperatures (SST). This underscores

the complex connection between atmospheric dynamics and the temperature patterns in the Agulhas Bank region of the ocean.

Although research has been conducted to investigate the warming of the Agulhas region, scientists still agree that there is a lack of research or understanding of the mechanisms that drive such warming. Rouault et al. (2009) suggest that increased transport of the Agulhas Current due to the increase in wind stress curl is one of the reasons that cause warming in the region. Due to the sea surface cooling in the Agulhas Current which is associated with an increase in latent heat fluxes (LHF) and sensible heat fluxes (SHF), Rouault et al. (2009) rules out local air-sea interaction as a possible contributor to the warming. Owing to the variations in sea surface temperature between WBC and their surroundings, the Agulhas Current has high evaporation rates, turbulent LHF and SHF (Rouault et al. 2003; Rouault et al. 2009; Beal et al. 2011; Imbol Nkwinkwa et al. 2019). The observations by Rouault et al. (2009) are supported by the findings of Han and Yan (2018), which shows that most of the increase in ocean heat content in the Agulhas Current does not happen at the surface but rather at a deeper layer (200–700 m). Han and Yan (2018) also argue that the warming in the accelerated period is driven by heave which increases in a monotonic manner, while the increase in heat accumulation rate during the slowdown period (1998 to 2013) is driven mostly by the spice component. According to Han and Yan (2018), the increase in salinity during the slowdown period strengthens spicing which causes a higher heat accumulation rate in the slowdown period than in the acceleration period.

Similar to Rouault et al. (2009), Wu et al. (2012) suggest that the rapid warming in subtropical WBCs including the Agulhas Current is consistent with intensification and/or a synchronous poleward shift of WBCs that is in conjunction with changes in winds. In support of Wu et al. (2012), Yang et al. (2016) reports that WBCs (except the Gulf Stream) are intensifying and shifting poleward thus increasing SST. Contrary to Rouault et al. (2009), Wu et al. (2012) and Yang et al. (2016), a study by Beal and Elipot (2016) insists that the Agulhas Current is not intensifying but broadening. According to Beal and Elipot (2016), the increase in wind intensity over the WBC may increase the eddy kinetic energy but not intensify the mean flow of these currents. Beal and Elipot (2016) further suggest that the warming trends in WBC are related to the broadening of WBC, although further investigation is needed. In building upon this foundation, Fadida et al. (2021) offer novel insights specifically into the Agulhas Return Current (ARC). Their research elucidates the ARC's variable responses to climate change, marked by significant meridional migrations and increasing eddy kinetic energy (EKE). The study reports different trends in the eastern and western segments of the ARC, with the former primarily

undergoing equatorward migration and the latter displaying a poleward tendency. This work further emphasizes the substantial role that bathymetry plays in shaping the ARC's dynamics, making it an essential component for understanding the broader Agulhas system's response to climate change.

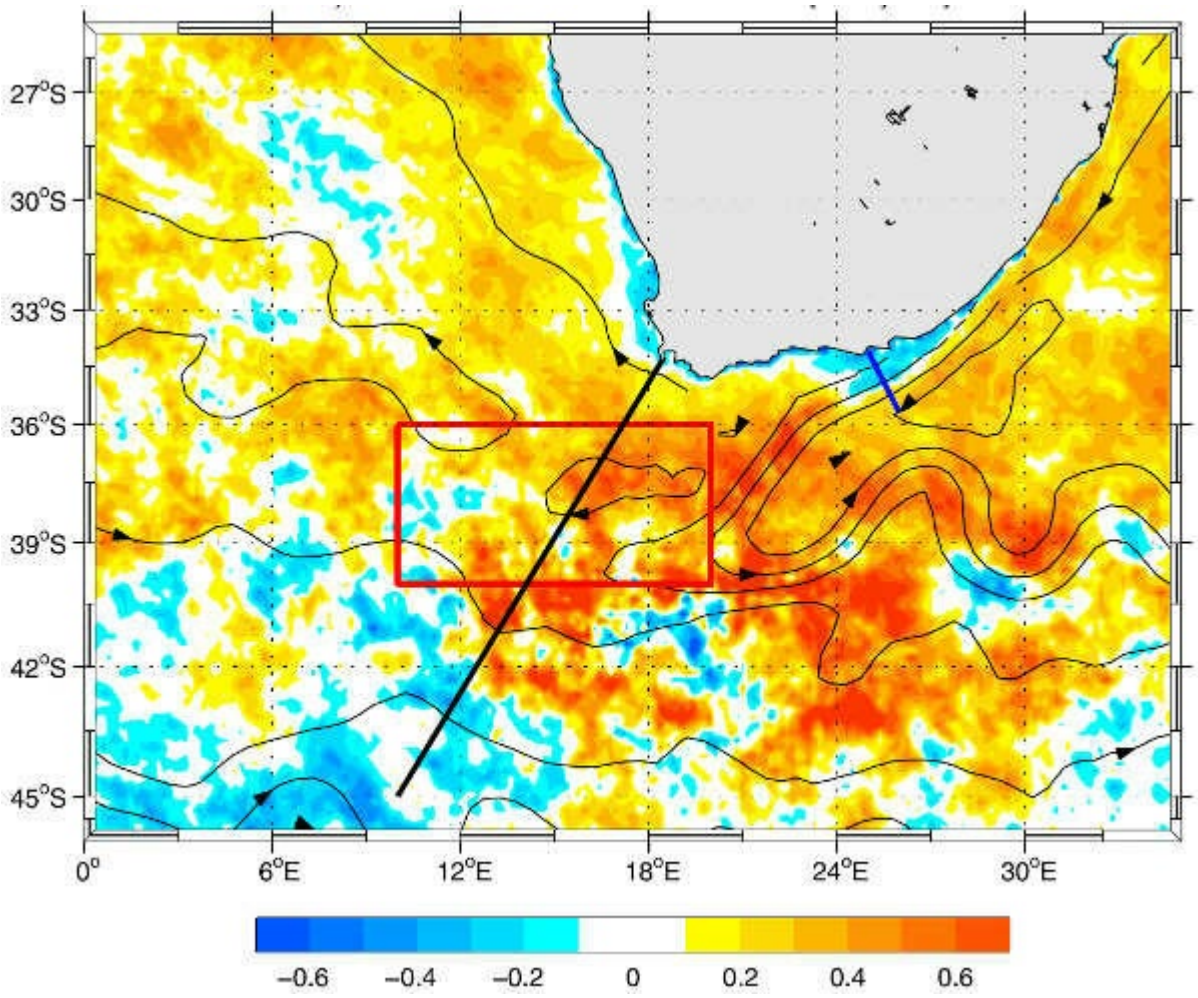

Figure 2.2: displays the warming patterns observed within the Agulhas Current, as adapted from the study conducted by Rouault et al. (2009). The data obtained from the Advanced Very High-Resolution Radiometer reveals a linear trend in sea surface temperatures between the years 1985 and 2006, indicating a warming rate of up to 0.7°C per decade. The presence of black contour lines on a map indicates the representation of average surface currents, while the inclusion of arrows serves to depict the direction in which these currents are flowing.

2.3 Influence of Climate Modes on the Agulhas Current

El Niño-Southern Oscillation (ENSO)

The ENSO is a prominent climatic phenomenon that is distinguished by two atypical ocean-atmosphere conditions known as El Niño and La Niña (Figure 2.3). El Niño and La Niña, which exhibit cyclical patterns ranging from 2 to 7 years, are predominantly observed within the equatorial Pacific Ocean (Sarachik and Cane, 2010). A deeper thermocline, higher sea surface temperatures (SST), and weaker trade winds are all characteristics of an El Nio phase in the eastern equatorial Pacific (Figure 2.3). On the other hand, La Niña events are characterised by a less pronounced thermocline and lower sea surface temperatures (SSTs), which are caused by the process of upwelling and the intensification of trade winds (Sarachik and Cane, 2010).

The impacts of ENSO, which originates in the equatorial Pacific, are widespread on a global scale as a result of teleconnections (Rouault and Richard, 2005). For example, the ENSO has a substantial impact on surface air temperatures and sea-ice concentrations in different areas of the Southern Ocean (Wang et al. 2017).

In Southern Africa, specifically the Agulhas Current, the occurrence of ENSO events affects the temperature and salinity signatures in the region. Jury, (2015) and Trott et al. (2021) found that there is warming after an El Niño event and cooling after a La Niña event. According to Trott et al. (2021), the effects of ENSO events on temperature in the Agulhas Current are noticeable 20 to 30 months after the peak of an ENSO event.

Putrasahan et al. (2017) corroborate the findings of Jury, (2015) and Trott et al. (2021) on the influence of ENSO on SST in the Agulhas Current, particularly concerning SST within the Agulhas leakage corridor. Utilising a high-resolution Community Climate System Model (CCSM3.5), Putrasahan et al (2017) illustrate the role of wind anomalies linked to ENSO cycles in initiating the propagation of oceanic Rossby waves in a westward direction. The aforementioned waves generate anomalies that propagate in a southwest direction along the African coastline, exerting an influence on the Agulhas leakage and contributing to approximately 20% to 30% of its annual variability in sea surface height (Putrasahan et al. 2017).

According to Rouault and Richard (2005), the rainfall patterns in Southern Africa are also influenced by the ENSO, which frequently leads to significant deviations from normal weather conditions. The El Niño events are typically linked to arid conditions and droughts, whereas La Niña phases are associated with heightened precipitation and a higher likelihood of flooding

(Rouault and Richard, 2005). These ENSO influenced changes have significant implications for various aspects such as food security, water resources, and human livelihoods in Southern Africa and require constant research (Rouault and Richard, 2005).

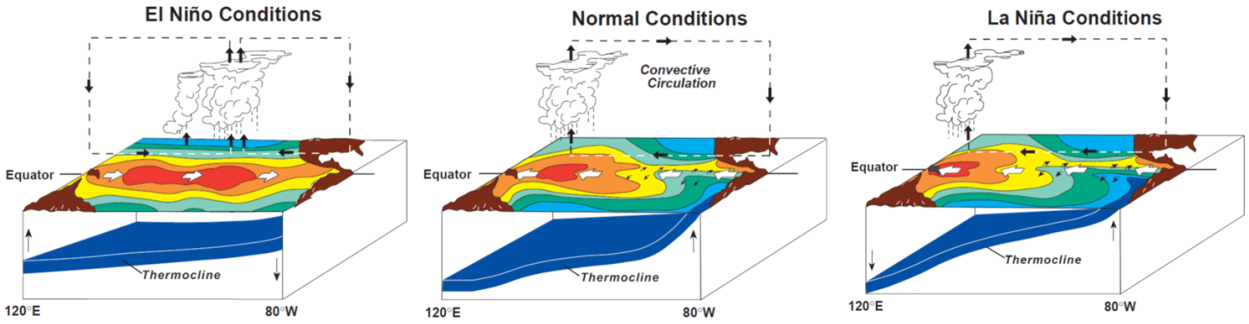

Figure 2.3: illustrates a schematic representation of the various conditions associated with the El-Niño Southern Oscillation (ENSO). The right panel depicts the La Niña conditions, the middle panel represents the Normal conditions, and the left panel portrays the El Niño conditions. The image was acquired from the PMEL TAO Project, which can be accessed at pmel.noaa.gov.

Southern Annular Mode (SAM)

In the Southern Hemisphere, the SAM is a key contributor to climate variability (Marshall, 2003; Ciasto and Thompson, 2008). According to Swart et al. (2015) and Thompson et al. (2011), the SAM is responsible for approximately 30% of the climate variability in the extra-tropical regions of the Southern Hemisphere. SAM is marked by the redistribution of atmospheric mass along latitudinal lines, specifically from higher latitudes located poleward of 50 °S to lower latitudes between 30 °S and 50 °S. The process of redistribution results in the generation of diversity in atmospheric characteristics, including wind speed, air temperature, and precipitation, over various periods, ranging from daily to decadal (Marshall, 2003; Marshall, 2007; Richard et al., 2013).

The spatial structure of the SAM is characterised by the presence of synchronous pressure anomalies with opposite signs at mid and high latitudes. Throughout the positive phase of the SAM, there is a notable lower atmospheric pressure over the region of Antarctica. In contrast, in the negative phase, there is a notable increase in atmospheric pressures over Antarctica (Figure 2.4). According to Swart et al. (2015), these pressure anomalies have a significant impact on the direction and intensity of the westerly winds. However, it has been indicated by recent studies that the association between the SAM and the characteristics of these winds is not a simple one and necessitates a more intricate comprehension (Swart et al., 2015).

The influence of SAM variability has garnered considerable scientific attention, However, while the ENSO-Agulhas Current linkage has been demonstrated by several studies (Putrasahan et

al., 2017), a direct SAM-Agulhas Current link remains less studied, with few studies highlighting the relationship.

According to Malan et al. (2019), SAM appears to have a long-term effect on Agulhas Bank temperatures, an ecologically important region. SAM influences the north-south migration of large-scale wind belts, which cause multidecadal temperature shifts over the Agulhas Bank. Yang et al. (2016) as well as Elipot and Beal, (2018) also suggest that SAM modulates basin-scale anticyclonic gyres that support the Agulhas Current by changing their latitude and intensity.

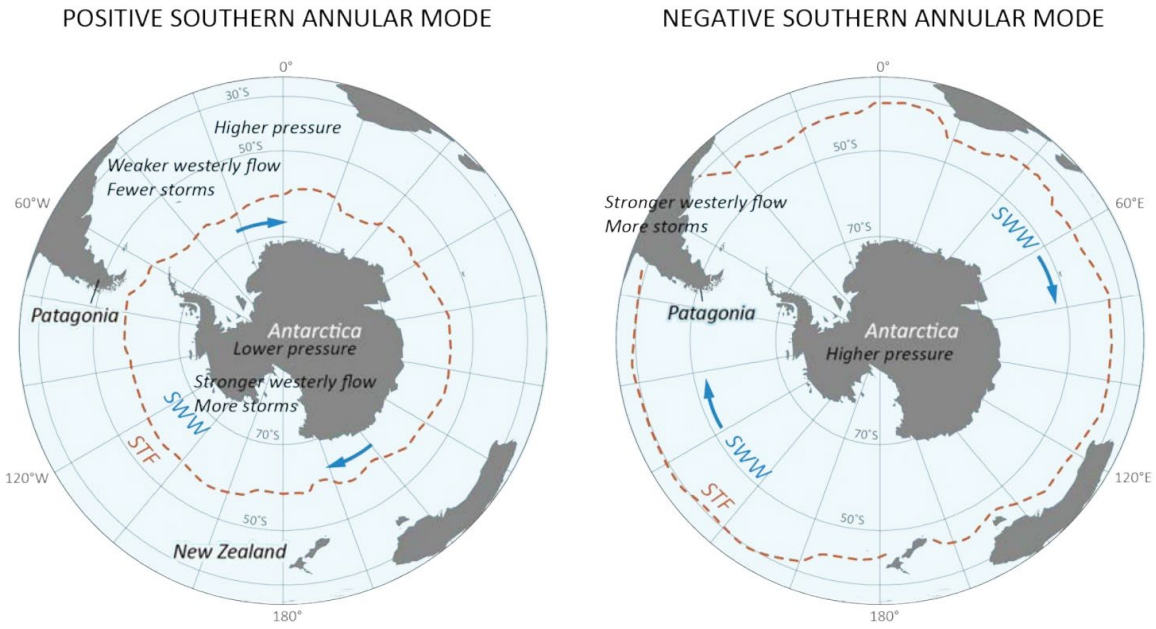

Figure 2.4: displays the Positive and Negative phases of the Southern Annular Mode (SAM) as obtained from Antarcticglacier.org. In this context, SWW refers to Westerly Winds, while STF stands for Subtropical Front

Table 2.1: Summary of all the previous studies that assessed warming trends in the Agulhas Current system and the various warming rates that have been reported for the Agulhas Current system. The various datasets, spatial resolution and the period covered by the study are also included in the table

Reference	Datasets	Spatial resolution	Warming rate	Period of the study.
Rouault et al. (2009)	AVHRR SST, NOAA OISST, Hadley SST	4 km by 4 km grid resolution for AVHRR SST, 1º x 1º Grid Globally for the other datasets.	0.7 ºC/decade	1985-2007
Rouault et al. (2010)	NOAA OISST	1º x 1º Grid Globally	0.55 ºC/decade	1982-2009
Wu et al. (2012)	Hadley Centre Sea Ice and SST version 1 (HadISST1); National Oceanic and Atmospheric Administration Extended Reconstructed SST version 2 (ERSSTv3b); Kaplan Extended SST version 2 (Kaplanv2); Simple Ocean Data Assimilation (SODA) SST product27; Hadley Centre SST version 2 (HadSST2).	1º x 1º Grid Globally for HadISST, 0.5º x 0.5º for SODA	0.8–1.8 ºC per century	1900–2008
Sweijd and Smit (2020)	NOAA OISST	0.25º x 0.25º Grid Globally	0.512 ºC/decade	1982-2019
Han and Yan (2018)	NOAA OISST	0.25^0 x 0.25^0 Grid Globally	~0.6 ºC/decade	1982-2013

3. CHAPTER 3: METHODS

3.1 Study Area

This study was conducted in the Southern African region; the latitudinal and longitudinal extents of the study area are 10 ºS-50 ºS and 0 ºE- 55 ºE respectively. Although the study covered the above-mentioned latitudinal and longitudinal extents, small areas within four domains in the Agulhas Current referred to as the Northern Agulhas Current, Southern Agulhas Current, Agulhas Retroflection, and the Agulhas Return Current (Figure 3.1) were selected for a focused analysis of the datasets used to fulfil the research objectives and address the research questions.

The square boxes in Figure 3.1 are the domains where the subsetting was done for this study and the black dots inside the boxes are the points where the timeseries were extracted to create an average timeseries for each domain. The author would like to emphasize that the boxes are there to only highlight the areas where the actual data point extraction took place as shown by the black dots, they are not the subsets.

The specific latitudinal and longitudinal coordinates for the data extraction can be seen in Figure 1 and are as follows:

Northern Agulhas Current: Latitude at -33.3 °S and -32.8 °S, Longitude at 28.6 °E and 29.1 °E.

Southern Agulhas Current: Latitude at -36.375 °S and -35.875 °S, Longitude at 22.5 °E and 23.0 °E.

Agulhas Retroflection: Latitude at -38.875 °S and -39.375 °S, Longitude at 19.125 °E and 19.625 °E.

Agulhas Return Current: Latitude at -39.625 °S and -39.125 °S, Longitude at 23.875 °E and 23.375 °E.

Each Latitude coordinate is paired with the longitude values to extract data for different locations.

The selection of these subset areas was guided by the predefined boundaries of the Agulhas Current System domains, as elaborated in Chapter 3 as well as the geostrophic currents shown in **Figure 3.1**. For instance, the Northern Agulhas Current is demarcated by latitudinal boundaries between 27°S and 34°S, whereas the Southern Agulhas Current extends from 34°S to the onset of the Agulhas Retroflection domain, which lies between 36°S and 40°S (Lutjeharms, 2006).

Rouault and Lutjeharms (2003), and Rouault et al. (2003) argued that, while some datasets (e.g., NOAA OISST) do not adequately show certain attributes of the coastal region and the core of the Agulhas Current due to the interpolation technique used and data spatial resolution, the datasets can be used quite satisfactorily by averaging over an area rather than extracting data from a single location.

When subsetting spatial data, it is essential to take more than one data point to ensure that the subset is representative of the region of interest and to avoid bias and errors in the analysis. The reason for using multiple data points in the spatial subset is underpinned by several important considerations:

1. Variability: Spatial data, including SST, are subject to significant spatiotemporal variations influenced by factors such as topography, ocean currents and atmospheric conditions. Using multiple data points allows for the capture of this inherent variability, thereby providing a more comprehensive representation of the spatial distribution of the data.

2. Sampling bias: Extracting single-point data can introduce sampling bias, potentially distorting the representation of the broader region of interest. Multipoint sampling mitigates this bias and increases the robustness of spatial variability estimates.

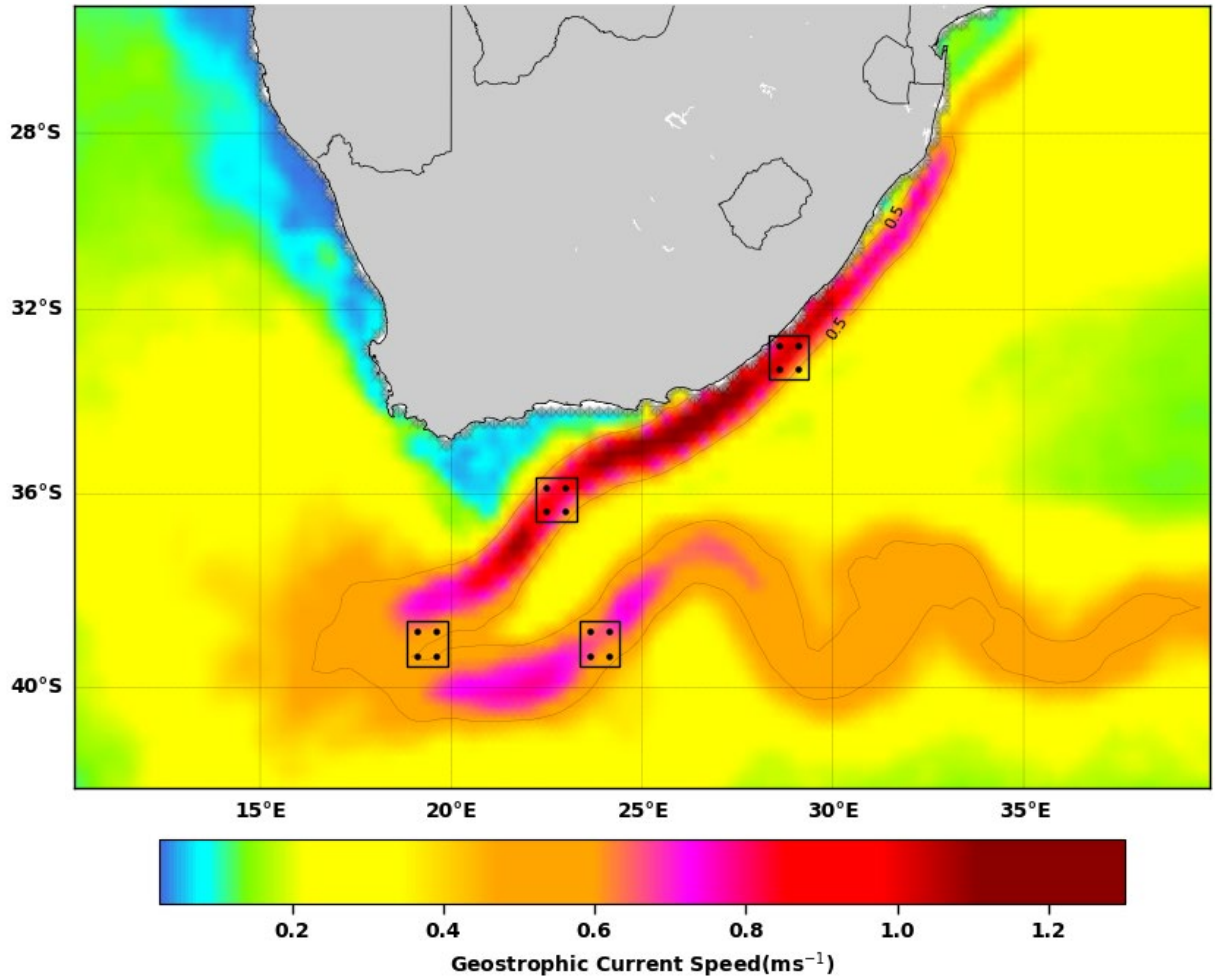

Figure 3.1: This map shows the mean ocean surface current speed (in m $s^{-1)}$ from 1993 to 2019 over the study area. The map is overlayed by the domains that were selected for the in-depth analyses of warming trends in the Agulhas Current. The domains selected for the focused analysis are highlighted by the black square boxes with black dots inside showing where the subsampling took place. All the boxes are placed within the latitudinal extents of each Agulhas Current system domain, the extents of each domain are explained in chapter 2. A 0.5 m s^{-1} contour line has been included just to get a general idea of the surface current speed in the map.

3.2 Data Sources

To address the key research questions and fulfil the research aims of this study, both SST and Geostrophic Current data were used. Both datasets are explained in detail below.

3.2.1 SST Data

A subset of the NOAA Optimum Interpolation SST (NOAA OI. v2 SST) version 2 daily average dataset (Reynolds et al. 2007) between 1982 and 2019 was used to conduct this study. The latitudinal and longitudinal extents of this study were used to make a subset of the SST data. Monthly fields are derived by averaging the 0.25° x 0.25° daily SST values over a month. The NOAA 0.25° x 0.25° daily OISST is a global grid-based product that combines data observations from ships, Argo floats, buoys, and high-resolution infrared satellite observations (9 km) from the AVHRR (advanced very high-resolution radiometer) sensor on NOAA (National Oceanic and Atmospheric Administration) satellites. SST data gaps are filled by interpolating the SST observations. The daily analysis uses in-situ and satellite SST, plus SST simulated by the sea-ice cover. Methodologies developed by Reynolds and Marsico (1993) are used to adjust the satellite data for biases, which improves the large-scale accuracy of the optimum interpolation.

The NOAA OISST data has been verified and has been used successfully in several studies in the Southern African region (Rouault and Lutjeharms, 2003). Benguela Ninos by Rouault, et al. 2003 and Rouault (2012), and the description of the SST trends in the Agulhas Current by Rouault et al. (2010) are some examples of such studies. The data that was used to conduct this study is freely available online through the following link (https://psl.noaa.gov/data/gridded/data.noaa.oisst.v2.highres.html)

3.2.2 Surface Geostrophic Current

A geostrophic current is an ocean current in which the Coriolis effect balances the pressure gradient force (Talley et al. 2011). The flow of geostrophic current is parallel to the isobars, with high pressure to the right of the flow in the Northern Hemisphere and to the left in the Southern Hemisphere. The surface geostrophic currents in the ocean can be determined using satellite altimetry data, which can be used to determine the horizontal gradient in sea level (Rio et al. 2014).

In order to determine the zonal (Equation 3.1) and meridional (Equation 3.2) components of geostrophic current, absolute dynamic topography (ADT) is used, which is determined by adding mean dynamic topography (MDT) and sea level anomalies (SLA) (Rio et al. 2014).

The formulars for the zonal and meridional components are written as follows:

$$u = -\frac{g}{f}\frac{\partial ADT}{\partial y} \quad (3.1)$$

$$v = \frac{g}{f}\frac{\partial ADT}{\partial x} \quad (3.2)$$

where g is the acceleration due to gravity (9.81 m s^{-2}), f=2Ωsinθ is the Coriolis parameter, x represents the longitudinal

direction and y represents the latitudinal direction, Ω = Rotation rate of Earth = 7.2921 x 10^{-5} rad s^{-1}, θ= latitude.

This study used global daily 0.25º x 0.25º gridded satellite altimetry data from 1993 to 2019. This dataset is only available from 1993 to the present date, hence its temporal scale is not the same as the SST dataset. The Copernicus Marine Environment Monitoring Service (CMEMS) distributes the altimetry product, which is available as a level 4 multi-mission product containing daily gridded Sea Surface Height (SSH), and its anomaly Sea Level Anomaly (SLA) and derived variables (Absolute and Anomalous geostrophic velocity: zonal and meridional components). CMEMS is a platform that provides systematic and regular data on the state of the physical ocean and regional seas. This product was produced by taking data from multiple altimetry missions and merging them with the same processing techniques, models, and geophysical corrections. During the merging of data from multiple altimetry missions, the OSTM and Jason-2 missions are used as a reference dataset, with accompanying data from Jason-3, Sentinel-3A, HY-2A, Saral/AltiKa, Cryosat-2, Jason-2, Jason-1, T/P, ENVISAT, GFO, and ERS1/2. An Optimum Interpolation is made by merging all the flying satellites to compute gridded Sea Level Anomalies (SLA) and Absolute Dynamic Topography (ADT). The geostrophic currents (geostrophic velocities anomalies and the absolute geostrophic velocities) are then derived from SLA and ADT, respectively.

The resultant geostrophic current speed was computed using the relation (Equation 3.3). The data for the geostrophic components can be accessed freely using the link below:

(https://resources.marine.copernicus.eu/?option=com_csw&view=details&product_id=SEALEVEL_GLO_PHY_L4_REP_OBSERVATIONS_008_047).

$$R = \sqrt{u^2 + v^2} \quad (3.3)$$

Where:

R = Resultant geostrophic current speed

u = zonal geostrophic current component

u = meridional geostrophic current component

3.2.3 Climate indices

Oceanic Niño Index (ONI)

The ENSO is a prominent climatic phenomenon that is distinguished by two atypical ocean-atmosphere conditions known as El Niño and La Niña. El Niño and La Niña, which exhibit cyclical patterns ranging from 2 to 7 years, are predominantly observed within the equatorial Pacific Ocean (Sarachik and Cane, 2010). The forecasting of ENSO events has been recognised as a crucial area of research due to the significant climatic consequences associated with these phenomena. To enhance the accuracy of predictive evaluations, the Climate Prediction Centre (CPC) under the National Oceanic and Atmospheric Administration (NOAA) employs a systematic approach to monitor deviations from the norm in Sea Surface Temperature (SST) across the tropical Pacific Ocean. The achievement of this is facilitated through the utilisation of a significant measurement known as the Oceanic Niño Index (ONI), which is represented in degrees Celsius.

To compute the ONI, a three-month moving average is calculated for sea surface temperature (SST) anomalies in the Niño 3.4 region, which is defined geographically as the area between latitudes 5°S and 5°N and longitudes 170°W and 120°E. To fulfil this objective, the data on SST are obtained from the Extended Reconstructed Sea Surface Temperature (ERSST) Version 5 dataset, which is a scientifically validated product that has undergone thorough scrutiny in peer-reviewed research (Trenberth, 1997; Huang et al., 2017; Trenberth, 2020).

After determining the three-month moving averages, they are compared to a long-standing baseline, which is the 30-year climatological mean of absolute sea surface temperature (SST) values. The reference baseline undergoes updates every five years, which ensures that it accurately reflects the current climate conditions and maintains its analytical strength. The discrepancy between the moving average and the established baseline results in the determination of the ONI index value. The current study used ONI values from January 1982 to

December 2019 to ensure both SST and geostrophic current speed are covered. The data is publicly available and can be accessed through the following link. https://legacy.bas.ac.uk/met/gjma/sam.html

SAM Index

The SAM is a major determinant of climatic variability in the Southern Hemisphere (Marshall, 2003; Ciasto and Thompson, 2008). According to seminal studies by Swart et al. (2015) and Thompson et al. (2011), SAM accounts for approximately 30% of the climate variability in the Southern Hemisphere's extratropical regions.

The SAM index used in this study was calculated using a rigorous method that included station-based observations of normalised monthly sea-level pressures at 40°S and 65°S latitudes. This calculation follows Gong and Wang (1999)'s empirical definition, which essentially quantifies the zonal pressure gradient between these two latitudes.

The SAM index is a quantitative representation of the oscillation of atmospheric mass in the Southern Hemisphere between mid and high latitudes. Positive SAM index values indicate increased westerly winds in the mid-high latitudes (50°S-70°S) and decreased westerly winds in the mid-latitudes (30°S-50°S).

The SAM index, which was created in 1957 till present and is based on data from six stations near 40°S, is available in a variety of temporal resolutions. The index calculated monthly was used for this study, providing a robust and temporally granular measure for analysing climate variability in the Southern Hemisphere. The SAM index data used in this study was from 1982 to 2019 and is freely and publicly accessible using the following link: https://legacy.bas.ac.uk/met/gjma/sam.html

3.3 Statistical Analysis

Python Programming Language was used for convenient analysis of the large data oceanographic dataset and visualisation of the results.

3.3.1 Analysis on Sea Surface Temperature

The NOAA OISST monthly values were used to calculate monthly climatology over the entire study area to describe the general temporal and spatial variation of SST. A monthly climatology is an average value over an extended time, often over 30 years, for each month of a given variable (Wilks, 1995). To conduct a focused analysis of the variations and trends within the Agulhas Current, in each domain 4 data points were selected to extract SST values (Figure 3.1).

The extracted data points were then used to derive a timeseries by averaging them for each domain over time. Monthly climatology was also calculated on the derived timeseries to further assess the variation of SST in time within domains and between the domains. Deviations from the usual monthly SST mean were assessed by calculating the monthly anomalies for each domain. The monthly anomalies were computed by subtracting the monthly climatology from the monthly SST values. The anomalies in this study were also normalised by dividing the anomalies by the climatological standard deviation to remove the influence of any dispersion.

Linear trends were calculated to determine the warming trends of the Agulhas Current. The SciPy module in Python was used to calculate the linear trends of the SST by using the linear least squares regression. The method of linear least squares is a statistical technique that is used for determining the best fit for a series of data measurements by reducing the sum of residuals from the plotted line or curve (Thomson and Emery, 2014). One of its advantages is that the data do not need to be equally spaced in time for this method to be applicable (Thomson and Emery, 2014). The linear trends were calculated for each data point or grid annually over the entire study area and the annual trends were converted to decadal (10 years) trends. Furthermore, monthly trends were calculated for the specific domains using the derived timeseries. The annual trends were used to better determine whether warming or cooling is the same across the entire Agulhas Current since they were calculated for each data point.

The statistical significance of these SST trends was assessed at a 95% confidence level using the Student t-test by calculating the p-value for each trend and comparing it to the determined threshold p-value (0.05). A p-value is a metric that expresses the probability that an observed difference may have happened by chance. The statistical significance of the observed difference increases as the p-value decreases (Thomson and Emery, 2014). The warming trends with a p-value of less than 0.05 were considered statistically significant.

3.3.2 Geostrophic Current

A statistical analysis similar to the one used for the SST analyses was used on the satellite altimetry dataset. The zonal and the meridional components of the geostrophic currents were analysed separately to assess their climatology, anomalies, and linear trends (annual and seasonal) both on a temporal and spatial scale. Then the resultant geostrophic current speed went through the same statistical analysis to determine its climatology, anomalies, and linear trends on a temporal and spatial scale. The p-values for the geostrophic current speed, zonal component and meridional component trends were calculated and compared to the established

threshold p-value (0.05) in order to ascertain the statistical significance of these trends at a 95% confidence level using the Student t-test.

3.3.3 Correlations

Pearson's correlation coefficient (r) was calculated to assess the spatial relationship between the monthly SST timeseries and the geostrophic current speed timeseries. Thomson and Emery (2014) describe Pearson correlation as a technique for determining the linear relationship between two variables. The Pearson's correlation coefficient (r) ranges between -1 and 1, the number indicates the strength (±1 is the strongest) while the sign of the Pearson's correlation coefficient indicates the direction of a relationship between two variables (Thomson and Emery, 2014). In this study, the strength of the Pearson's correlation coefficients was classified according to Hogg et al. (2014) as illustrated in Table 3.1.

The statistical significance of the correlation between SST and geostrophic current speed was assessed using the Student t-test by calculating the p-value for each data point and comparing it to the determined threshold p-value (0.05). Correlation coefficient values with a p-value that is less than 0.05 were considered statistically significant.

Lagged Pearson's correlation analyses were used to examine the relationships between SST anomalies, geostrophic current speed anomalies, and climate indices, specifically, the ENSO and SAM across various regions of the Agulhas Current system. The regions encompassed in this study consist of the Northern and Southern Agulhas Current regions, the Agulhas Retroflection, and the Agulhas Return Current.

Since the intensification of the Agulhas Current is regarded as one of the causes of warming in the Agulhas Current, SST anomalies were the dependent variable for the SST and geostrophic current speed lag correlation analysis. This enabled the geostrophic current speed anomalies to lead the variations in SST.

However, SST and geostrophic current speed anomalies were both the dependent variables for the lagged correlation involving the climate indices. All the dependent anomalies underwent temporal shifting within a range of 0 to 49 months. This enabled the climate indices (Oceanic Niño Index and SAM Index), to serve as leading indicators for the observed variations in SST and surface geostrophic current speed.

Following this, Pearson correlation analyses were conducted to examine the relationship between the time series of the prominent climate modes and the time series of the dependent parameters, which were shifted in terms of lag.

The decision to choose a lag interval of up to 49 months was based on existing research and relevant statistical approaches used to ensure reliable results. According to Hogg et al. (2014), as the number of lags increases, the degrees of freedom decrease, affecting the statistical power and significance of the results. With fewer lags, the sample size remains robust, improving the reliability of the correlation coefficients obtained. Therefore, it is important to have a balanced number of lags for your analysis.

Trott et al. (2021) has previously examined the time-dependent relationship between sea surface temperature (SST) in the Agulhas Current system and the impacts of ENSO. According to Trott et al. (2021), the effects of ENSO events on temperature in the Agulhas Current are noticeable 20 to 30 months after the peak of an ENSO event.

The aforementioned precedent played a crucial role in establishing the specific time intervals utilised in the research, thereby ensuring consistency with previously observed temporal patterns.

Table 3.1 The meaning of the correlation coefficient values as reported by Hogg et al. (2014)

Correlation coefficient interval	**Relationship**	**Direction**
1 (-1)	Perfect positive (negative) correlation	A positive correlation coefficient means as one variable increases (decreases), the other also increases (decreases). A negative correlation coefficient means as one variable increases, the other decreases.
1 > r ≤ 0.8 (-1 < r ≤ -0.8)	Strong positive (negative) Correlation	
0.8 > r ≤ 0.5 (-0.8 < r ≤ -0.5)	Moderate positive (negative) Correlation	
0.5 > r ≤ 0.3 (-0.5 < r ≤ -0.3)	Weak positive (negative) Correlation	
0.3 > r < 0 (-0.3 < r < 0)	Negligible positive (negative) Correlation	
0	No Correlation	

4. CHAPTER 4: RESULTS

4.1 Sea Surface Temperature variation and warming trends

A detailed description of the SST variation, SST anomalies and warming trends in the Agulhas Current system in temporal and spatial terms are provided in this section. The results presented in this section were obtained through the SST data analysis done on the NOAA OISST dataset covering the 1982 to 2019 period.

4.1.1 Annual Cycle of SST

To facilitate the interpretation of both regional and local features of the Agulhas Current system, a relatively larger domain of the Southern Africa region has been inspected. The monthly SST in the Agulhas Current system varied spatially from 1982 to 2019 (Figure 4.1). A general north-south negative SST gradient on the east coast of South Africa was observed, while on the west coast, the inshore edge was cooler than the offshore regions (Figure 4.1). There was a variation in mean SST among the 4 domains of the Agulhas Current (Figure 4.1).

Generally, the Northern Agulhas Current was the warmest domain with a maximum SST of 27 ^{o}C (Figure 4.1), followed by the Southern Agulhas Current as the second warmest domain with a slightly lower maximum SST value of 24 ^{o}C (Figure 4.1). The Agulhas Retroflection and the Agulhas Return Current shared similar mean SST values which were lower than the other two domains. The maximum monthly SST for the Agulhas Retroflection and the Agulhas Return Current was approximately 21 ^{o}C and 19 ^{o}C respectively (Figure 4.1). Figure 4.1 also highlighted the monthly patterns of mean SST that were observed within and among the domains in the Agulhas Current system. Despite the different maximum and minimum monthly SST values that were observed between the domains, the patterns of SST changes were similar in all the domains during all months (Figure 4.1). February was the warmest month in all the domains with SST values of greater than 25 ^{o}C found on the Northern Agulhas Current. August and September were the coolest months, SST was less than 21 ^{o}C in all the domains during these two months (Figure 4.1).

Figure 4.2 is consistent with Figure 4.1 in highlighting the domains which had the lowest or the highest SST, as well as months which had higher or lower SST values. The lowest monthly mean SST value of approximately 15 ^{o}C was found in September in the Agulhas Return Current (Figure 4.2).

Distinct seasonal patterns of mean SST were also observed in each domain and between domains (Figure 4.1 and Figure 4.2). Austral summer which included December to February

(DJF) was the warmest season in all the domains with SST reaching its peak in February as depicted in Figure 4.1 and Figure 4.2.

In austral autumn (March to May: MAM), there was cooling which intensified towards the winter season (June to August: JJA) in all domains. In the Northern Agulhas Current, SST decreasing from around 25.3 ^{o}C in March to around 22.3 ^{o}C in early winter (June) was observed, a decrease of 3 ^{o}C (Figure 4.2). In the Southern Agulhas Current, a decrease of 2.9 ^{o}C was observed, while in the Agulhas Retroflection and the Agulhas Return Current SST decreased by 3 ^{o}C and 3.5 ^{o}C, respectively.

Generally, winter (JJA) was the coolest season for all the domains and the lowest SST values for the Northern Agulhas Current (~21 ^{o}C), Southern Agulhas Current (~19 ^{o}C), Agulhas Retroflection (~17.3 ^{o}C), and the Agulhas Return Current (~16.6 ^{o}C) were observed in August (Figure 4.2 and Figure 4.1). In austral spring (SON) the monthly mean SST increased in all the domains (Figure 4.2). The SST in the Northern Agulhas Current increased by around 1 ^{o}C from early spring to late spring (Figure 4.2). Based on Figure 4.2, spring monthly SST increased by 1.4 ^{o}C in the Southern Agulhas Current, while in the Agulhas Retroflection and the Agulhas Return Current SST increased by 1.75 ^{o}C and 1.67 ^{o}C respectively.

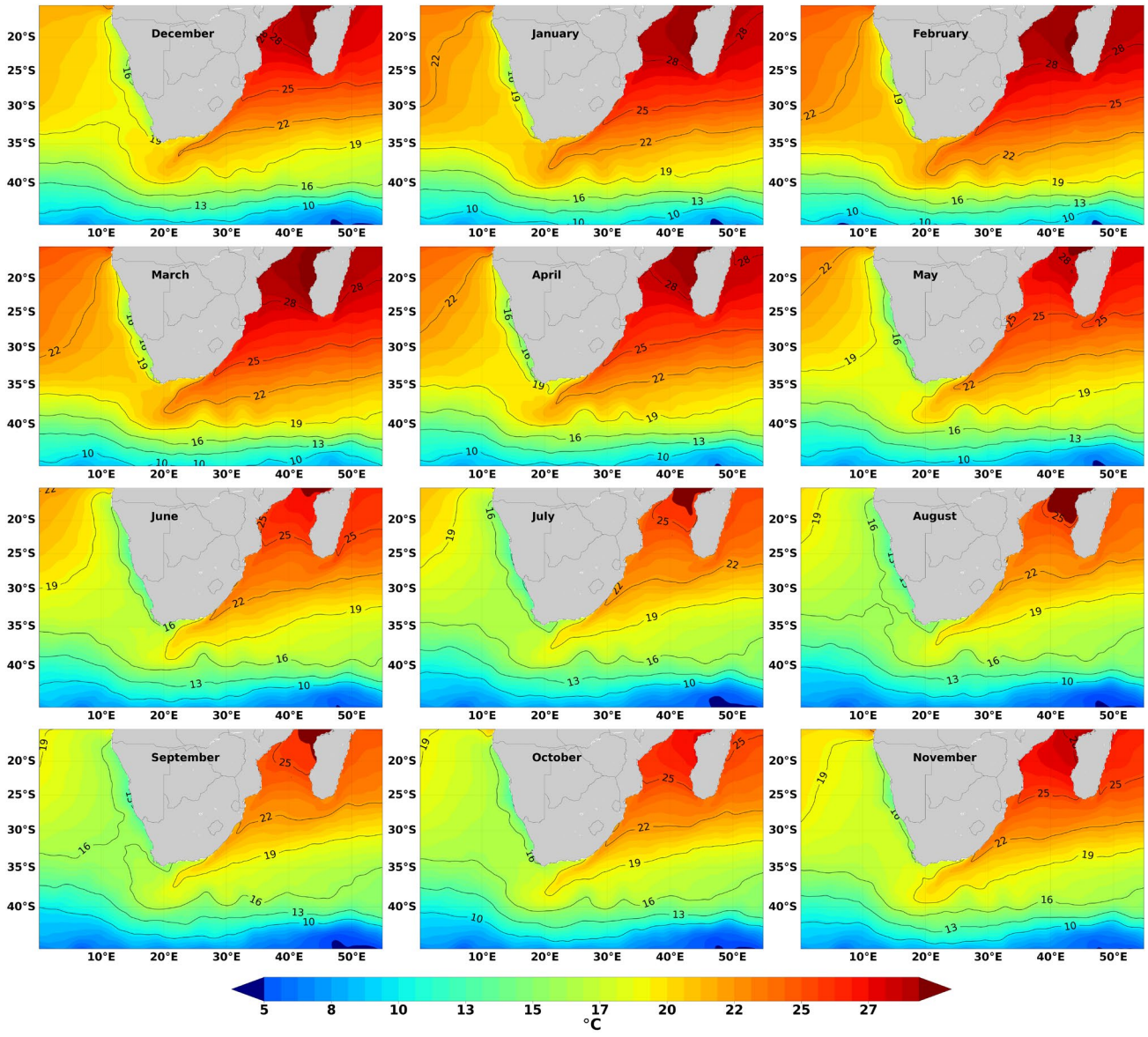

Figure 4.1: Spatial monthly SST climatology around Southern Africa in degrees Celsius derived from the NOAA OISST dataset for the 1982 to 2019 period. The contour lines are showing isotherms of 10, 13,16, 19, 22,25 and 28 ºC

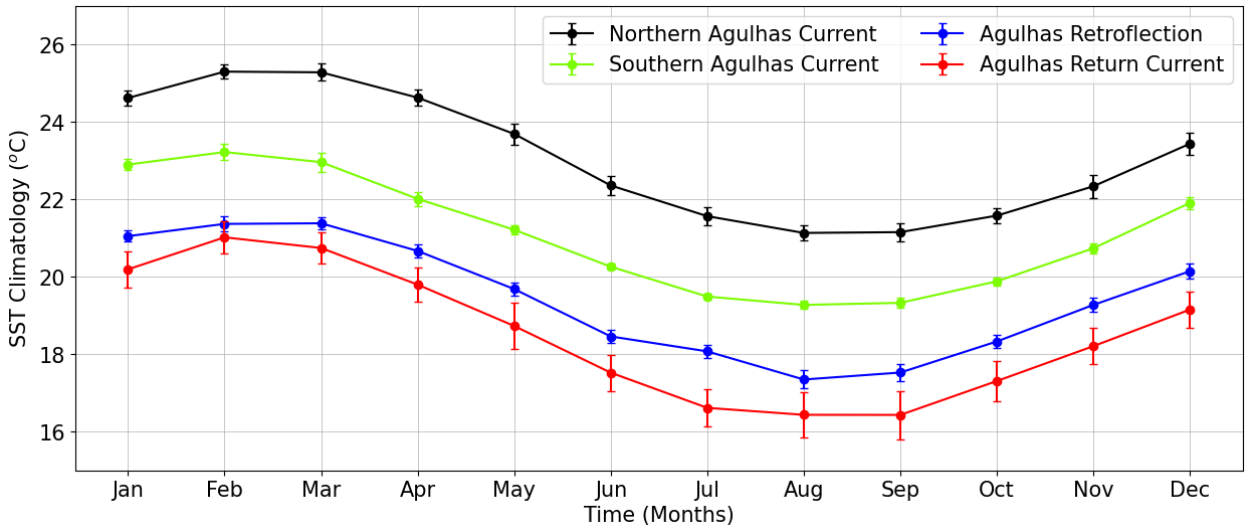

Figure 4.2: Monthly SST climatology from the 4 different domains (Northern Agulhas Current, Southern Agulhas Current, Agulhas Retroflection, and the Agulhas Return Current) of the Agulhas Current (see *Figure 3.1*). The timeseries data used to derive the monthly climatology is from the NOAA OISST dataset for the 1982 to 2019 period. The solid lines with error bars represent the respective sections in the Agulhas Current system.

4.1.2 Time Series Analysis

Long-term monthly SST Timeseries

The monthly SST timeseries and long-term linear trends for the domains selected for the focused analysis of the warming trends in the Agulhas Current are shown in Figure 4.3. Figure 4.3 depicts the trends using the line of best fit (dashed line) and the slope of the line of best fit, with the p-value indicating the significance of the trends. The monthly SST values depicted in Figure 4.3 are generally consistent with the SST climatology patterns seen in Figure 4.1 and Figure 4.2. All long-term SST trends were relatively small and positive. Except for the trends reported in the Northern Agulhas Current (Figure 4.3a), the long-term trends observed in other domains were statistically significant ($p<0.05$), showing that the regions have warmed from 1982 to 2019 (Figure 4.3b, c, and d).

In agreement with the preceding sections (Figure 4.1 and Figure 4.2), Figure 4.3a reveals that the Northern Agulhas Current was the warmest domain and had the smallest statistically insignificant increase in SST (0.0029 °C/decade; $p > 0.05$) from 1982 to 2019. Clear interannual SST variation was evident in the Northern Agulhas Current (**Figure 4.3**). with the maximum (26.59 °C) SST in February 2003 and the minimum (19.95 °C) in September 1994 (Figure 4.3a).

The Southern Agulhas Current (Figure 4.3b) was the second warmest domain, with minimum SST values of 17.5 °C found in August and a maximum of 25.15 °C in January. Contrary to the Northern Agulhas Current, the Southern Agulhas Current had a statistically significant and stronger increase in SST (0.0125 °C/decade; $p < 0.05$) from 1982 to 2019 (Figure 4.3b).

Similarly, the Agulhas Retroflection (0.0098 °C/decade; $p<0.05$) and Return Current (0.0060 °C/decade; $p<0.05$) demonstrated statistically significant long-term increases in SST from 1982 to 2019 (Figure 4.3c and d). The increase in SST from 1982 to 2019 was greater in the Southern Agulhas Current (Figure 4.3b) compared to the Northern Agulhas Current (Figure 4.3a), Agulhas Retroflection (Figure 4.3c), and Agulhas Return Current (Figure 4.3d) domains.

Maximum SST values of around 23.63 °C in March 2012 and a minimum SST value of around 14.75 °C in September 2008 were found in the Agulhas Retroflection (Figure 4.3c). Additionally, SST values in the Agulhas Return Current (Figure 4.3d) were close to the values observed in the Agulhas Retroflection with a maximum of 23.91 °C in February 2014, and a minimum of 13.24 °C in August 1990.

Long-term seasonal SST Timeseries

The SST in all domains showed distinct seasonal variations, with the warmest temperatures mostly occurring in the summer and the coolest in the winter, except in the Northern Agulhas Current, where the coolest temperatures were in the spring (Figure 4.4).

Notably, the Northern Agulhas Current was generally the warmest domain, exhibiting maximum SST (25.34 °C) in summer (December 1999) and minimum SST (20.7 °C) in spring, as seen in Figure 4.4a. Seasonal warming trends of the Northern Agulhas Current were statistically insignificant ($p > 0.05$).

The Southern Agulhas Current (Figure 4.4b) was the second warmest domain, with minimum SST values of 18.47 °C found in winter and a maximum of 23.83 °C in summer. In contrast to the Northern Agulhas Current, the Southern Agulhas Current had a statistically significant and stronger increase in SST (0.0125 °C/decade; $p<0.05$) from 1982 to 2019 (Figure 4.4b).

The Agulhas Retroflection (0.0098 °C/decade; $p<0.05$) and Return Current (0.0060 °C/decade; $p<0.05$) also demonstrated statistically significant long-term increases in SST from 1982 to 2019 (Figure 4.3c and d). The increase in SST from 1982 to 2019 was greater in the Southern Agulhas Current (Figure 4.3b) compared to the Northern Agulhas Current (Figure 4.3a), Agulhas Retroflection (Figure 4.3c), and Agulhas Return Current (Figure 4.3d) domains.

In the Agulhas Retroflection seasonal SST values of around 22.15 ºC in autumn (March) and a minimum SST of around 16.57 ºC in spring were observed (Figure 4.3c). Additionally, SST values in the Agulhas Return Current (Figure 4.3d) were similar to the values observed in the Agulhas Retroflection, with a maximum of 22.13 ºC in summer, while the minimum was 14.24 ºC in winter.

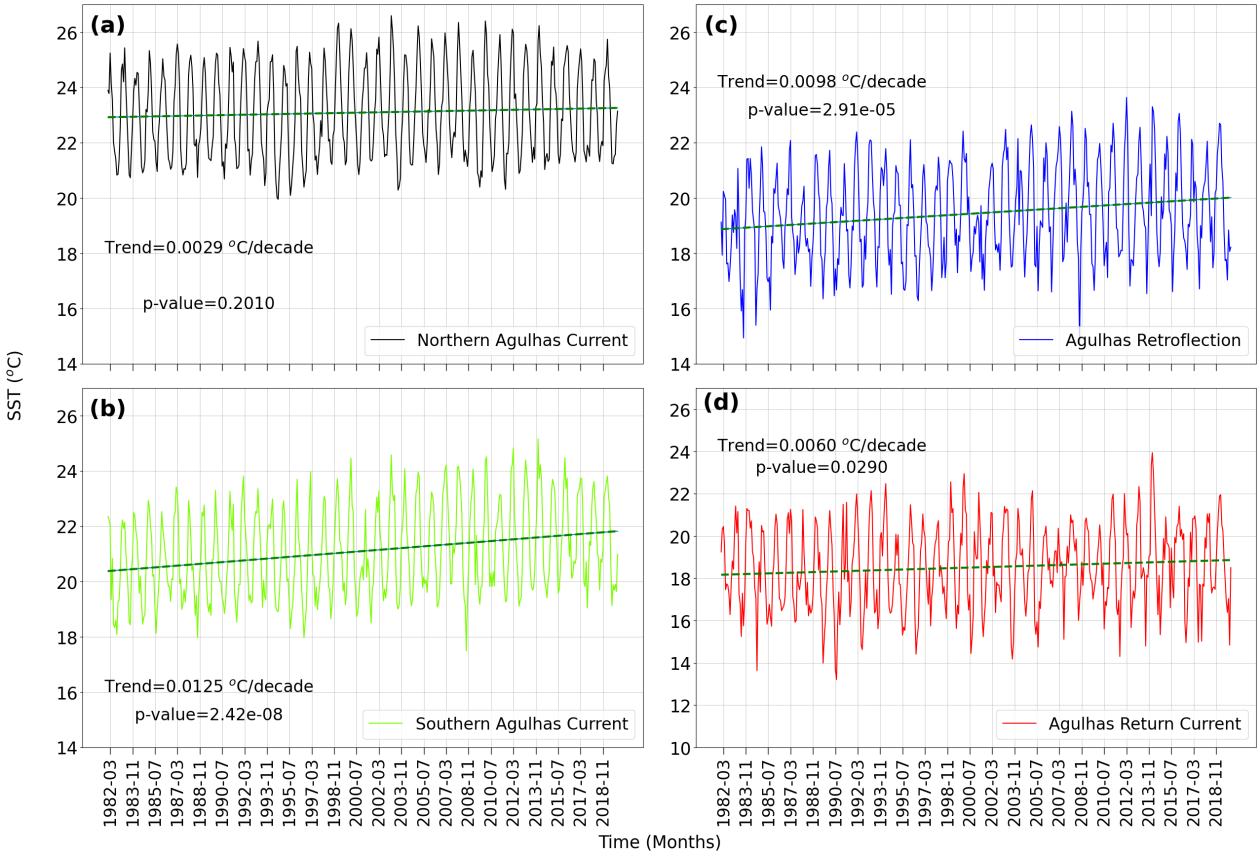

Figure 4.3: Long-term monthly SST timeseries from the 4 domains used to divide the Agulhas Current system. (**a**) Northern Agulhas Current, (**b**) Southern Agulhas Current, (**c**) Agulhas Retroflection area, and (**d**) Agulhas Return Current. The solid lines represent the SST timeseries for that specific domain, and the dashed line shows the linear fitted trend. The trends shown are significant at the 95% level only if the p-value associated with them is less than 0.05.

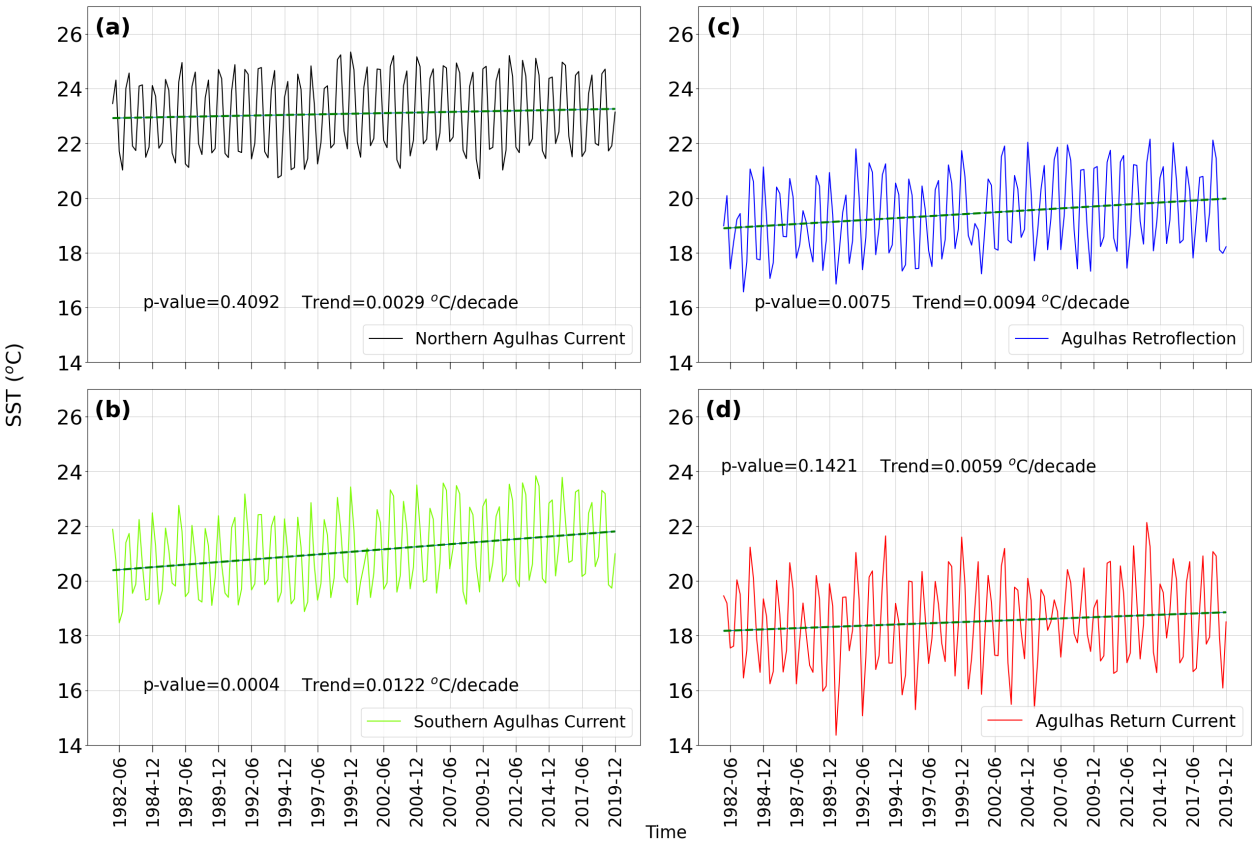

Figure 4.4 Long-term seasonal SST timeseries from the 4 domains used to divide the Agulhas Current system. (**a**) Northern Agulhas Current, (**b**) Southern Agulhas Current, (**c**) Agulhas Retroflection area, and (**d**) Agulhas Return Current. The solid lines represent the SST timeseries for that specific domain, and the dashed line shows the linear fitted trend. The trends shown are significant at the 95% level only if the p-value associated with them is less than 0.05.

.

4.1.3 Spatial SST Trends

Annual Spatial SST Trends

Figure 4.5 shows the Southern Africa region's decadal spatial SST warming trends from 1982 to 2019. The decadal spatial SST warming trends per season are shown in Figure 4.6. The spatial patterns and rate of warming over the Agulhas Current shown in Figure 4.5 will be explained and linked to the long-term timeseries trends found in Figure 4.3. Overall, trends exhibited a maximum spatial SST warming of approximately 0.57 ^{o}C/decade in most parts of the Agulhas Current system and some of these trends were statistically significant ($p<0.05$; Figure 4.5). Some small coastal regions mostly along the South Coast of South Africa and the southwestern coastal areas of Southern Africa depicted cooling trends of up to -0.36 ^{o}C/decade (Figure 4.5a). However, the cooling trends were not statistically significant ($p>0.05$; Figure 4.5b).

The Northern Agulhas Current domain has warmed by around 0.12 ^{o}C/decade to 0.3 ^{o}C/decade (Figure 4.5). The inshore trends in the Northern Agulhas Current were statistically significant however most trends in the offshore region were statistically insignificant ($p>0.05$) (Figure 4.5b). The Southern Agulhas Current's warming trends were stronger than the linear trends observed in the Northern Agulhas Current and ranged between 0.12 ^{o}C/decade to 0.4 ^{o}C/decade (Figure 4.5). However, some regions (around 36 ^{o}S and 22 ^{o}E) had warmed at an intense rate of approximately 0.57 ^{o}C/decade and this intense warming was statistically significant ($p<0.05$) (Figure 4.5b). The Agulhas Retroflection domain and the Agulhas Return Current shared similar warming trends with a general minimum of approximately 0.2 ^{o}C/decade and a maximum of approximately 0.57 ^{o}C/decade (Figure 4.5). The linear trends were statistically significant mostly around the Agulhas Retroflection (Figure 4.5b), and the area covered by statistically significant trends within the Agulhas Return Current was not big (Figure 4.5b).

Figure 4.3 and Figure 4.5 depicted consistent trends in terms of which domains warmed the most from 1982 to 2019. For example, both Figure 4.3 and Figure 4.5 agree that the Northern Agulhas Current has warmed less than the other three domains, and the Agulhas Retroflection and Agulhas Return Current have warmed more. The differences in the rate or magnitude of the trends shown in Figure 4.3 and Figure 4.5 are probably due to the subsetting used to get the timeseries in Figure 4.3.

Seasonal Spatial SST Trends

Figure 4.6, shows seasonal warming trends around Southern Africa for the period 1982 to 2019. The Agulhas Current system generally showed significant ($p<0.05$) warming trends of differing magnitude with maximum warming trends greater than 0.5 °C/decade observed in all seasons (Figure 4.6). Very small patches of significant cooling especially in the summer and autumn seasons were observed along South Africa's south coast (Figure 4.6a and, b).

According to Figure 4.6, the Northern Agulhas Current was the least warming domain in all the seasons. During all the seasons, warming trends in the region ranged between 0.1 °C/decade to 0.47 °C/decade (Figure 4.6). Figure 4.6 also shows that statistically significant warming trends in the Northern Agulhas Current were mostly found over the Agulhas Current path (Figure 4.6). Autumn was the season with the strongest warming trends, reaching a maximum warming rate of 0.47 °C/decade (Figure 4.6b), while the maximum warming rate for other seasons (summer, winter and spring) was around 0.36 °C/decade (Figure 4.6a,c and d).

The Southern Agulhas Current's warming trends were stronger than the trends observed in the Northern Agulhas Current in all the seasons (Figure 4.6). Overall, the seasonal warming trends ranged between 0.06 °C/decade and 0.76 °C/decade. However, based on Figure 4.6, the maximum warming trends in the region varied seasonally in terms of spatial coverage and magnitude (warming rate). The strongest significant warming season in the Southern Agulhas Current is autumn with warming rates of around 0.76 °C/decade, while summer, winter and spring ranged between 0.06 °C/decade and ~0.5 °C/decade (Figure 4.6a, b and, c).

Generally, the Agulhas Retroflection had stronger warming trends than the Northern Agulhas Current region, but weaker trends compared to the Southern Agulhas Current in all seasons (Figure 4.6). The overall trends in the Agulhas Retroflection ranged between 0.1 °C/decade and 0.5 °C/decade (Figure 4.6). Autumn was the strongest warming season with maximum warming rates of around 0.5 °C/decade (Figure 4.6b), followed by winter(Figure 4.6c) at around 0.4 °C/decade while summer and spring shared similar warming rates of ~0.34 °C/decade (Figure 4.6a and, d).

Based on Figure 4.6, the Agulhas Return Current only experienced warming during the autumn, winter, and spring seasons. Overall, during autumn and winter, the Agulhas Return Current is the second strongest warming region after the Southern Agulhas Current with maximum significant warming rates of around 0.71 °C/decade in winter (Figure 4.6c) and 0.63 °C/decade in autumn (Figure 4.6b). Although warming trends were observed during spring (0.5 °C/decade, $p>0.05$) their spatial coverage is very small (Figure 4.6d).

Summary

The annual SST trends in the Agulhas Current system represent a general warming scenario, with maximum warming rates of up to 0.57 ºC per decade, particularly around 36 ºS and 22 ºE. Notably, the Southern Agulhas Current showed stronger annual warming trends, ranging from 0.12 to 0.5 ºC per decade and even peaking at a statistically significant 0.57 ºC per decade. In contrast, the Northern Agulhas Current showed weaker annual warming, with rates of 0.12 to 0.3 ºC per decade. For Agulhas Retroflection and Agulhas Return Current, annual warming trends were consistent with general lows of about 0.2 °C/decade and highs of about 0.5 °C/decade, but the Agulhas Return Current showed stronger statistically significant annual warming especially around the Retroflection area, with peaks of up to 0.57 °C/decade.

When it comes to seasonal variations, all areas of the Agulhas Current System generally showed significant warming trends, with rates exceeding 0.5 ºC per decade in certain seasons. The southern Agulhas Current was found to be the region with the highest warming, especially in autumn, with a peak rate of 0.76 ºC per decade. Meanwhile, the Agulhas reverse current showed strong warming in autumn and winter, with maximum rates of about 0.71 ºC per decade. The Northern Agulhas Current has consistently been the lowest warming area across all seasons, with rates as low as 0.1 ºC per decade. Overall, the seasonal data confirm the annual trends and emphasize that the southern Agulhas Current and the Agulhas Return Current are the fastest-warming regions both annually and seasonally.

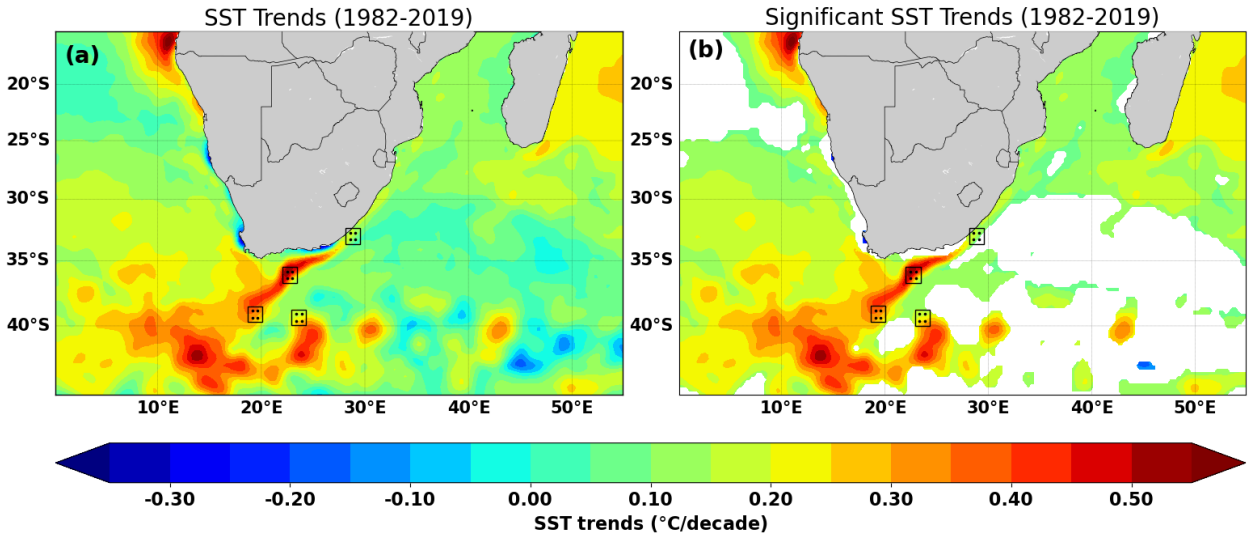

Figure 4.5: Spatial SST trends around Southern Africa derived from the NOAA OISST dataset for the 1982 to 2019 period. The red colour shows a warming trend per decade, and the blue signifies a cooling trend. The SST trends, including areas that are not significant are shown in (**a**), while (**b**) only highlights areas where the warming is significant with a 95% confidence level.

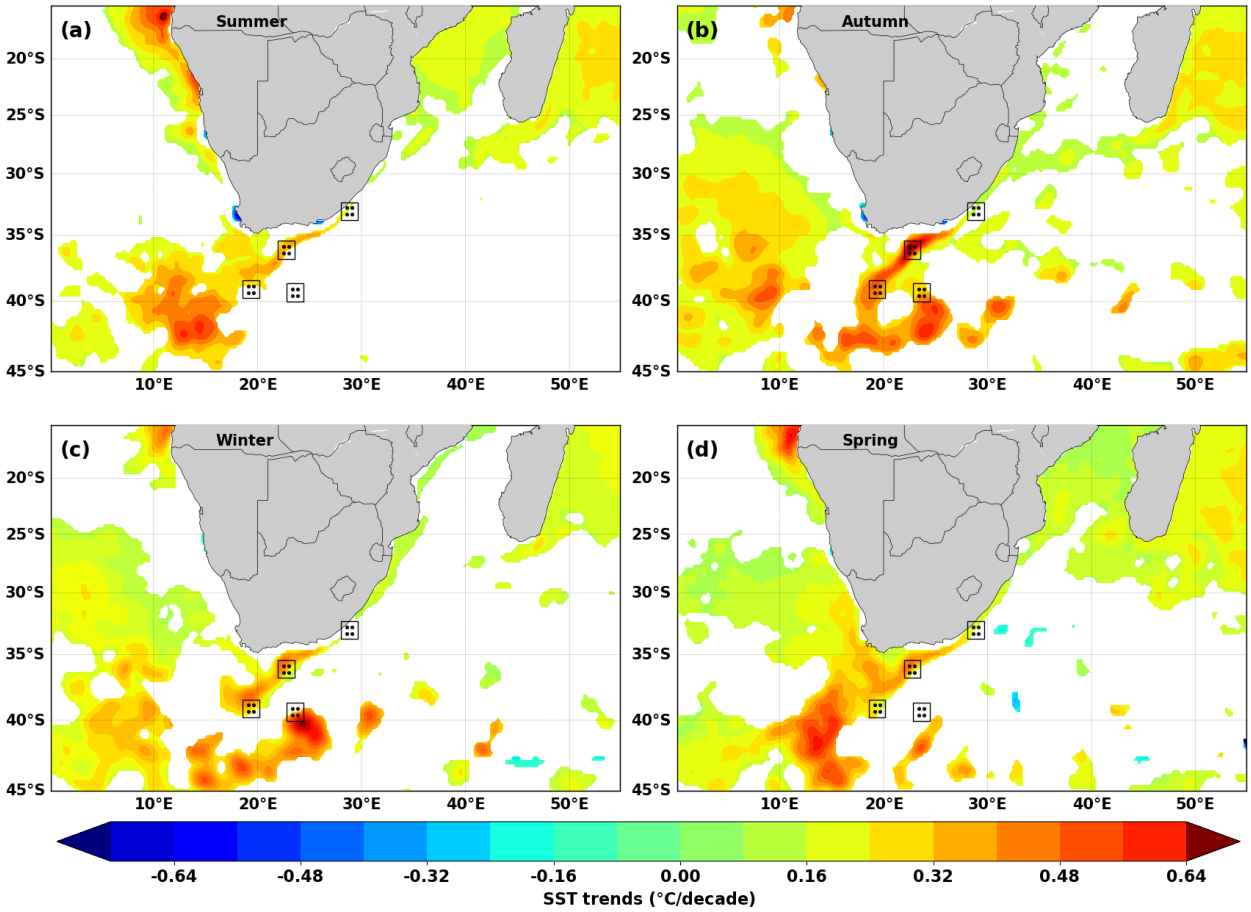

Figure 4.6 Spatial SST trends around Southern Africa per season derived from the NOAA OISST dataset for the 1982 to 2019 period. The red colour shows a warming trend per decade, and the blue signifies a cooling trend. The SST trends, including areas that are not significant are shown in (**a**), while (**b**) only highlights areas where the warming is significant with a 95% confidence level.

4.1.4 SST Anomalies

The monthly time series of SST anomalies for the period 1982–2019 were calculated for four different areas in the Agulhas Current region (Figure 4.7). Positive anomalies indicate warmer-than-average conditions, while negative anomalies indicate cooler-than-average conditions. The anomalies are presented using a bar graph, with blue bars indicating cooler-than-average SSTs in a particular month, while red bars depict warmer-than-average SSTs. A variation in the intensity of cooler-than-average and warmer-than-average SSTs between the four domains was observed (Figure 4.7).

In the northern Agulhas Current (Figure 4.7a), SST anomalies ranged from -3.33 °C to 2.7 °C. Clusters of extreme SST anomalies were observed during specific periods, such as 1994–1995 and 1997–1998. The most extreme negative anomaly occurred in May 1985 with a value of -3.33 °C, while the most extreme positive anomaly was observed in May 1991 with a value of 2.7 °C. For the southern Agulhas Current (Figure 4.7b), the SST anomalies were between -3.35 °C and 2.66 °C. Clusters of extreme negative anomalies can be seen in 1982, and in January 2001 a maximum extreme negative value of -3.35 °C was recorded. On the other hand, extreme positive anomalies show some clustering in the period 2007-2009, with the highest value of 2.66 °C recorded in September 2007.

In the region of Agulhas Retroflection (Figure 4.7c), SST anomalies ranging from -2.97 °C to 2.37 °C were observed. Notably, a cluster of extreme negative anomalies occurred in 1982, and another cluster occurred in the early 2000s. The most extreme negative anomaly was observed in February 1982 with a value of -2.95 °C, while the most extreme positive anomaly was in January 2016 at 2.37 °C (Figure 4.7c).

Finally, extreme SST anomalies between - 2.93 °C and 2.76 °C were observed for the Agulhas Return Current (Figure 4.7d). There is a notable cluster of extremely positive anomalies around 2014. The most extreme negative anomaly was detected in November 2019 and recorded a value of -2.93 °C, while the highest extreme positive anomaly was in February 2014 at 2.76 °C (Figure 4.7d).

The intra-annual fluctuation in all domains is another noticeable aspect of Figure 4.7. The annual cycles exhibited monthly fluctuations; certain anomalies changed rapidly and dramatically from month to month. Figure 4.7 also depicts the variation between the first two decades (1982-2000) and the final two decades (2000-2019). Cooler-than-average SST anomalies predominated from 1982 to 2000, but warmer-than-average anomalies were primarily seen in the subsequent two decades (Figure 4.7).

Summary

The monthly time series of SST anomalies from 1982 to 2019 in four areas of the Agulhas Current system exhibits both spatial and temporal variability (Figure 4.7). Positive and negative anomalies indicate warmer and cooler conditions, respectively. Because monthly SST anomalies fluctuated, anomalies above −2 °C or 2 °C were considered extreme cooling or warming events. Extreme SST anomalies with maximums of -3.33°C to 2.7°C and -3.35°C to 2.66°C occurred in the Northern and Southern Agulhas Currents respectively, with notable clusters of extreme anomalies in specific periods such as 1994-1995, 1997-1998 and 2007-2009. Compared to the Agulhas regions highlighted above, the Agulhas Retroflection showed relatively weaker extreme cooling and warming events of about -2.97°C to 2.37°C. This shows some consistency with the spatial warming trends highlighted in Figure 4.5 which showed the Southern Agulhas Current as one of the strongest warming regions. The Agulhas Return Current showed similar extreme cooling and warming events with the largest negative anomaly of -2.93°C and a maximum positive anomaly of 2.76°C. In addition, temporal clusters of extreme SST anomalies have been observed, for example in 1982 and 2014 for the Agulhas Retroflection. Intra-annual fluctuations were noticeable, with rapid month-to-month changes in SST anomalies. There were also visible interannual variations and decadal variations in SST anomalies, with cooler conditions prevailing from 1982 to 2000 and warmer conditions prevailing from 2000 to 2019.

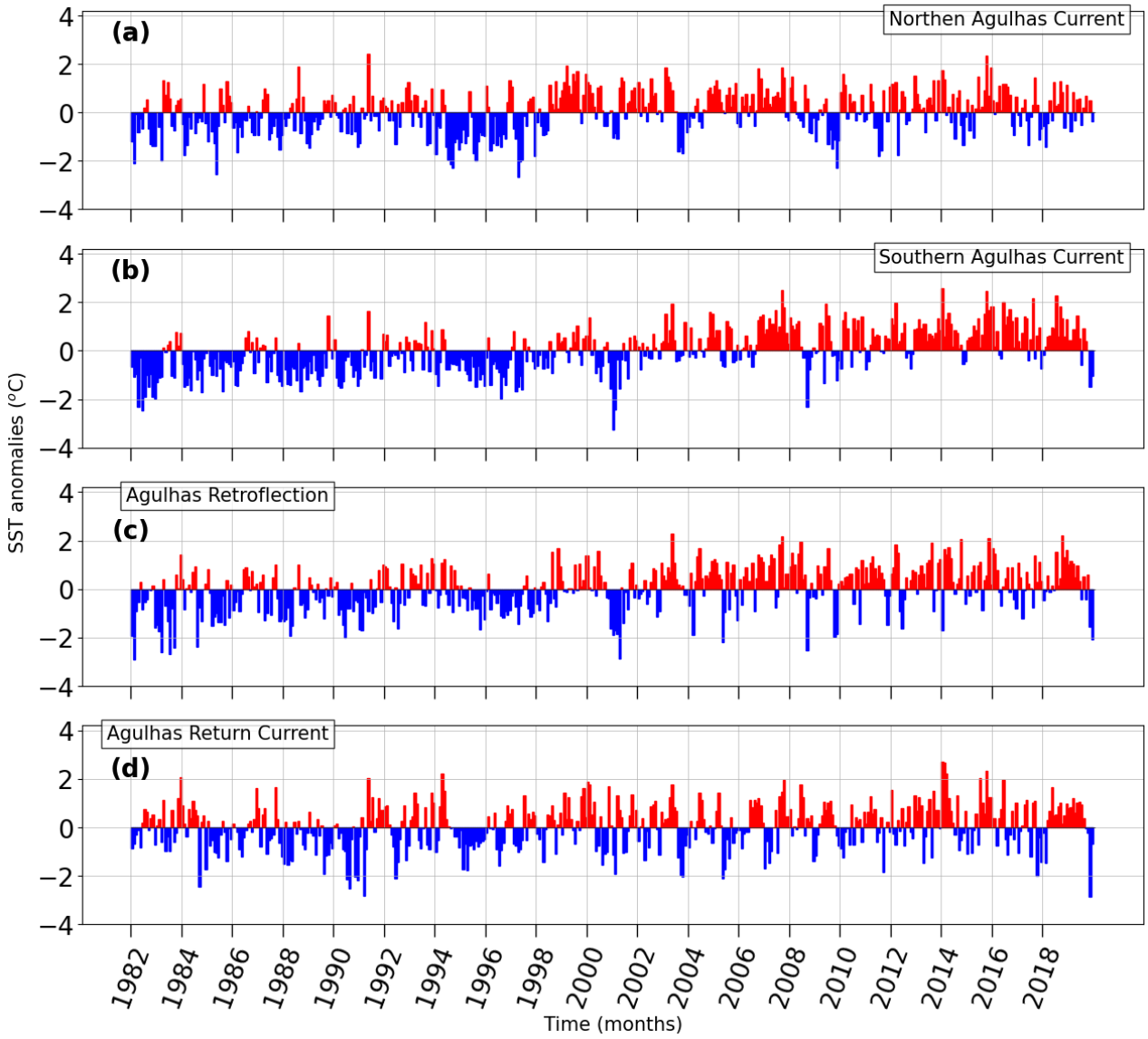

Figure 4.7: Monthly normalised SST anomalies from the 4 domains of the Agulhas Current system derived from the NOAA OISST dataset for the 1982 to 2019 period. (**a**) Northern Agulhas Current, (**b**) Southern Agulhas Current, (**c**) Agulhas Retroflection and (**d**) Agulhas Return Current. The red bars signify warming, while the blue bars show cooling.

4.2 Geostrophic Currents

A detailed description of the geostrophic current speed and its components (zonal and meridional) variations, and derived anomalies, as well as their strengthening or weakening trends from 1993 to 2019 in the Agulhas Current system in their respective temporal and spatial scales, are provided in this section. The correlation between SST and geostrophic current speed from 1993 to 2019 is also described sufficiently in this section.

4.2.1 Seasonal Cycle

The spatial presentation of the monthly climatology for the geostrophic current speed around South Africa from 1993 to 2019 is shown in Figure 4.8. To comprehensively understand the surface circulation patterns within the Agulhas Current system, an investigation was conducted that focused not only on the overall geostrophic current speed but also on its zonal and meridional components. By analysing these components individually, deeper insights were gained into the changes in the direction of the geostrophic currents across various regions of the Agulhas Current system. The monthly climatology for the geostrophic current speed, meridional component, and zonal component for all domains in the Agulhas Current is presented in Figure 4.9. It is crucial to delineate that a positive or negative zonal component signifies a latitudinal flow in the east-west direction, while a positive or negative meridional component denotes a longitudinal flow in the north-south direction.

While Figure 4.8 shows a current speed of up to 1.4 m s^{-1}, the monthly climatology for the geostrophic current speed shown in Figure 4.9a for all the domains ranged between 0.39 m s^{-1} and 0.89 m s^{-1}, with little variation between the domains. Some of the maximum geostrophic current speeds shown in Figure 4.8 are not visible in Figure 4.9a, probably due to spatial subsetting and averaging done to generate the climatology in Figure 4.9a. An immediate prominent feature depicted was the path of the Agulhas Current (Figure 4.8). An increasing offshore gradient of surface current speed from the coast to the core of the Agulhas Current was observed, followed by a gradual decline further offshore (Figure 4.8).

Generally, the surface geostrophic current speeds of the southwestward flowing Northern Agulhas Current were between 0.6 m s^{-1} and 1 m s^{-1} (Figure 4.8). According to Figure 4.9a, the Northern Agulhas Current has a relatively constant annual geostrophic current speed ranging between 0.69 m s^{-1} and 0.86 m s^{-1}. The Northern Agulhas Current maintains a south-westerly flow with negative meridional and zonal components, both varying between -0.48 m s^{-1} and -0.60 m s^{-1} (Figure 4.9b and c). These components exhibit minor seasonal variations, reaching their lower thresholds in winter (July) and peaking in summer (January and February) and fall

seasons (March and April). The Southern Agulhas Current (Figure 4.9a) mirrors the Northern Agulhas Current in terms of average geostrophic current speed, within a narrower range of 0.68 m s^{-1} to 0.84 m s -1. Notably, the Southern Agulhas Current experiences an increase in speed as the current moves southwestward, reaching peak speeds of 1.4 m s^{-1} in certain locations (Figure 4.8). This current also flows in a south-westerly direction, with the negative meridional and zonal components between -0.45 m s^{-1} and -0.54 m s^{-1} and -0.46 m s^{-1} and -0.62 m s^{-1}, respectively (Figure 4.9b and c). Seasonal fluctuations are more pronounced in the meridional component, especially in February, June, and October.

Based on Figure 4.9a Agulhas Retroflection had a geostrophic current speed between 0.47 m s^{-1} and 0.65 m s^{-1}. Compared to the Northern and Southern Agulhas Currents, the Agulhas Retroflection exhibited more variable flow directions, manifested in both positive and negative values for the zonal (Figure 4.9c) and meridional components (Figure 4.9b). These components showed significant seasonal fluctuations and had different flow directions depending on the month. In the Agulhas Retroflection, the zonal component ranged from -0.31 m s^{-1} to -0.01 m s^{-1} (Figure 4.9c). This indicates that flow direction may be variable, with negative values indicating westward flow and positive values indicating eastward flow. In the Agulhas Retroflection region, these changes in the direction of the current might be changes associated with the presence of eddies. The meridional component ranged from -0.28 m s^{-1} to -0.13 m s^{-1}, with negative values indicating a southward flow direction (Figure 4.9b).

Finally, according to Figure 4.9a, the Agulhas Return Current had a geostrophic current speed ranging from 0.53 m s^{-1} to 0.71 m s^{-1}. This flow exhibited stronger flows near the Agulhas Retroflection and weakened as it extended eastward (Figure 4.8). The Agulhas Return current flowed mainly eastward, as evidenced by a positive zonal component (Figure 4.9c) varying between 0.28 m s^{-1} and 0.45 m s^{-1}. The meridional component (Figure 4.9b) varied with both positive and negative values ranging from -0.24 m s^{-1} to 0.17 m s^{-1} and had a seasonal dependence that varied depending on the month, indicating the possibility of both northward and southward flow depending on seasonal factors.

Summary

Generally, geostrophic current speeds are higher in the Northern and Southern Agulhas Currents, reaching speeds of up to 1 m s^{-1} and 1.4 m s^{-1}, respectively, than in the Agulhas Retroflection and Return Current, which had speeds of up to 0.65 m s^{-1} and 0.71 m s^{-1}, respectively. Notably, the Northern Agulhas Current exhibited a relatively constant with little variation in terms of seasonal geostrophic current speed flow and maintained a south-westerly

flow with negative zonal and meridional components. The Southern Agulhas Current had similar speeds but with greater seasonal fluctuations. Generally, the Southern Agulhas Current also flows in a south-westerly direction, with negative meridional and zonal components. Seasonal fluctuations are more pronounced in the meridional component, especially in February, June, and October. The Agulhas Retroflection was characterized by variable flow directions with both positive and negative values in zonal and meridional components, possibly influenced by the presence of eddies. Meanwhile, the Agulhas return current flowed mainly eastward, but had seasonally varying meridional components to both north and south. This study also highlights the absence of specific peak speeds in the monthly climatology (Figure 4.9) which are visible in Figure 4.8, which may be due to spatial subsetting and averaging done to generate the timeseries.

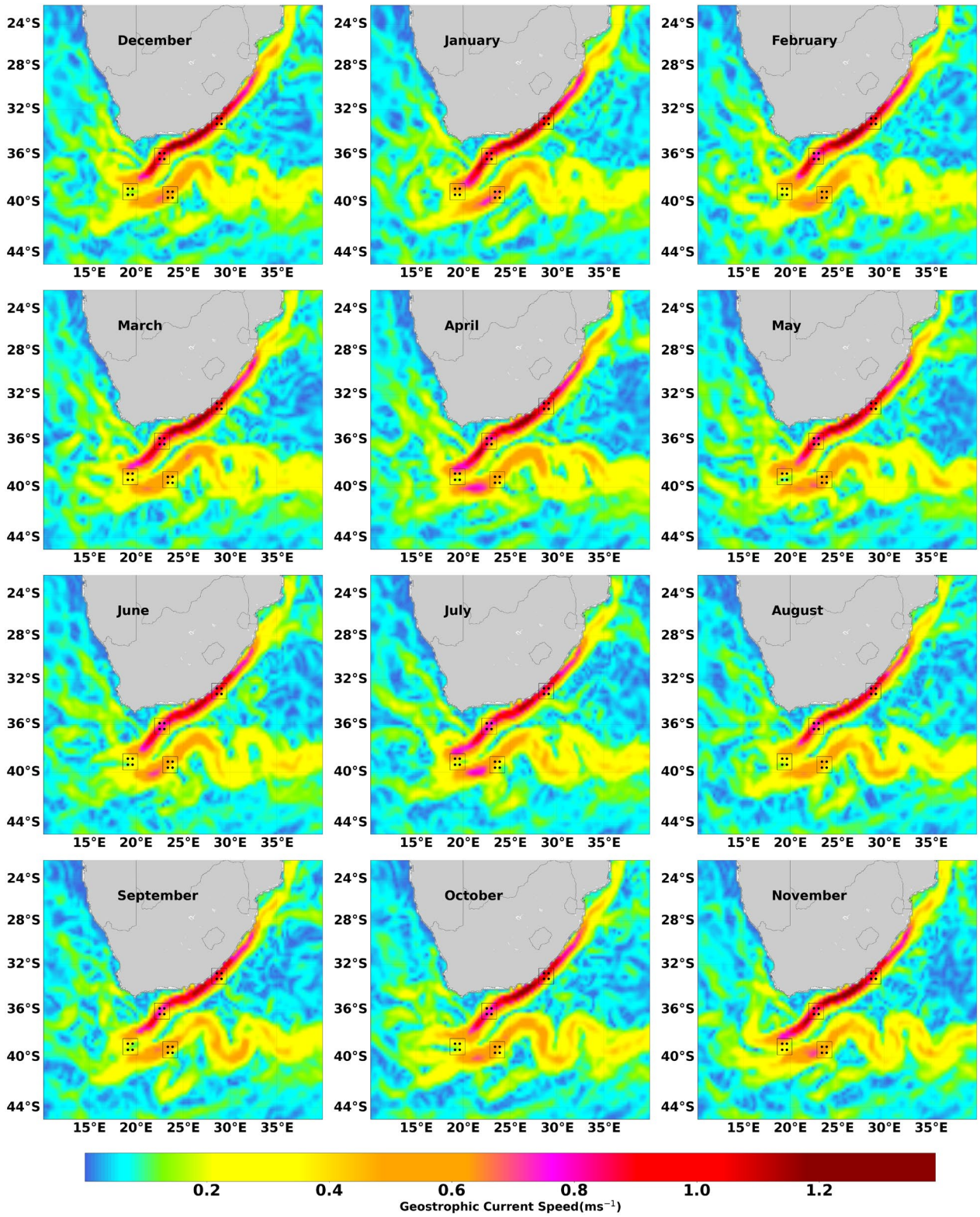

Figure 4.8: Geostrophic current speed climatology around the Southern Africa region for the 1993 - 2019 period. The colour shading represents the geostrophic current speed strength in m s^{-1}

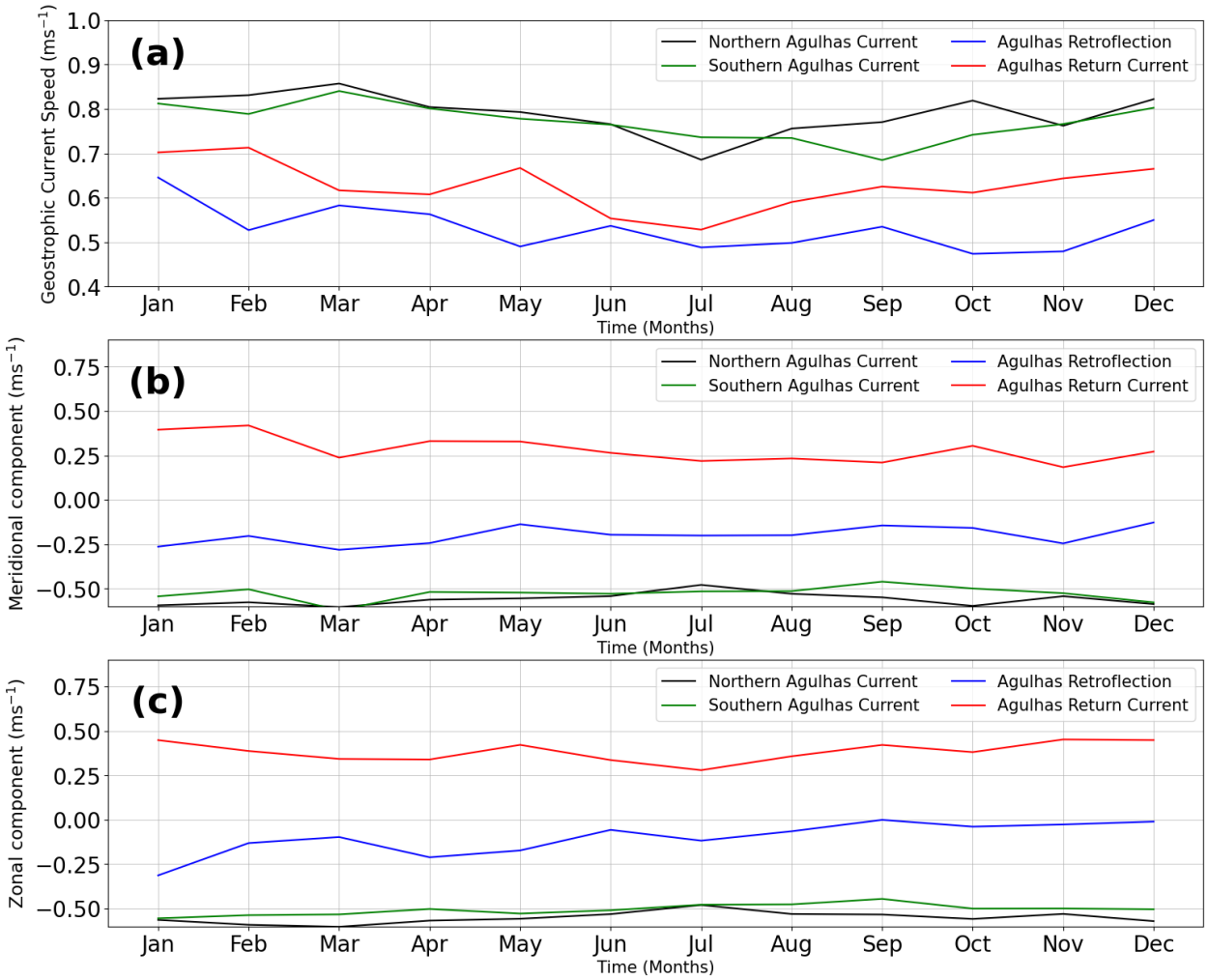

Figure 4.9: Monthly geostrophic current speed (**a**), meridional geostrophic component (**b**), and zonal geostrophic component (**c**) climatology from the 4 different domains (Northern Agulhas Current, Southern Agulhas Current, Agulhas Retroflection, Agulhas Return Current) of the Agulhas Current. The timeseries data used to derive the monthly climatology covers the 1993-2019 period. For the meridional geostrophic component, a negative value highlights a southward flow while a positive value represents a northward flow. For the zonal component, negative is a sign for a westward flow, while positive is for an eastward flow of the current

4.2.2 Geostrophic Current Time Series

The monthly timeseries of the resultant geostrophic current speed for all domains of the Agulhas Current system are shown in Figure 4.10. The monthly timeseries for the zonal and meridional component flows are also displayed in Figure 4.12. The solid lines show the monthly current speed, while the dashed line shows the decadal trend of the current speed over the 1993 to 2019 period.

Geostrophic current speeds between 0.16 m s^{-1} and 1.2 m s^{-1} were observed in the Northern Agulhas Current with a decreasing statistically significant current speed trend of about -0.0008m

s^{-1}/decade (p=0.0188) (Figure 4.10a). The flow of the zonal (Figure 4.12b) and meridional (Figure 4.12a) components ranged between -0.01 m s^{-1} and -89 m s^{-1}, indicating a southwestward flow in the Northern Agulhas Current. Furthermore, the linear trend for the meridional component (Figure 4.12a) was statistically significant and around 0.00058 m s^{-1}/decade (p=0.04) from 1993 to 2019, while the zonal component (Figure 4.12b) had a statistically significant linear trend of 0.00056 m s^{-1}/decade (p=0.011).

The geostrophic current speeds in the Southern Agulhas Current ranged between 0.2 m s^{-1} and 1.1 m s^{-1} (Figure 4.10b). Small geostrophic current speed trends of around -0.0006 m s^{-1}/decade were observed in the Southern Agulhas Current (Figure 4.10b) however they were statistically insignificant (p=0.1375). The zonal component in the Southern Agulhas Current mostly depicted a westward flow, with some eastward flow in certain months probable due to the meandering of the current in the region. The zonal component ranged between -0.83 m s^{-1} and 0.18 m s^{-1} (Figure 4.12d). Based on Figure 4.12d, a statistically insignificant (p=0.6718) trend for the zonal component was observed in the Southern Agulhas Current.

Variations in the current direction for the meridional component in the Southern Agulhas Current were observed (Figure 4.12c). Some months depicted a southerly flow (negative values) while others showed a northerly flow (positive values). The flow for the meridional component in the Southern Agulhas Current (Figure 4.12c) ranged between -0.88 m s^{-1} and 0.41 m s^{-1} with statistically significant long-term changes of 0.00097 m s^{-1}/decade (p=0.032).

The geostrophic current speed in the Agulhas Retroflection (Figure 4.10c) ranged between 0.14 m s^{-1} and 1.2 m s^{-1} with a statistically non-significant current speed trend of -0.0007 m s^{-1}/decade (p=0.133). Figure 4.12e shows the meridional component flow in the Agulhas Retroflection domain ranged between -1 m s^{-1} and 0.84 m s^{-1} with a statistically insignificant linear trend of 0.00133 m s^{-1}/decade (p=0.089) from 1993 to 2019. The mix of positive and negative meridional component speed was probable due to the presence of rings and eddy formation in the Agulhas Retroflection area. Similarly, the zonal component in the Agulhas Retroflection (Figure 4.12f) showed positive but statistically insignificant trends over the years (1993 to 2019), a trend of up to 0. 00148 m s^{-1}/decade (p=0.204). As illustrated in Figure 4.12f, the speed for the zonal component in the Agulhas Retroflection ranged between -1 m s^{-1} and 0.97 m s^{-1}.

The geostrophic current speed in the Agulhas Return Current showed a statistically non-significant trend of around -0.0011 m s^{-1}/decade (p=0.0057), with general geostrophic current speed values ranging between 0.12 m s^{-1} and 1.14 m s^{-1} (Figure 4.10d). Surface current flow ranging between -0.5 m s^{-1} and 1 m s^{-1} was observed for the zonal component in the Agulhas

Return Current (Figure 4.12h). According to Figure 4.12h, the zonal component had statistically significant trends around -0.000171 m s^{-1}/decade (p=0.016) from 1993 to 2019. A meridional surface component flow ranging between -0.8 m s^{-1} and 1 m s^{-1} was observed in the Agulhas Return Current (Figure 4.12g). Furthermore, the results shown in Figure 4.12g revealed a statistically non-significant meridional component trend in the Agulhas Return Current, the trend was around -0.00102 m s^{-1}/decade (p=0.144) from 1993 to 2019.

The analysis of the seasonal geostrophic current speed in the Agulhas Current system from 1993 to 2019, encompassing multiple domains, reveals distinct trends with varying degrees of statistical significance (Figure 4.11). The analysis of the Northern Agulhas Current (Figure 4.11a) revealed a notable decrease in the seasonal geostrophic current speed, with a rate of -0.0008 m s^{-1}/decade. This trend was statistically significant, as evidenced by a p-value of 0.0222. The observed speeds within this particular area exhibited a range of values, with the lowest recorded speed being 0.553 m s^{-1} and the highest reaching 0.996 m s^{-1}. On the other hand, the Southern Agulhas Current showed a negative trend of -0.0007 m s^{-1}/decade, although not have statistical significance with a p-value of 0.0796 (Figure 4.11b). The current's speed varied between 0.501 m s^{-1} and 0.977 m s^{-1}. The Agulhas Retroflection exhibited a negative trend of -0.0006 m s^{-1}/decade, however, its p-value of 0.1724 indicates that the trend was statistically non-significant (Figure 4.11c). The speeds within Agulhas Retroflection ranged from 0.346 m s^{-1} to 0.808 m s^{-1}. The Agulhas Return Current demonstrated the most substantial decrease in seasonal geostrophic flow speed, with a rate of -0.0012 m s^{-1}/decade (Figure 4.11d). The trends were statistically non-significant in the Agulhas Return Current as shown by a p-value of 0.049. The geostrophic current speed ranged from 0.278 m s^{-1} to 1.015 m s^{-1}.

Summary

Monthly trends in the Northern Agulhas Current showed a statistically significant decrease in overall flow speed, complemented by significant trends in both the zonal and meridional components indicating southwestward flow. The Southern Agulhas Current experienced small, statistically insignificant declines in overall geostrophic current flow speed, with its zonal and meridional component exhibiting primarily southwestward flow with some months showing eastward flow probably due to the meandering of the current. The meridional component in Southern Agulhas Current exhibited significant long-term changes. In the Agulhas Retroflection, the general flow showed a statistically non-significant decline, and the zonal and meridional components both showed positive and negative speeds with insignificant trends. The fluctuation in speed was probably due to the presence of rings and eddies in the region. The Agulhas return current showed statistically non-significant decreases in both monthly and seasonal geostrophic

current flow as well as the meridional component, although the zonal component showed a statistically significant negative trend. Seasonally, a decline in speed can be observed in all areas, although the statistical significance varies. In particular, the seasonal trends of the Southern Agulhas Current, Agulhas Retroflection, and Agulhas Return Current were not statistically significant.

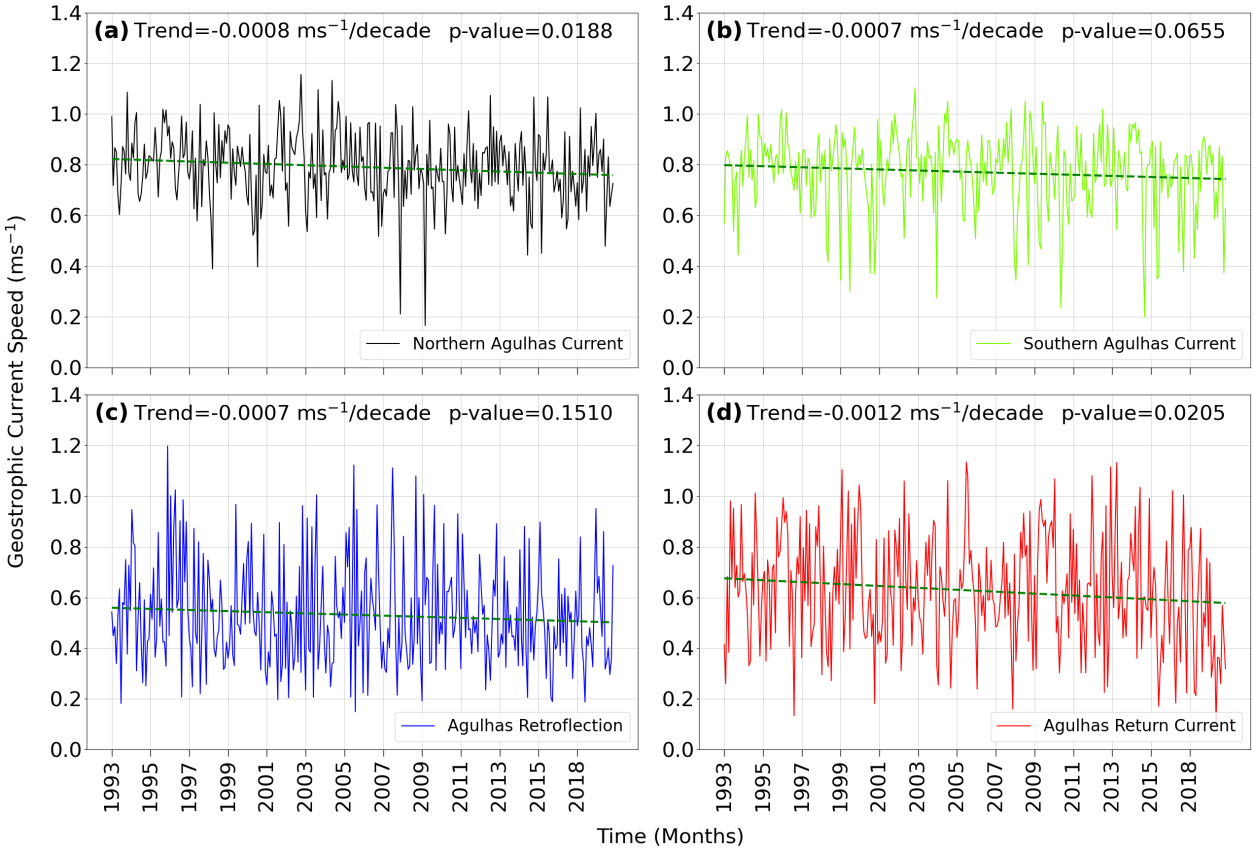

Figure 4.10: Monthly resultant geostrophic current speed timeseries and linear trends for the 1993-2019 period for all the domains in the Agulhas Current. (**a**) Northern Agulhas Current, (**b**) Southern Agulhas Current, (**c**) Agulhas Retroflection area, and (**d**) Agulhas Return Current. The solid lines show the resultant current speed timeseries while the slope of the linear trend is shown using the dashed line.

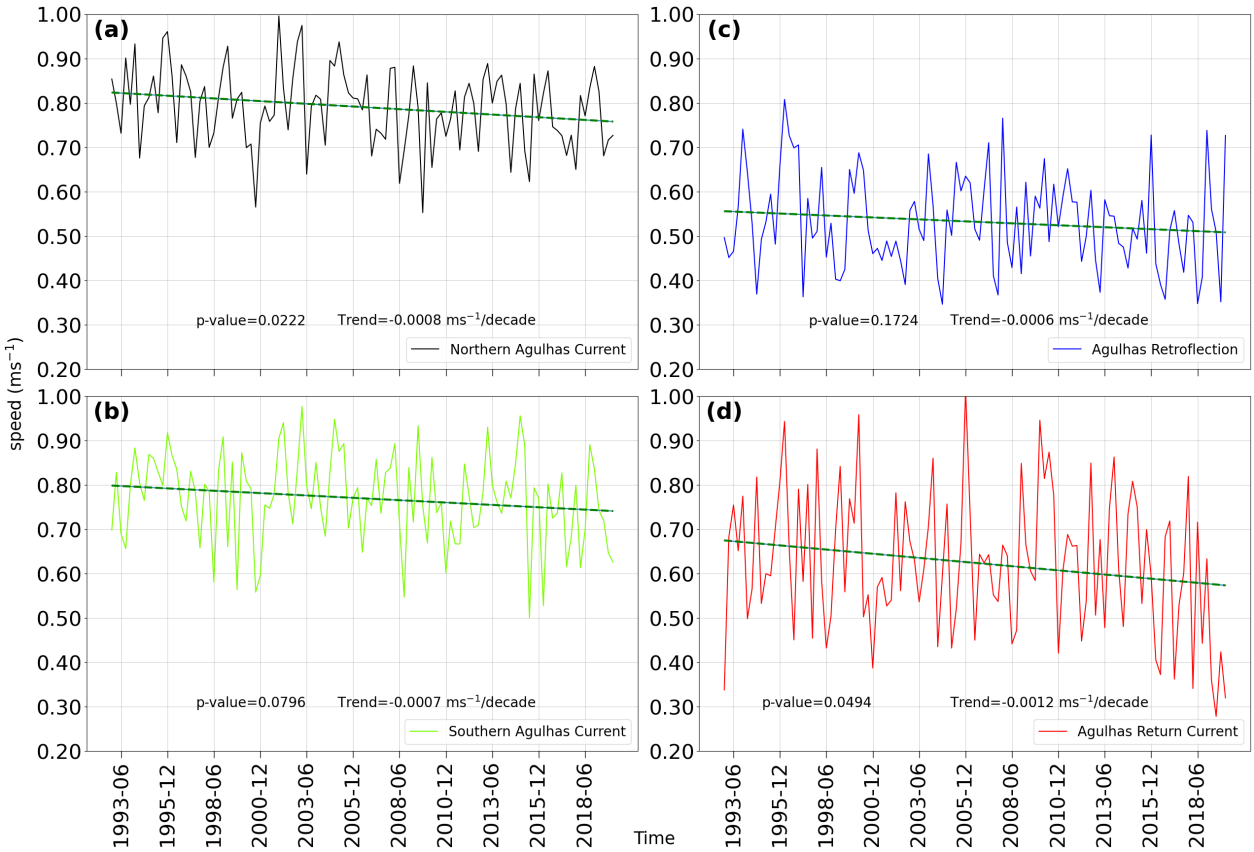

Figure 4.11: Seasonal resultant geostrophic current speed timeseries and linear trends for the 1993-2019 period for all the domains in the Agulhas Current. (**a**) Northern Agulhas Current, (**b**) Southern Agulhas Current, (**c**) Agulhas Retroflection area, and (**d**) Agulhas Return Current. The solid lines show the resultant current speed timeseries while the slope of the linear trend is shown using the dashed line.

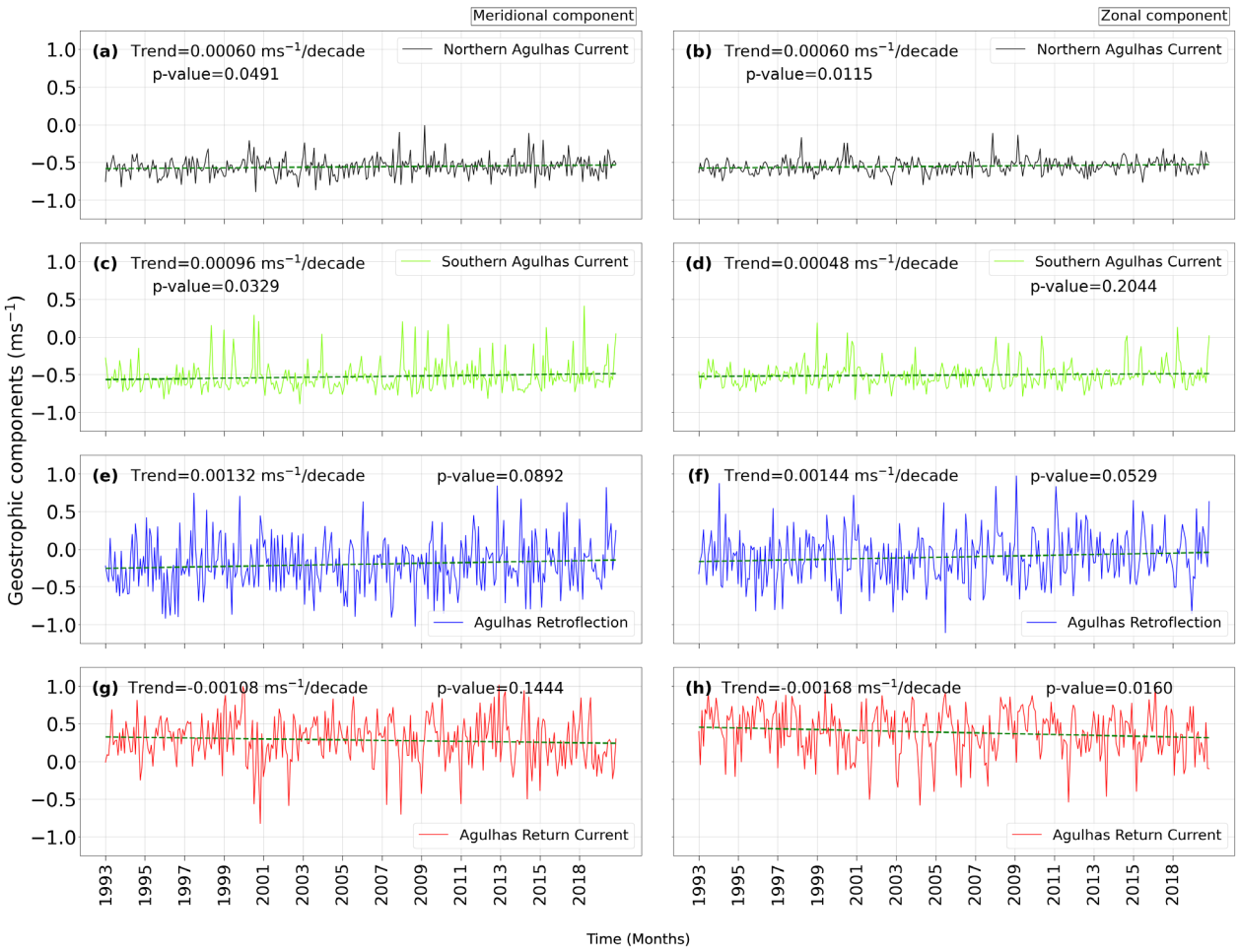

Figure 4.12: Monthly timeseries and linear trends for the meridional and zonal components during the 1993-2019 period, for all the domains. (**a**) Northern Agulhas Current, (**b**) Southern Agulhas Current, (**c**) Agulhas Retroflection area, and (**d**) Agulhas Return Current. The solid lines show the timeseries for the components while the slope of the linear trend is shown using the dashed line

4.2.3 Geostrophic Current Trends

Annual geostrophic current trends for the Southern African region are shown in Figure 4.13. The trends are for the geostrophic current speed, the meridional component, and the zonal component (Figure 4.13). Seasonal trends for the geostrophic current speed are shown in Figure 4.14

The trends showed little statistical significance for both the geostrophic current speed and the components as shown by the small patches in Figure 4.13. The statistically significant trends for the geostrophic current speed ranged between -0.103 m s^{-1}/decade and 0.101 m s^{-1}/decade (Figure 4.13b). For the zonal component, the significant trends were between -0.857 m s^{-1}/decade and 0.97 m s^{-1}/decade (Figure 4.13f). The strongest weakening of the flow was observed in the meridional component with the minimum trends as low as -1.53 m s^{-1}/decade, while the maximum was 0.966 m s^{-1}/decade (Figure 4.13d).

The seasonal trends for the geostrophic current were similar to the annual spatial trends, showing little statistical significance (Figure 4.14). Seasonal trends for the different seasons ranged between -0.093 m s^{-1}/decade and 0.128 m s^{-1}/decade for summer (Figure 4.14a), -0.12 m s^{-1}/decade and 0.135 m s^{-1}/decade for autumn (Figure 4.14b), -0.112 m s^{-1}/decade and 0.11 m s^{-1}/decade for winter (Figure 4.14c) and between -0.1 m s^{-1}/decade and 0.107 m s^{-1}/decade for spring (Figure 4.14d).

The significant trends observed in Figure 4.13 and Figure 4.14 show no overall strengthening or weakening of the current but of small areas. Considering the studies of Braby et al. (2016), and Beal and Elipot (2016), the areas that show significant strengthening or weakening might be areas of intensified mesoscale activities although further investigations with high-resolution datasets are needed to confirm. According to Braby et al. (2016), the presence of eddies both anticyclonic and cyclonic eddies in the Agulhas Current results in a transfer of momentum, subsequently impacting the average velocity and offshore location of the current. The speed of the Agulhas Current experiences an increase of 0.16 ± 0.17 m s^{-1} when anticyclonic eddies are included, while the inclusion of cyclonic eddies leads to a decrease in speed of 0.13 ± 0.16 m s^{-1}. Beal and Elipot (2016) argue that there are no signs that the Agulhas Current has intensified, however, there is the presence of the intensification of mesoscale eddy activity in the Agulhas Current.

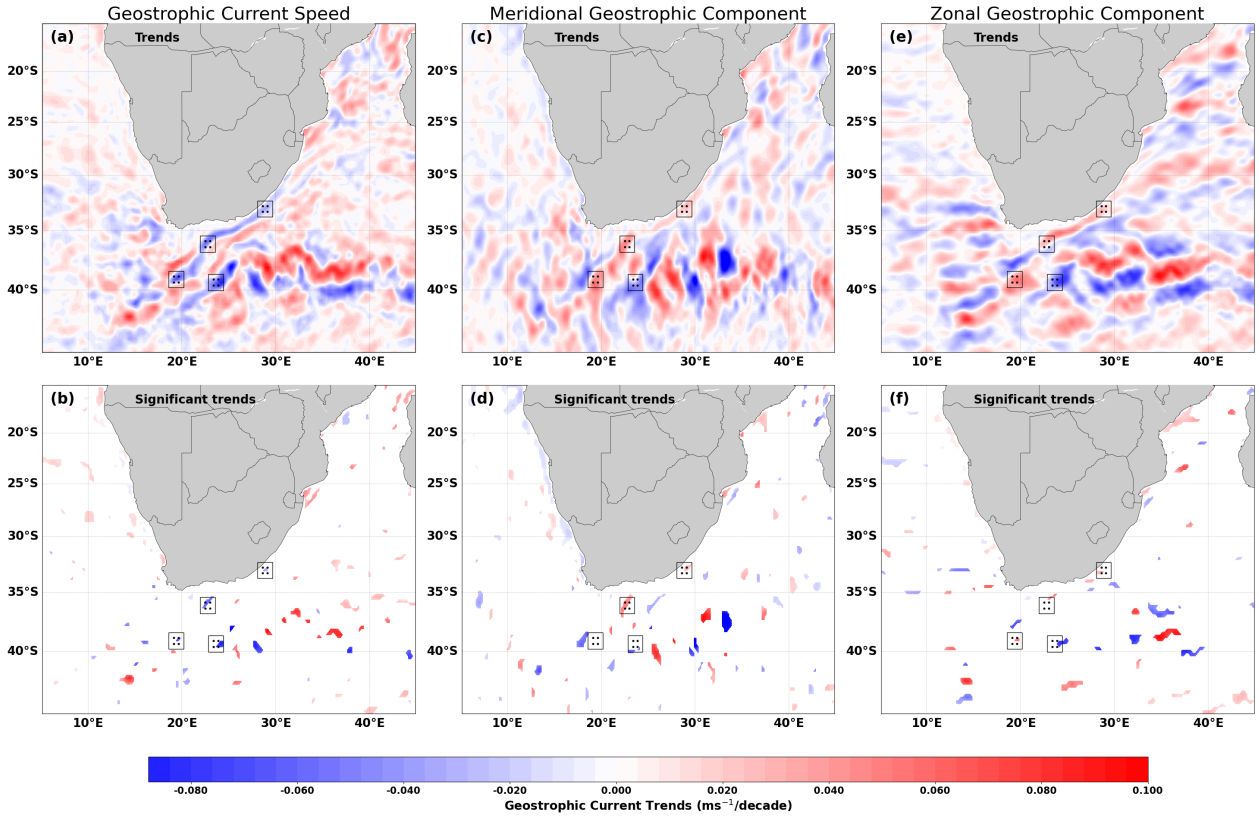

Figure 4.13: Geostrophic current trends for the resultant current speed (**a** and **b**), meridional (**c** and **d**) and zonal (**e** and **f**) components around the Southern Africa region for the 1993 to 2019 period. The figure shows both non-significant and significant trends with the appropriate labels. The confidence level for the significant trends is 95%

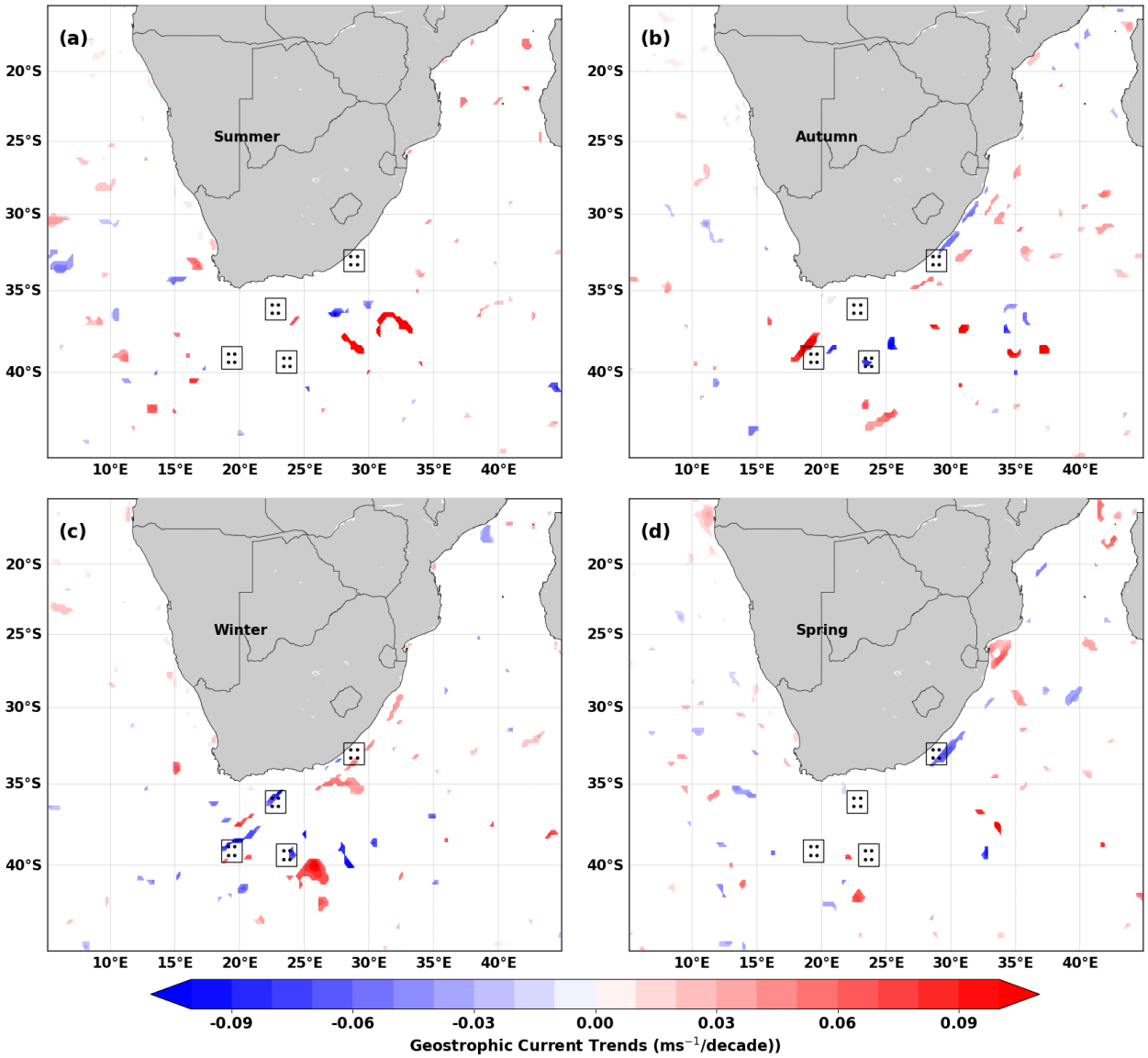

Figure 4.14: Decadal spatial geostrophic current speed trends around Southern Africa per season derived from the NOAA OISST dataset for the 1982 to 2019 period. The red colour shows a strengthening trend, and the blue signifies a weakening trend

4.2.4 Geostrophic Current Anomalies

Monthly anomalies for the geostrophic current speed anomalies were calculated for all domains from 1993 to 2019 to determine whether the Agulhas Current has strengthened or weakened (Figure 4.15). For the geostrophic current speed (Figure 4.15), negative anomalies indicate that the current has weakened while the positive anomalies indicate a strengthened current flow.

The geostrophic current speed (Figure 4.15) and geostrophic components (Figure 4.16) fluctuated rapidly and dramatically from one month to the next. Most monthly geostrophic current speed anomalies were between -1 and 1 m s^{-1} for all the domains (Figure 4.15). However, some anomalies that are greater than the general range of 1 m s^{-1} and -1 m s^{-1} were observed in all the regions but with more intensity in the Agulhas Retroflection and Agulhas Return Current (Figure 4.15b and d).

The Northern Agulhas Current exhibited varying geostrophic current speed anomalies. Positive anomalies ranged from 0.001 m s^{-1} to 1.973 m s^{-1} (Figure 4.15a). The highest and lowest values were recorded in September 2015 and December 2009, respectively. Negative anomalies varied between -0.007 m s^{-1} and -2.551 m s^{-1}, with them occurring in June 2015 and the minimum in November 2009 respectively (Figure 4.15a). The Southern Agulhas Current exhibited periodic positive geostrophic current speed anomalies ranging from 0.002 m s^{-1} to 1.284 m s^{-1} (Figure 4.15b). The peak was recorded in September 1998 and the lowest in January 2009. Negative anomalies varied between -0.014 and -2.303 m s^{-1}, although most negative anomalies were below -0.099 m s^{-1} (Figure 4.15b). In the Agulhas Retroflection (Figure 4.15c), positive anomalies ranged from 0.001 to 2.179 m s^{-1}, with the highest recorded in February 2008 and the lowest in August 2017. Negative anomalies ranged from -0.007 to -1.424 m s^{-1} and represented periods when the geostrophic current speed was weaker compared to its long-term mean (Figure 4.15c). According to Figure 4.15d, in the Agulhas Return Current, positive anomalies ranged from a minimum of 0.001 m s^{-1} to a maximum of 1.672 m s^{-1}. The highest value was recorded in July 2013 and the lowest in September 2016. Negative anomalies were also observed, with the most significant being -1.719 m s^{-1} (Figure 4.15d).

Anomalies in various regions of the Agulhas system revealed substantial variation in the zonal and meridional components of the current. In the Northern Agulhas region, the zonal component (Figure 4.16a) exhibited a peak positive anomaly of 2.522 m s^{-1} in June 1998, in contrast to a minimum positive anomaly of 0.003 m s^{-1} in July 2003. The zonal component exhibited negative anomalies ranging from -0.011 m s^{-1} in December 2011 to approximately -1.913 m s^{-1} in March 2003. The variability observed in the zonal component was also observed in the meridional

component (Figure 4.16b). In November 2009, the meridional component exhibited a maximum positive anomaly of 2.861 m s^{-1}, whereas in August 1999, it reached a minimum of 0.008 m s^{-1}. The observed negative anomalies exhibited a range of values, with the lowest anomaly recorded as -2.367 m s^{-1} in September 2015 and the highest anomaly recorded as -0.014 m s^{-1} in July 1994 (Figure 4.16b).

In the Southern Agulhas region, the zonal component anomaly exhibited a maximum positive value of 2.502 m s^{-1} in November 2000, and a minimum value of 0.003 m s^{-1} in July 2016 (Figure 4.16c). In March 1994, negative anomalies were observed with the smallest value of -0.012 m s^{-1}, while the largest negative anomaly value of -1.801 m s^{-1} was recorded in September 1998. The meridional component (Figure 4.16d) anomalies exhibited significant variability, reaching a peak positive value of 3.264 in November 2000 and a minimum value of 0.001 m s^{-1} in September 2001. The observed negative anomalies ranged from -0.018 in December 1999 to -1.168 m s^{-1} in April 2003 (Figure 4.16d).

Within the Agulhas Retroflection region, the zonal component exhibited a notable positive anomaly of 3.019 m s^{-1} in November 2011, followed by a minimum value of 0.003 m s^{-1} in October 2019 (Figure 4.16e). The negative anomalies exhibited a range of values, with the smallest recorded at -0.016 m s^{-1} in October 2007 and the largest at -2.291 m s^{-1} in July 2000 (Figure 4.16). According to Figure 4.16f, the meridional component exhibited a peak positive anomaly of 2.509 m s^{-1} in February 2000 and a trough of 0.009 in December 1995. Negative anomalies were observed within the range of -0.041 m s^{-1} in July 2005 to -2.256 m s^{-1} in May 2009 (Figure 4.16f).

Regarding the Agulhas Return Current, the zonal component (Figure 4.16g) exhibited positive anomalies that varied between a peak of 1.803 m s^{-1} in July 1993 and a nadir of 0.001 m s^{-1} in May 2009. The observed negative anomalies ranged from the smallest anomaly of -0.010 m s^{-1} in October 2015 to -2.686 m s^{-1} in January 2002 (Figure 4.16g). Regarding the meridional component (Figure 4.16h), it is worth noting that the highest positive anomaly recorded was 2.108 m s^{-1} in July 2013, while the lowest anomaly observed was 0.020 in August 2001. The observed negative anomalies exhibited a range of values, with the largest negative anomaly being -2.793 m s^{-1} in August 2008 and the smallest being -0.013 m s^{-1} in December 2013 (Figure 4.16h).

Summary

Geostrophic current speed anomalies, as well as their zonal and meridional components, were investigated in this study of the Agulhas Current system from 1993 to 2019. The majority of

anomalies ranged from -1 m s^{-1} to 1 m s^{-1}, but intense anomalies that exceeded the general range were also observed in all domains. Positive anomalies in geostrophic current speed indicate that the current is strengthening, while negative anomalies indicate that the current is weakening. The Agulhas Retroflection and Agulhas Return Current showed the most intense strengthening of the geostrophic current flow in the Agulhas Current system, as represented by high positive anomalies. The Northern Agulhas Current, on the other hand, showed the most pronounced weakening with negative anomalies reaching -2.551 m s^{-1}.

The Northern Agulhas Current showed variability in both the zonal and meridional components, with the highest positive anomaly in the zonal component at 2.522 m s^{-1} and the lowest negative anomaly at -1.913 m s^{-1}. The meridional component of the Southern Agulhas Current had the highest positive anomaly at 3.264 m s^{-1}, indicating a strong strengthening in the southward flow in the region. The Agulhas Retroflection had the highest positive zonal anomaly at 3.019 m s^{-1}, while the Agulhas Return Current was significantly weaker, with a negative zonal anomaly of -2.686 m s^{-1}.

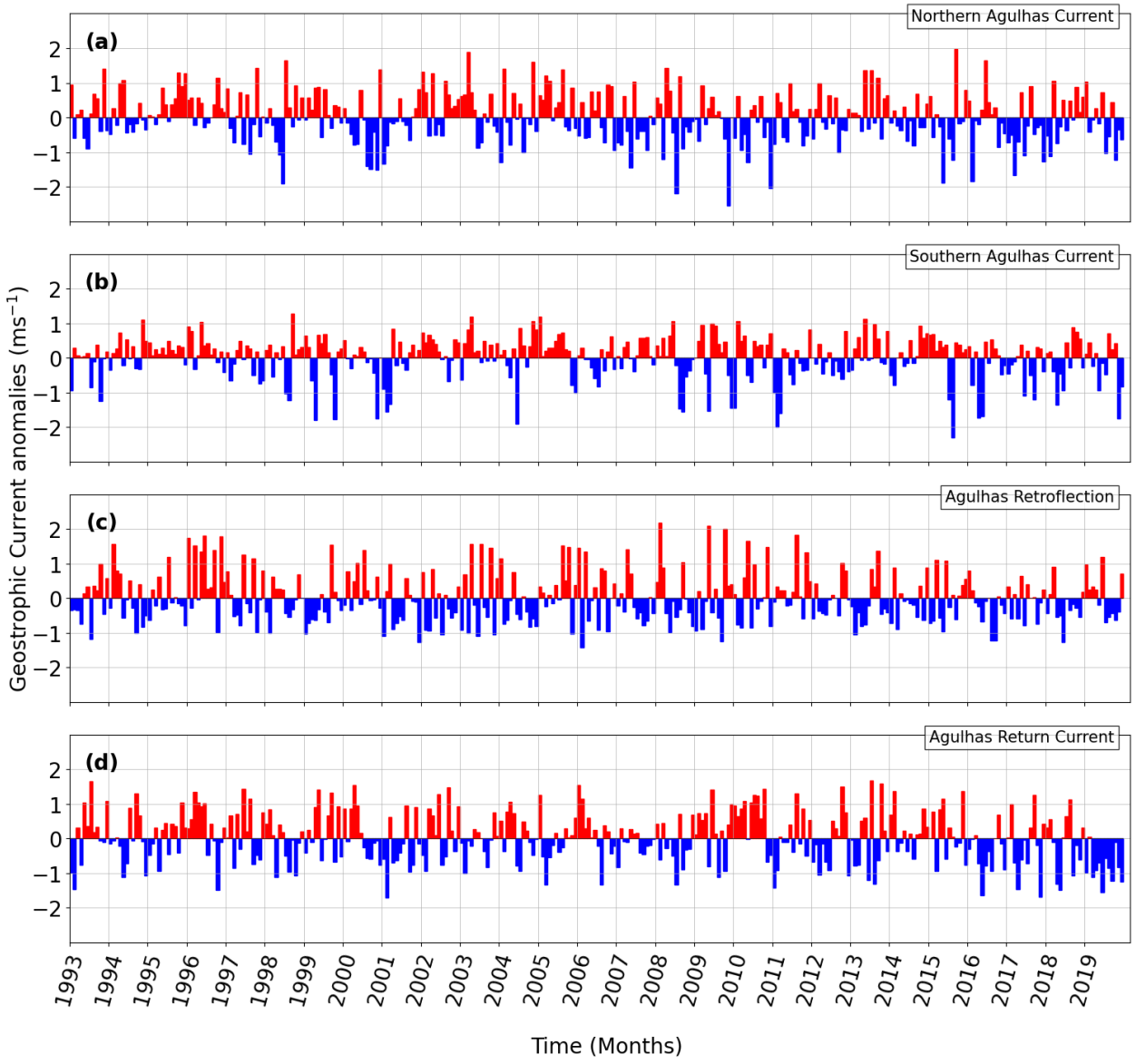

Figure 4.15: Normalised monthly geostrophic current speed anomalies from 1993 to 2019 for the 4 domains of the Agulhas Current system. (**a**) Northern Agulhas Current, (**b**) Southern Agulhas Current, (**c**) Agulhas Retroflection and the (**d**) Agulhas Return Current. The blue colours show negative anomalies, while red signifies all the positive anomalies.

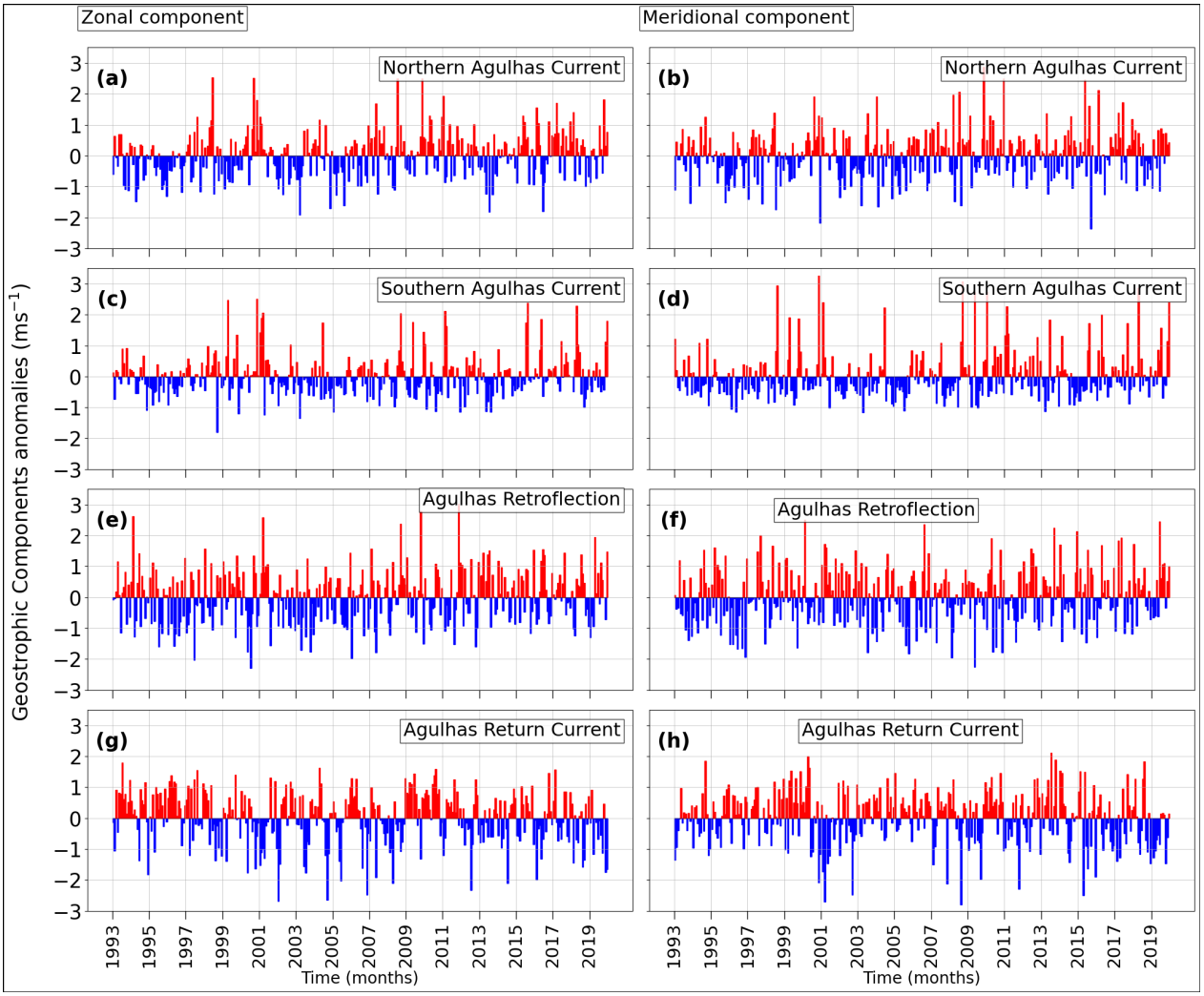

Figure 4.16: Monthly geostrophic current anomalies for the meridional and zonal components from the 4 domains (Northern Agulhas Current (**a** and **b**), Southern Agulhas Current (**c** and **d**), Agulhas Retroflection (**e** and **f**) and the Agulhas Return Current (**g** and **h**)) of the Agulhas Current system. The anomalies are for the 1993 to 2019 period. The blue colours show negative anomalies while red signifies all the positive anomalies

4.3 SST and Geostrophic Current Relationship

4.3.1 Monthly and Seasonal Correlation

Figure 4.17 shows Pearson's correlation coefficients between the monthly normalised SST anomalies and the monthly normalised geostrophic current speed anomalies over the Southern Africa region from 1993 to 2019. Pearson's correlation coefficient highlights the strength of the linear relationship between the geostrophic current speed anomalies and SST anomalies and the statistically significant linear relationship was assessed at a 95% confidence level.

Based on Figure 4.17b statistically significant ($p < 0.05$) Pearson's correlation coefficients ranged between -0.4 and 0.63. The most distinct feature was the statistically significant ($p < 0.05$) weak to moderate positive correlation (0.25 to 0.58) visible over the whole Agulhas Current system path (Figure 4.17b). The positive correlation coefficient ($r>0$) highlighted a positive relationship between monthly SST anomalies and geostrophic current speed anomalies in the Agulhas Current system (Figure 4.17a).

Spatial variation was prominent in the monthly correlation shown in Figure 4.17a. A statistically significant weak positive correlation ($p < 0.05$) of around 0.25 to 0.35 was observed in the Northern and the Southern Agulhas Current domains (Figure 4.17a and b). Even though the correlation in the Northern and Southern Agulhas Current was statistically significant, most of the correlations were however considered to be negligible as they were exceedingly small ($r<0.3$) (Figure 4.17a and b). Agulhas Retroflection and the Agulhas Return Current demonstrated a moderate positive statistically significant correlation of around 0.58 ($p < 0.05$) (Figure 4.17b). The offshore edge of the Northern and Southern Agulhas domains had a weak negligible negative correlation of around -0.25 which was statistically insignificant (Figure 4.17a and b). Both edges of the Agulhas Retroflection and Agulhas Return Current had statistically insignificant weak to moderate negative correlation (Figure 4.17a and b).

Figure 4.18 depicts a statistically significant seasonal Pearson's correlation between SST anomalies and geostrophic current speed anomalies within the Agulhas Current region from 1993 to 2019. The seasonal correlation over the Agulhas Current mostly showed a positive linear relationship, with some small patches of negative correlation around the Southern Agulhas Current in summer and autumn (Figure 4.18). The correlation coefficients ranged from 0.82 to -0.59 during the summer season (Figure 4.18a), indicating a strong relationship between SST anomalies and geostrophic current speed anomalies. The autumn season (Figure 4.18b) echoed the summer season (Figure 4.18a) in terms of a maximum correlation value of 0.82, but had a more pronounced negative correlation of -0.67, indicating a stronger inverse relationship during

this season. Winter (Figure 4.18c) had the highest positive correlation of 0.88 among all seasons, as well as the most pronounced negative correlation of -0.76. This points to a stronger relationship between SST anomalies and geostrophic current speed anomalies during the winter months. The spring season (Figure 4.18d), on the contrary, had a slightly lower maximum correlation value of 0.86 compared to winter, although higher than the other seasons.

4.3.2 Lag Correlation

Figure 4.19 shows the lag correlation between changes in monthly SST anomalies and geostrophic current speed anomalies over time for the respective Agulhas Current regions. The study looks at these changes from the same time point to as far as 47 months apart, allowing us to understand both immediate and delayed interactions. All the lag correlation between SST anomalies and geostrophic current anomalies was weak ($0.5 > r \leq 0.3$; $-0.5 < r \leq -0.3$) or negligible ($0.3 > r < 0$; $-0.3 < r < 0$).

In the Northern Agulhas Current (Figure 4.19a), a statistically significant immediate (lag 0) relationship between SST and current speed, with a correlation coefficient of $r = 0.3954$ (p-value < 0.05) was observed. The immediate significant relationships weakened slightly at lag 1, with $r = 0.1868$ (p-value < 0.05). A statistically significant negative relationship appears at lag 18 ($r = -0.1131$), and short periods of positive correlation show up between lag 30- and lag 33, with coefficients ranging from $r = 0.1186$ to $r = 0.1527$ (p-value < 0.05).

For the Southern Agulhas Current (Figure 4.19b), there was also a statistically significant immediate relationship, expressed by $r = 0.3883$ (p-value < 0.05). The relationship was weaker but statistically significant at a lag 1, marked by $r = 0.1397$ (p-value < 0.05). There were occasional statistically significant negative relationships at the lag 10 and 12 ($r = -0.1356$ and $r = -0.1178$, respectively), followed by rare positive relationships at the 28th and 29th months, with values of $r = 0.1150$ and $r = 0.1551$ (p-value < 0.05).

In the Agulhas Retroflection area (Figure 4.19c), a statistically significant correlation was observed at a lag 5 with a negative value of $r = -0.1538$ (p-value < 0.05), followed by another negative one at lag 6 with $r = -0.1179$ (p-value < 0.05). A positive statistically significant correlation at lag 27 was observed, indicated by an r-value of 0.1287 (p-value < 0.05).

Finally, in the Agulhas Return Current region (Figure 4.19d), a variation of relationships was observed over time. At lag 6 and 7, statistically significant (p-value < 0.05) positive relationships were present noted by the r values ($r = 0.1625$ and $r = 0.1323$), respectively. A negative correlation was also observed at lag 15, marked by $r = -0.1257$ (p-value < 0.05), and another

statistically significant positive correlation reappeared at lag 28 and 46, noted by r = 0.1367 and r = 0.1316 (p-value < 0.05), respectively.

Summary

This study looked at the relationship between monthly normalised SST anomalies and geostrophic current speed anomalies in the Agulhas Current region from 1993 to 2019. Figure 4.17 depicts a weak to moderate positive correlation along the Agulhas Current system path, with some areas exhibiting negligible correlation (r<0.3). Figure 4.18 delves into the seasonal aspect, revealing strong positive correlations, especially during the winter season, with a maximum coefficient of 0.88, and a significant negative correlation in autumn with a minimum coefficient of -0.67. This seasonal variation suggests that there may be an enhanced linear relationship between SST anomalies and geostrophic current speed anomalies during these times.

Figure 4.19 shows lag correlations, revealing both immediate and delayed interactions up to 47 months apart. The Northern and Southern Agulhas Current regions show significant immediate relationships, with correlation coefficients of r = 0.3954 and r = 0.3883, respectively. The Agulhas Retroflection and Return Current regions show a variety of significant correlations across different lags, indicating complex temporal dynamics. These findings shed light on the complex interactions between SST anomalies and geostrophic current speed anomalies, allowing for a better understanding of the oceanic and atmospheric interactions within the Agulhas Current system over time.

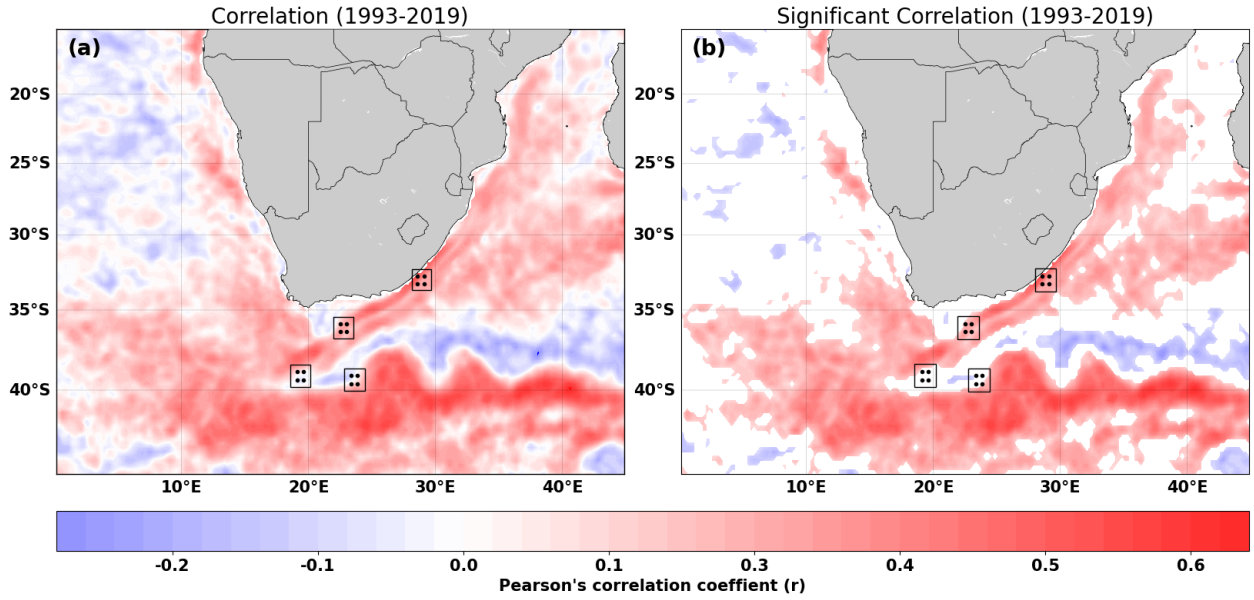

Figure 4.17: Monthly spatial correlation between SST and geostrophic current speed around Southern Africa derived for the 1993 to 2019 period. The colour shading shows the strength of the relationship between variables. Red demonstrates a positive relationship between the parameters, while blue represents a negative relationship. The figure shows both (**a**) insignificant and (**b**) significant correlation coefficients. The correlation significance is shown for a 95% confidence level.

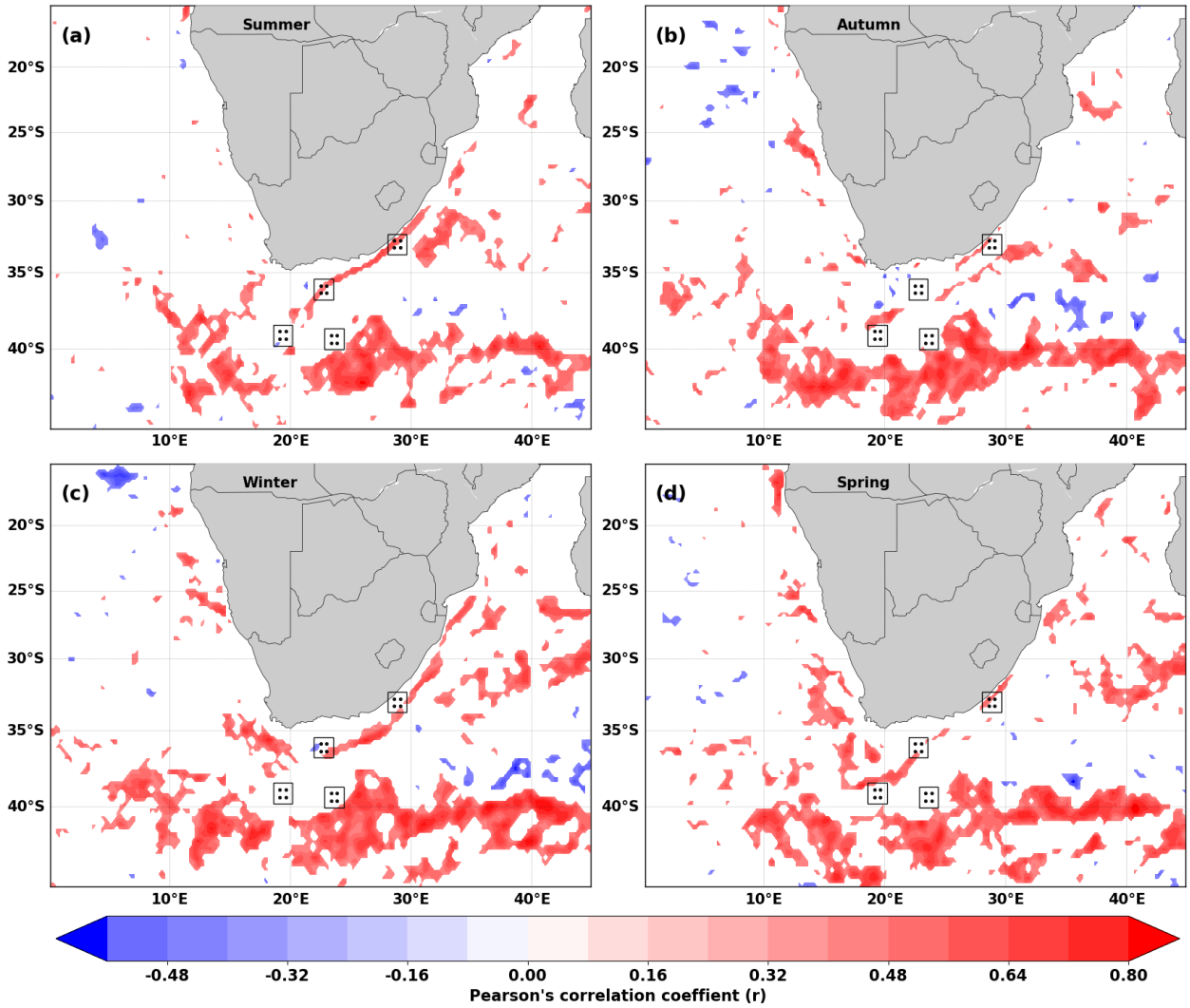

Figure 4.18: Seasonal spatial correlation between normalised SST and geostrophic current speed anomalies around Southern Africa derived for the 1993 to 2019 period. The colour shading shows the strength of the relationship between variables. Red demonstrates a positive relationship between the parameters, while blue represents a negative relationship. The figure only shows the significant correlation coefficients for a 95% confidence level.

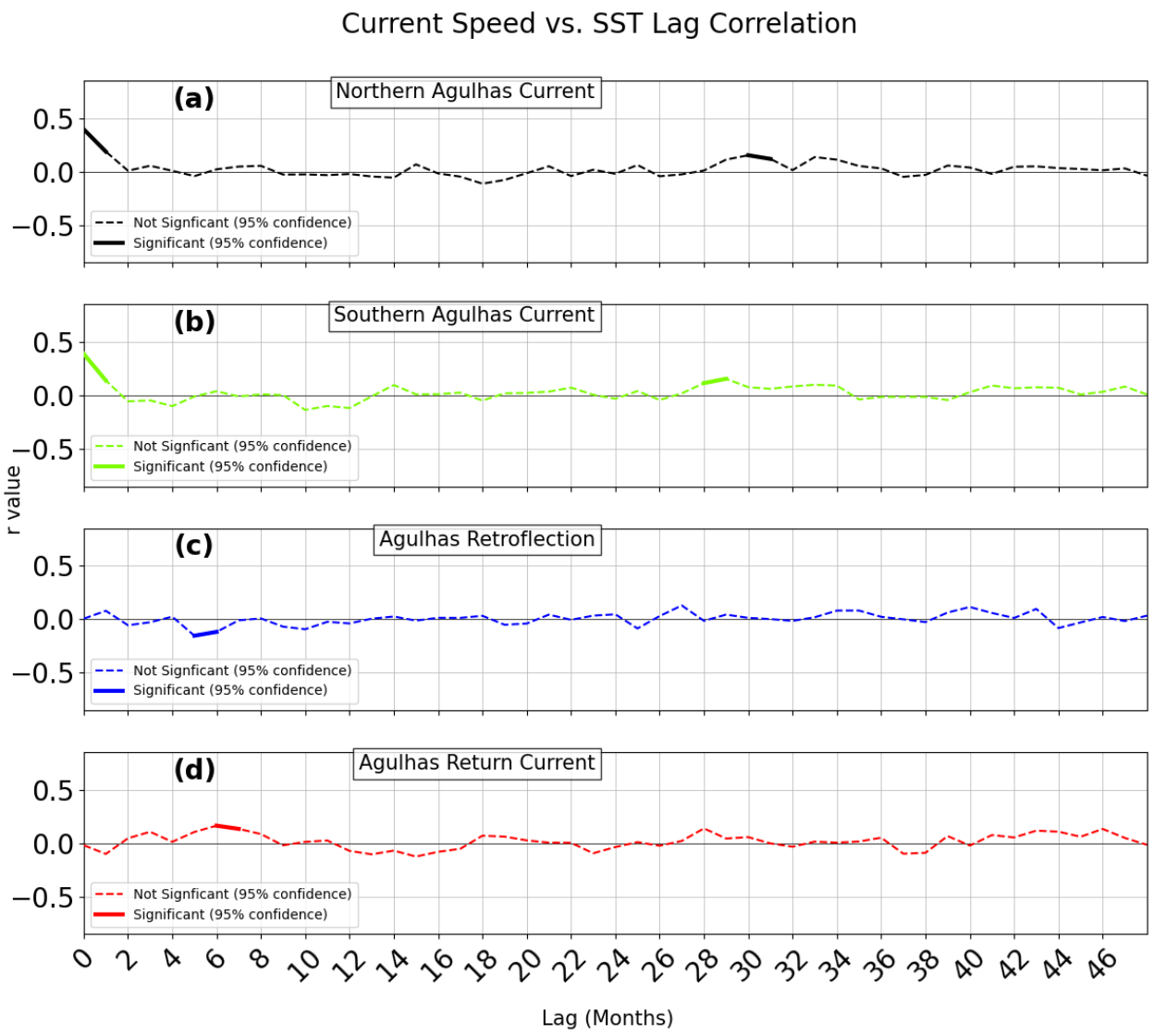

Figure 4.19: Lag correlation between SST and geostrophic current speed anomalies around Southern Afr in the (**a**) Northern Agulhas Current, (**b**) Southern Agulhas Current, (**c**) Agulhas Retroflection and the (**d**) Agulhas Return Current at lags ranging between 0 and 47 months. The dashed line indicates that the correlation is insignificant ($p > 0.05$), and the solid lines show that the correlation is significant ($p < 0.05$)

4.4 Influence of Climate Indices on SST and Geostrophic Current.

The Oceanic Niño Index (ONI, in °C) shown in Figure 4.20 was used to identify the different phases of the ENSO and to determine the long-term patterns and significant events of ENSO (Figure 4.22). The National Oceanic and Atmospheric Administration (NOAA) defines an El Niño event as a positive ONI exceeding 0.5 ^{o}C over at least five successive overlapping intervals, while a La Niña event is defined as a negative ONI falling below -0.5 °C.

According to Figure 4.20, twelve El Niño and eight La- Niña events occurred between 1982 and 2019. The most intense El Niño event, with an ONI greater than 2.5 °C, occurred between April 2015 and April 2016. Another notable El Niño event occurred from May 1997 to May 1998, with an ONI exceeding 2.0 °C. The most pronounced and long-lasting La Niña event, with an ONI less than -2.0 °C, occurred between May 1988 and April 1989 (Figure 4.20). Furthermore, two other significant La Niña events occurred from July 1998 to June 2000 and from July 2010 to May 2012 (Figure 4.20).

In addition to ENSO, the SAM is a significant climate mode influencing oceanographic conditions in the Southern Hemisphere (Yang et al. 2016; Elipot and Beal, 2018). A SAM index was therefore developed to assess and document the impact of SAM (Marshall et al. 2018). A positive SAM index indicates a poleward migration of the core of the westerly wind belt (Marshall et al. 2018), resulting in reduced wind circulation at Agulhas Current latitudes. A negative SAM index, on the other hand, indicates an equatorward migration of the core of the westerly wind belt, resulting in enhanced wind circulation at Agulhas Current latitudes. According to Figure 4.21, the SAM index was primarily positive throughout the study period. The positive SAM index peaked at 4.92 in February 2015, and it peaked again in March 2016 at 4.36. The peak negative SAM index (-6.03) occurred in October 1988, and in 2002, there were two significant negative SAM indices, -4.42 in March and -5.77 in October.

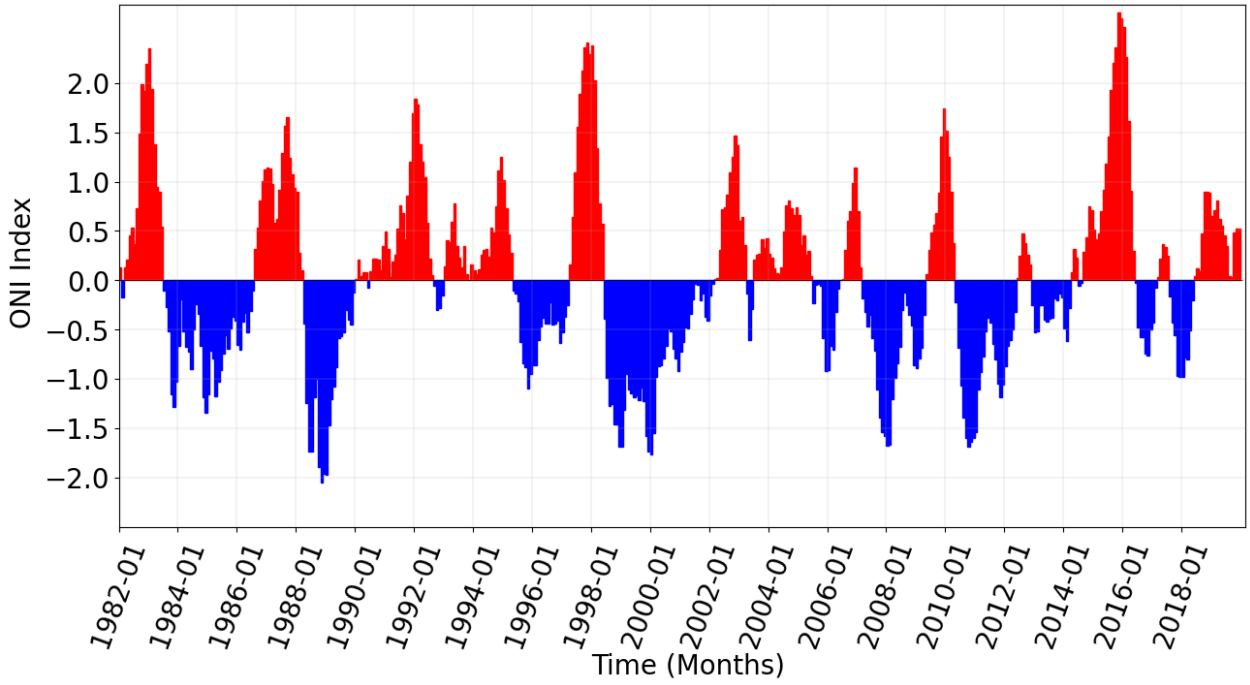

Figure 4.20: The time series of the monthly Oceanic Nino index (ONI; °C) from 1982 to 2019.

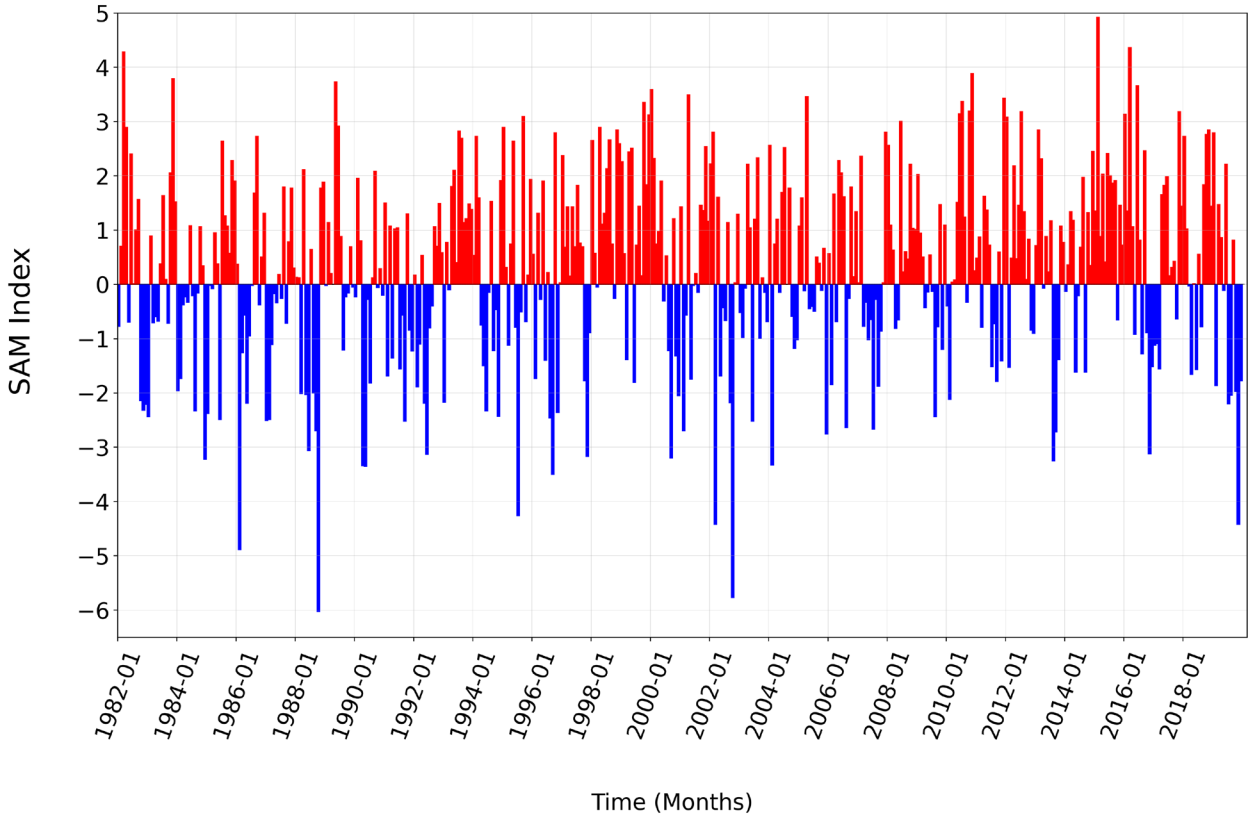

Figure 4.21: The time series of the monthly SAM index from 1982 to 2019.

4.4.1 Relationship between climate indices and SST

To determine the impact of the ENSO on SST anomalies in the various regions of the Agulhas Current, lag correlation analyses were performed, as shown in Figure 4.22, spanning a range of lag 0 to lag 47 to reveal immediate or delayed correlations.

Concerning the Northern Agulhas Current, Figure 4.22a primarily exhibits correlations that are not statistically significant across lags ranging from lag 0 to lag 33. However, starting from lag 34, a sequence of negligible but statistically significant negative correlations emerges, displaying coefficients ranging from -0.0974 to -0.1466 until lag 38.

On the contrary, the Southern Agulhas Current, as depicted in Figure 4.22b, exhibits negligible but statistically significant positive correlations from lag 6 to lag 11, with coefficients ranging from 0.0995 to 0.1062. After lag 12, the aforementioned correlations undergo a shift towards statistical insignificance. However, it is worth noting that a resurgence of negligible negative correlations was observed between lags 35 and 42.

In relation to the Agulhas Retroflection, Figure 4.22c reveals no significant correlations up to lag 17. Then positive but negligible statistically significant correlations from lag 18 to lag 25 were observed, with coefficients ranging from 0.1069 to 0.1244. Another pattern of negative correlations with coefficients ranging from -0.1048 to -0.1377 within lag 37 to 42 was also observed in Agulhas Retroflection.

In the context of the Agulhas return current, as illustrated in Figure 4.22d, the correlations with ENSO exhibit no statistically significant results until lag 34. However, a shift towards weak negative correlations was observed between lags 35 and 41, starting at -0.1112 and progressively strengthening to -0.1403 by lag 38.

The correlation analysis of the SAM index and normalised SST anomalies across the Agulhas Current reveals intriguing trends (Figure 4.23). A lag correlation was performed for each region with lags ranging from 0 to 47.

The correlation in the Northern Agulhas Current remained not significant across lags 0 to 37 (Figure 4.23a). However, at lags 38 and 39, there were negligible but significant positive correlations with coefficients of 0.0999 and 0.1186, indicating a delayed response in SST anomalies to SAM fluctuations. Following lag 39, the correlations return to non-significance until lag 47 (Figure 4.23a).

In the Southern Agulhas Current (Figure 4.23b), lags 27 and 28, showed negligible statistically significant negative correlations of -0.1060 and -0.1018, indicating an inverse relationship between SAM and SST anomalies during these lags. A negligible positive correlation of 0.1250 reappears at lag 39.

The Agulhas Retroflection exhibited negligible but statistically significant positive correlations at lags 0 to 2, with coefficients ranging from 0.1030 to 0.1412 (Figure 4.23c). However, at lags 12, 23, 25, and 26, there is a shift to negligible negative correlations with coefficients ranging from -0.0961 to -0.1137, indicating a potential inverse and delayed relationship between SAM and SST anomalies during these periods in the region (Figure 4.23c).

Lastly, in the Agulhas Return Current (Figure 4.23d), there were negligible positive correlations at lags 0, 1, and 11, with coefficients of 0.1401, 0.1005, and 0.1080, respectively and all these were statistically significant. At lag 24, a negligible but statistically significant negative correlation with a coefficient of -0.0984 emerged, followed by a return to a negligible significant positive correlation with a coefficient of 0.1408 at lag 39 (Figure 4.23d).

Summary

The analysis of the ENSO influence on SST anomalies in the Agulhas Current regions (as depicted in Figure 4.22) demonstrates a range of correlation patterns across various time lags, spanning from lag 0 to lag 47. Notable results include the occurrence of negligible negative correlations after Lag 34 in the Northern Agulhas Current and a change between positive and negative correlations in the Southern Agulhas Current and the Agulhas Retroflection at different lags. Negligible negative correlations appear in the Agulhas return current after lag 34, suggesting different impacts of ENSOs over different lags and regions in the Agulhas Current. Similarly, correlation analysis of the SAM index with SST anomalies (Figure 4.23) reveals a series of correlation patterns from lag 0 to lag 47 in the Agulhas Current regions. The analysis highlights patterns of negligible positive and negative correlations at specific lags in the Northern and Southern Agulhas Current, Agulhas Retroflection and Agulhas Return Current. These results reflect the complicated, delay-dependent relationship between SAM, ENSO and SST anomalies in the Agulhas Current regions and require more detailed studies to better understand the underlying climatic interactions in detail.

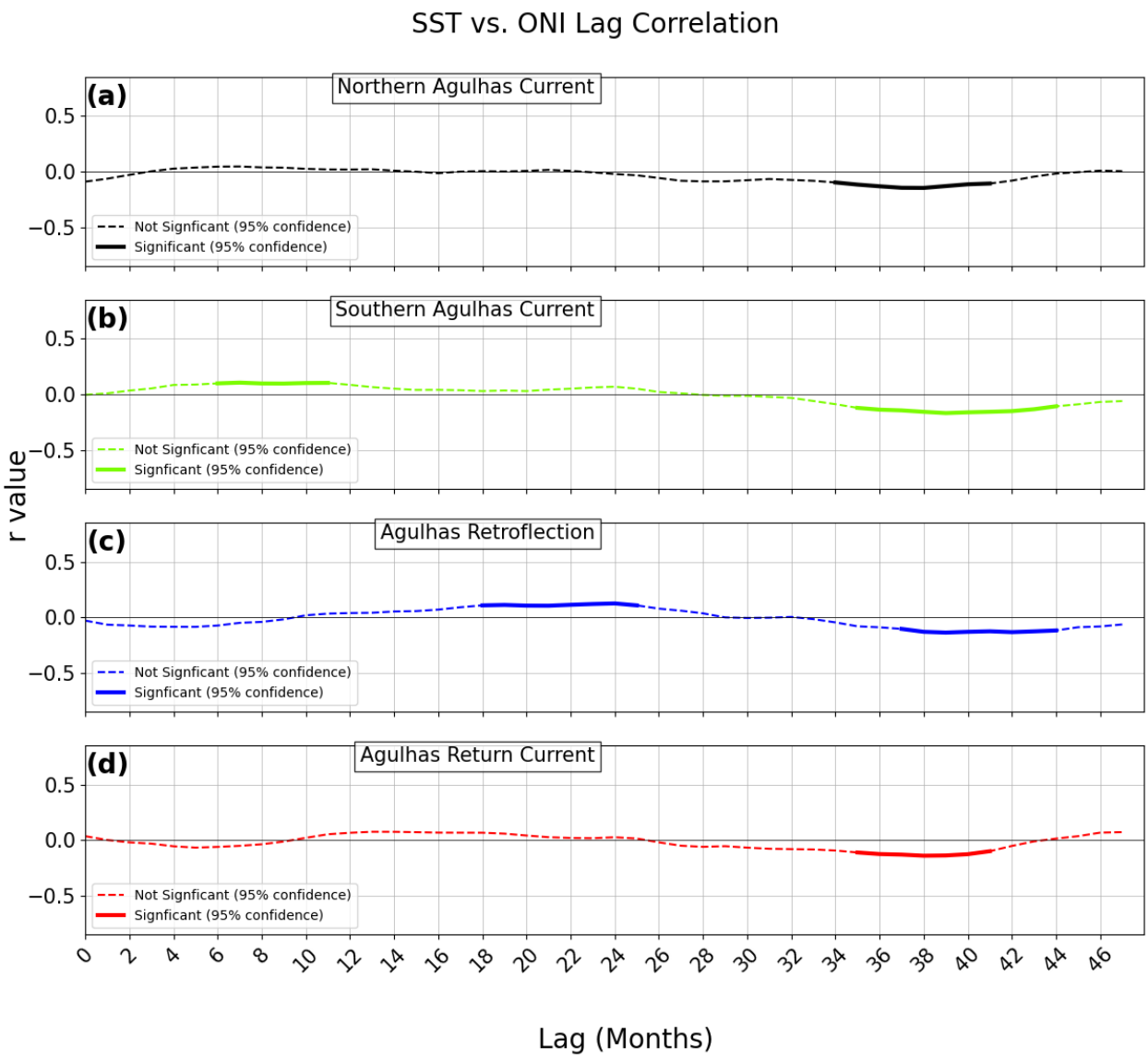

Figure 4.22: The lag correlation coefficients obtained from the analysis between normalised SST anomalies and the ONI index in the (**a**) Northern Agulhas Current, (**b**) Southern Agulhas Current, (**c**) Agulhas Retroflection and the (**d**) Agulhas Return Current at lags ranging between 0 and 47 months. The dashed line indicates that the correlation is insignificant ($p > 0.05$), and the solid lines show that the correlation is significant ($p < 0.05$)

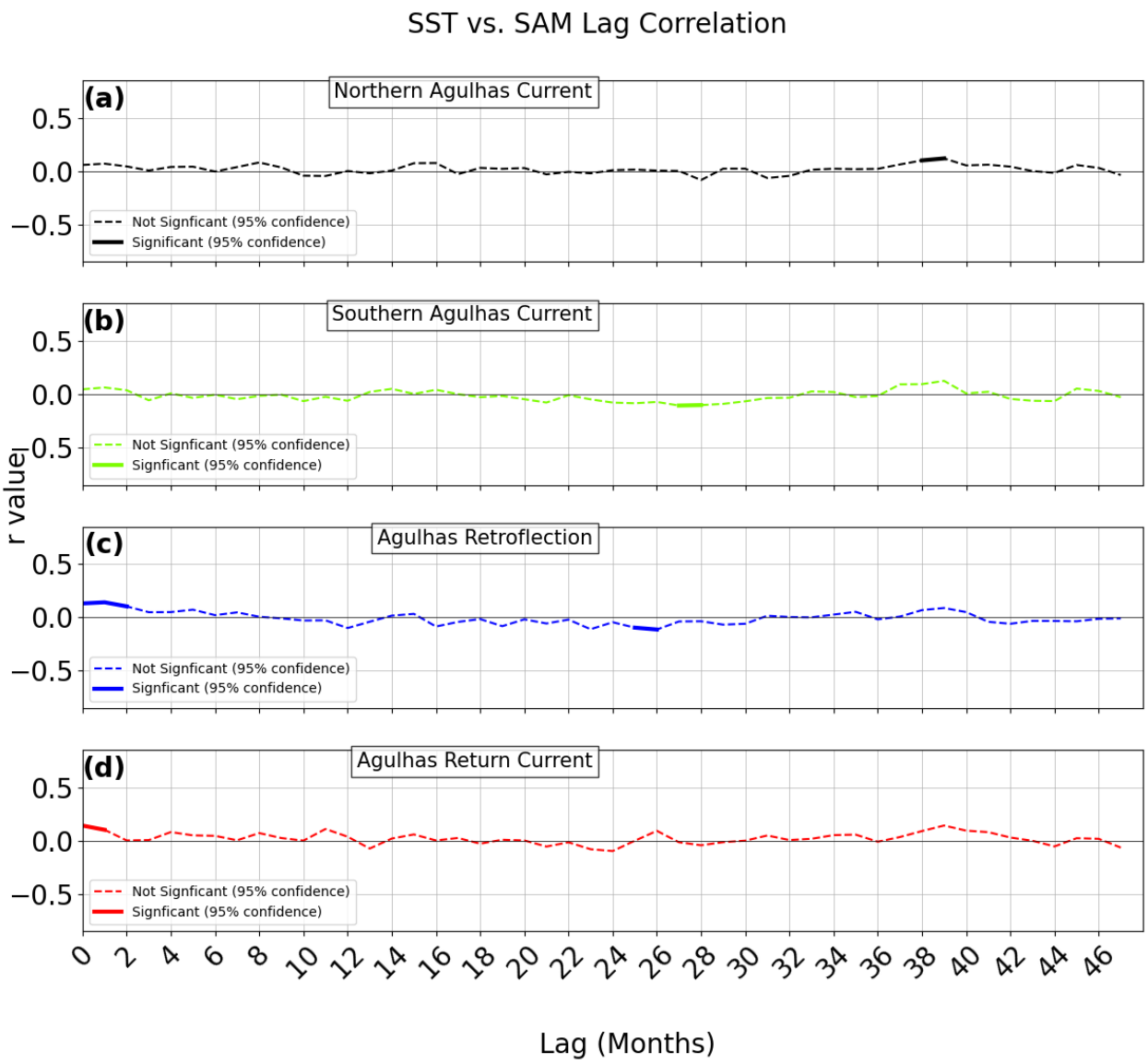

Figure 4.23: The lag correlation coefficients obtained from the analysis between normalised SST anomalies and the SAM index in the (**a**) Northern Agulhas Current, (**b**) Southern Agulhas Current, (**c**) Agulhas Retroflection and the (**d**) Agulhas Return Current at lags ranging between 0 and 47 months. The dashed line indicates that the correlation is insignificant ($p > 0.05$), and the solid lines show that the correlation is significant ($p < 0.05$)

4.4.2 Relationship between Climate Nodes and Geostrophic Current Speed

To discern the impact of the Oceanic Niño Index (ONI) on normalised geostrophic current speed anomalies across different regions of the Agulhas Current, lag correlation analyses were conducted, extending from lag 0 to lag 47 to unveil immediate or delayed correlations (Figure 4.24).

In the Northern Agulhas Current (Figure 4.24a), Southern Agulhas Current (Figure 4.24b) and Agulhas Retroflection (Figure 4.24c) regions, the correlations were found to be statistically non-significant across all lags. According to Figure 4.24d, the Agulhas Return Current exhibited no statistically significant correlations until lag 39, followed by a change towards negligible but statistically significant negative correlations from lag 40 to lag 47. The statistically significant correlation coefficient ranged between -0.135 and -0.18 in the Agulhas Return Current (Figure 4.24d).

Simultaneously, the correlation analysis regarding the SAM elucidates varied patterns (Figure 4.25). In the Northern Agulhas Current, correlations across lags from lag 0 to lag 37 were non-significant. However, at lags 38 and 39, negligible but statistically significant positive correlations emerged, with coefficients of 0.1733 and 0.1269, respectively (Figure 4.2a). According to Figure 4.2b, in the Southern Agulhas Current, negligible significant negative correlations at lags 8 and 11 with coefficients of -0.1129 and -0.1125 were observed, then again at lag 26 with a coefficient of -0.1156, and a shift to a negligible positive correlation occurred at lag 45 with a coefficient of 0.1560 (Figure 4.2b). In the Agulhas Retroflection (Figure 4.2c), a negligible significant positive correlation with a coefficient of 0.1167 was noted at lag 4, then shifted to a negligible negative correlation at lag 26 with a coefficient of -0.1240 and a negligible positive correlation at lag 45 with a coefficient of 0.1212 was observed again. Lastly, within the Agulhas Return Current, a sequence of negligible negative correlations was witnessed starting from lag 38 to lag 39, with coefficients of -0.1407 and -0.2299 respectively (Figure 4.2d).

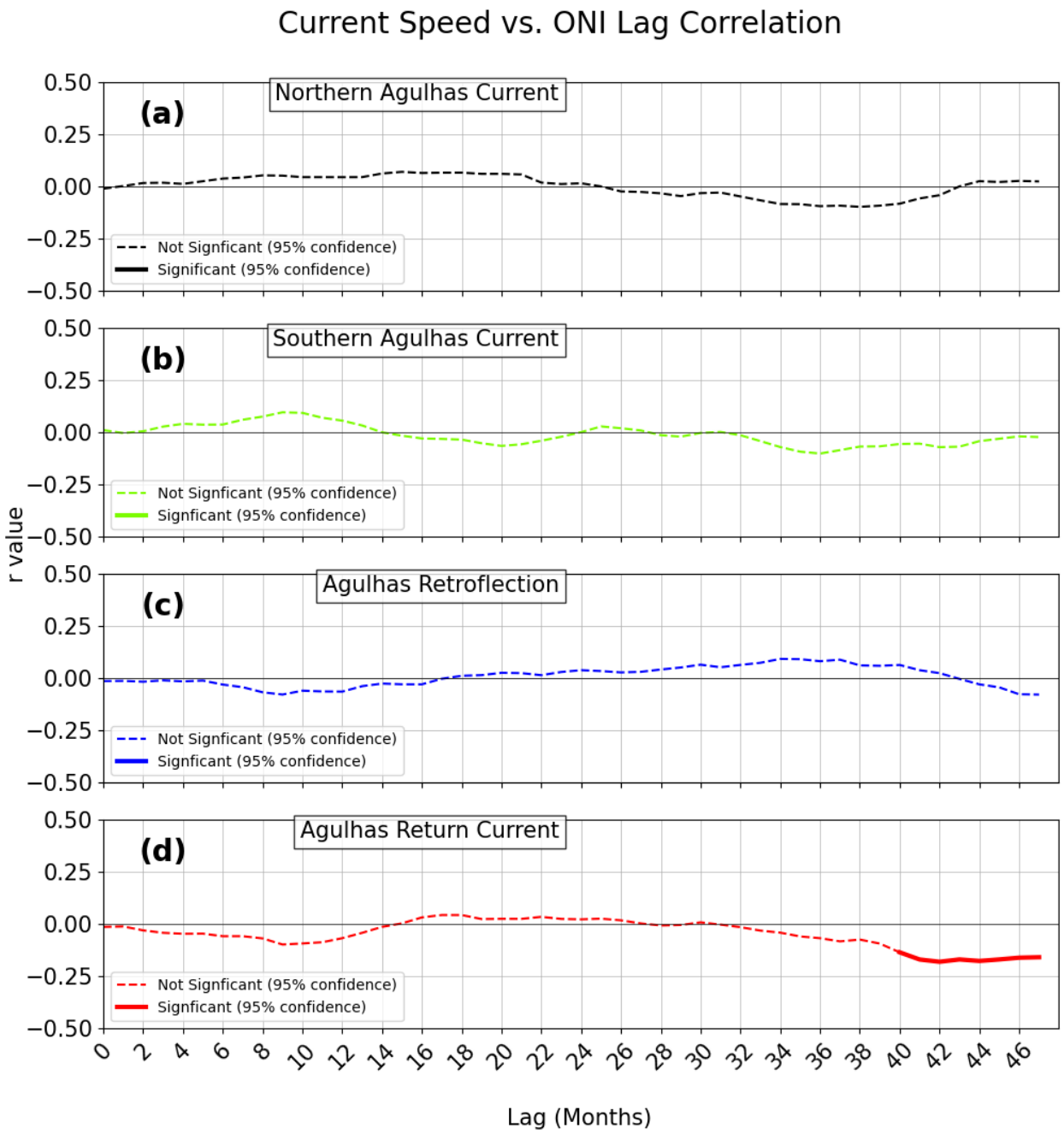

Figure 4.24: The lag correlation coefficients obtained from the analysis between normalised geostrophic current speed anomalies and the ONI index in the (**a**) Northern Agulhas Current, (**b**) Southern Agulhas Current, (**c**) Agulhas Retroflection and the (**d**) Agulhas Return Current at lags ranging between 0 and 47 months. The dashed line indicates that the correlation is insignificant ($p > 0.05$), and the solid lines show that the correlation is significant ($p < 0.05$)

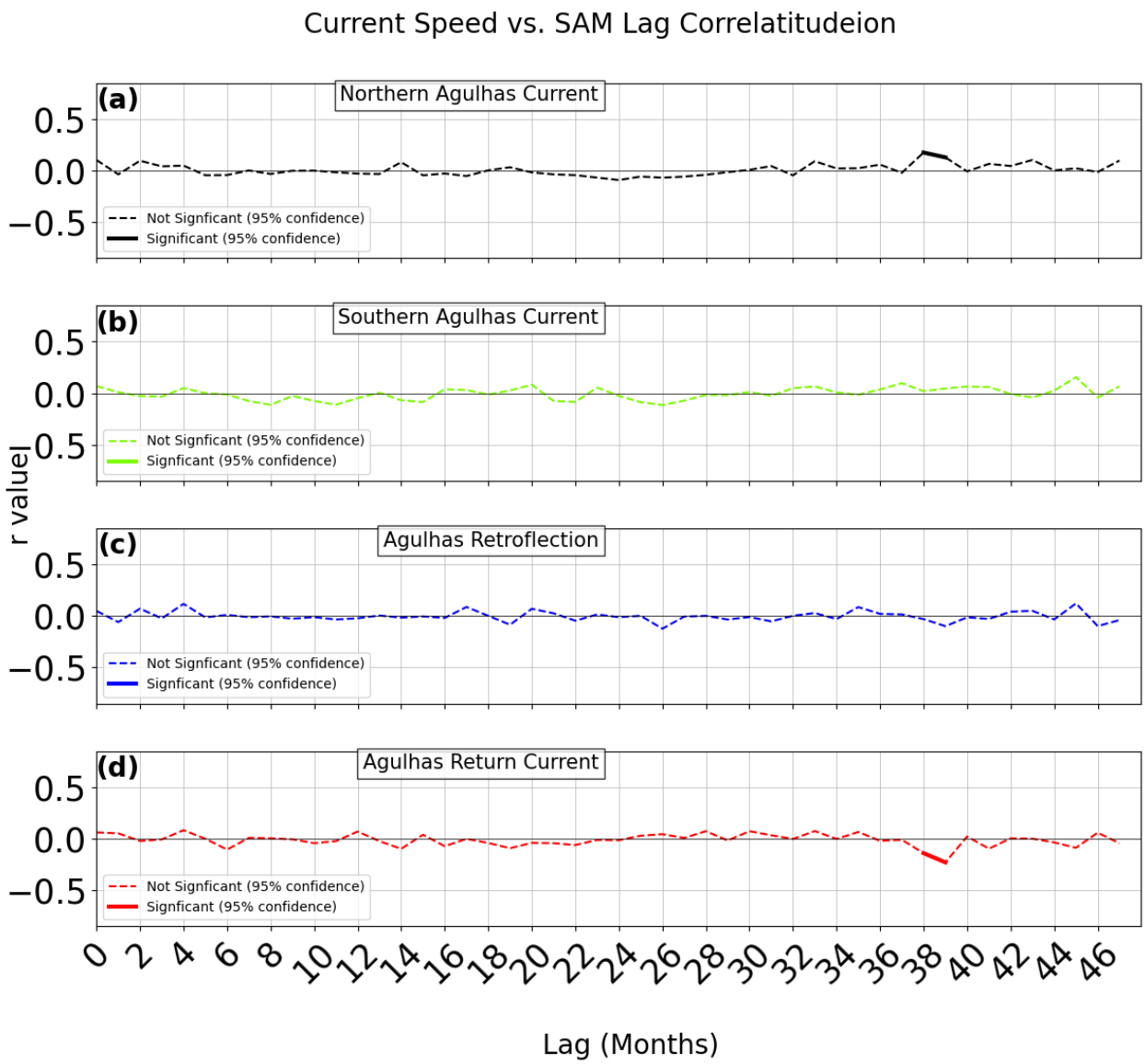

Figure 4.25: The lag correlation coefficients obtained from the analysis between normalised geostrophic current speed anomalies and the ONI index in the (**a**) Northern Agulhas Current, (**b**) Southern Agulhas Current, (**c**) Agulhas Retroflection and the (**d**) Agulhas Return Current at lags ranging between 0 and 47 months. The dashed line indicates that the correlation is insignificant ($p > 0.05$), and the solid lines show that the correlation is significant ($p < 0.05$)

5. CHAPTER 5: DISCUSSION

This study's results section (Chapter 4) has provided insight into the regional SST and geostrophic current speed variations, spatial and temporal trends, and anomalies of both the SST and geostrophic current speed in the Agulhas Current system. Insight into the relationship between the SST and geostrophic current speed has also been provided through results obtained by performing correlation analysis. Therefore, this chapter will discuss and synthesise the study's aim and the key findings reported in Chapter 4. The main aim of this study was to investigate the warming trends in the Agulhas Current from 1982 to 2019. The datasets used for this study are explained in Chapter 3. Key research questions that were asked to guide the study and fulfil the research objectives are answered below.

6.1: SST and Geostrophic Current Variations

Compared to the surrounding area, the Agulhas Current has a warm SST, with the highest temperatures of around 27 ^{o}C in summer and 22 ^{o}C in winter (Figure 3), and these observations are comparable to observations made by Christensen (1980), Lutjeharms (2006) and Imbol Nkwinkwa et al. (2019). In agreement with Imbol Nkwinkwa et al. (2019) and McMonigal et al. (2020), this study highlighted the seasonal cycle in SST in the Agulhas Current, demonstrating a warmer austral summer with the highest SST in February and a cooler winter with the lowest SST in August–September (Figure 4). According to Schumann et al. (1995), the seasonal variation of SST in coastal areas of southeast Africa is to an extent driven by the variation of solar insolation in the region. The Agulhas Current showed higher SST in summer possibly due to increased levels of solar insolation, furthermore, lower SST values in winter were observed due to the reduced level of insolation. Moreover, McMonigal et al. (2020) argue that a seasonal cycle of this nature is expected in the Southern Hemisphere subtropics, which are affected by sea surface fluxes.

This study also demonstrated regional SST variations previously described by Lutjeharms (2006), highlighting a westward negative SST gradient in the Agulhas Current (Figure 4.1, Figure 4.2, and Figure 4.3). The Northern Agulhas Current was the warmest domain with SST values of around 27 ^{o}C, followed by the Southern Agulhas Current, while the coolest domain is the Agulhas Return Current (Figure 4.1, Figure 4.2, and Figure 4.3).

In agreement with Lutjeharms (2007) a general southwestward flow for the geostrophic current speed was observed in the Northern and Southern Agulhas Current (Figure 4.8, Figure 4.9, and Figure 4.10). This study reported a maximum current speed of 1 m s^{-1} in the Northern Agulhas Current which is not consistent with the maximum geostrophic current speed (1.5 m s^{-1}) reported

by Bryden et al. (2005). The strongest current speed was found in the Southern Agulhas Current domain with a maximum speed of up to 1.4 m s^{-1}(Figure 4.8), however, this is considerably less than the maximum speed of 2 m s^{-1} reported by Bryden et al. (2005) and Lutjeharms (2007) in the region. These discrepancies in the geostrophic current speed could be due to several factors. Firstly, this study used a satellite product to study the current speed in the Agulhas Current system while the current speeds reported by both Bryden et al. (2005) and Lutjeharms (2007) are based on in-situ data collected using current meter moorings. Another reason for the differences in the current speed in the Northern and Southern Agulhas Current could be due to the different temporal scales which are covered by the studies, for instance, the dataset used in this study covers 26 years starting from 1993 to 2019 while Bryden et al. (2005) used which was collected over 1 year (March 1993 to April 1994).

Previous studies investigating the current flow in the Agulhas Current have not focused on the variation and flow strength of the meridional and zonal components, therefore there is limited literature about the speed of the geostrophic components in the region, however, the direction of the flow for both components follows the expected path based on the known trajectory of the Agulhas Current system. In this study, a southerly meridional flow was observed in the Northern and the Southern Agulhas Current domains, with a negative current speed gradient westward (Figure 4.9). The zonal component showed a westward flow in the Northern and the Southern Agulhas Current domains (Figure 4.9).

The Agulhas Retroflection and the Agulhas Return Current showed similar current speed patterns, but the Agulhas Return Current's speed decreased eastward (Figure 4.8). The surface current flow in the Agulhas Return Current domain ranged between 0.2 m s^{-1} to 0.8 m s^{-1}, considerably lower than the 2.1 m s^{-1} near the Agulhas Retroflection and the 1.1 m s^{-1} further east that was reported by Boebel et al. (2003). Differences seen between this study and Boebel et al. (2003) might be caused by the different datasets used and the difference in the timeframe of both studies. Contrary to this study, Boebel et al. (2003) studied the Agulhas Retroflection and the Agulhas Return Current using a combined kinematic, hydrographic, and dynamic data gathered during the 1997-1999 Cape of Good Hope Experiments.

Consistent with previously reported findings in several studies (e.g., Boebel et al. 2003; Bryden et al. 2005; Lutjeharms, 2006; Lutjeharms, 2007), meandering of the current was observed in the Agulhas Return Current in this study (Figure 4.8). Changes in the flow direction for the meridional component in the Agulhas Retroflection and Agulhas Return Current were observed, probably due to the meandering of the current in those domains (Boebel et al. 2003; Bryden et al. 2005; Lutjeharms, 2006; Lutjeharms, 2007). In the Agulhas Retroflection and the Agulhas

Return Current, an eastward zonal current flow was observed during all months. The strongest flow for the zonal component was observed in the Northern Agulhas Current, while the weakest flow was observed in the Agulhas Retroflection domain (Figure 4.9). Similar to Krug and Tournadre (2012) as well as Beal et al. (2015), this study shows that the Agulhas Current has seasonality (Figure 4.8 and Figure 4.9), stronger speed in the summer and weaker speed in the winter were observed, with geostrophic current speeds of up to 1.4 m s^{-1} in March to 1.18 m s^{-1} in June. However, on the contrary, Matano et al. (2002) and Lutjeharms (2006) suggested that the strongest flow occurs in winter and spring, while a weaker flow occurs in summer and autumn. Consistent with Lutjeharms (2006), this study demonstrated that the current speed in the Agulhas Current increased from the coast to the current maxima, followed by a more gradual decline in current speeds offshore (Figure 4.8).

These findings confirm and expand our understanding of the Agulhas Current's spatiotemporal variation in SST and current speed. They also highlight that methodological, datasets and temporal scale factors may explain geostrophic speed discrepancies between previous and current studies in the Agulhas Current. This calls for more in-depth research into the Agulhas current hydrographic conditions, and its meridional and zonal components speeds.

6.2: What are the warming trends of the Agulhas Current system?

Early studies that assessed SST trends in the Agulhas Current (e.g., Rouault et al. 2009 and Rouault et al. 2010) observed warming and cooling in certain regions since the 1980s. Several studies later supported their findings (e.g., Wu et al. 2012; Han and Yan, 2018; Sweijd and Smit, 2020). The trends found in this study and trends observed by Sweijd and Smit (2020) are likely to agree since both studies use the same SST dataset. Warming trends of up to 0.55 ^{o}C/decade were observed in various parts of the Agulhas Current in previous studies (Rouault et al. 2010). Rouault et al. (2010) also observed cooling trends between -0.4 ^{o}C and −0.35 ^{o}C/decade, along the southern coastline of South Africa. According to Sweijd and Smit (2020), most regions of the Agulhas Current have general warming trends of up to 0.11 ^{o}C/decade. However, Sweijd and Smit (2020) observed hotspot areas with warming trends of up to 0.512 ^{o}C/decade, near the edge of the Agulhas Bank. Additionally, Sweijd and Smit (2020) state that the Agulhas Current has a small region of cooling in the southern coastline of South Africa due to the intensification of coastal upwelling.

This study has highlighted warming in the Agulhas Current that varies spatially. Although the rate of the warming trends is not entirely the same as in previous studies, the spatial variation of warming trends in the Agulhas Current region since 1982 is consistent with the findings of

previous studies (e.g., Rouault et al. 2009; Rouault et al. 2010; Sweijd and Smit, 2020). This study has found that most regions in the Agulhas Current system have warmed by approximately 0.57 ºC/decade from 1982 to 2019 (Figure 4.5). All the domains of the Agulhas Current had statistically significant warming trends; however, these statistically significant warming trends vary spatially (Figure 4.5). Although the general average warming rates (0.11 ºC/decade) reported by Sweijd and Smit (2020) in the Agulhas Current were smaller than the warming rates in this study, the maximum warming rates (0.57 ºC/decade) found in this study are similar in terms of magnitude and location with the warming rates (0.512 ºC/decade) they found in hotspot regions within the Agulhas Current. Sweijd and Smit (2020) calculated the spatial linear trends over each grid cell within the Agulhas Current an approach similar to the one used in this study. Statistically insignificant annual cooling trends of up to -0.35 ºC/decade were also observed near the southern coastline of South Africa consistent with the findings of Rouault et al. (2009) and Rouault et al. (2010) (Figure 4.5).

Seasonal trends revealed that the Agulhas Current system predominantly warmed across all seasons, and the warming trends varied spatially. The seasonal trends were consistent with the annual trends, both in spatial variation and the overall warming rate. Although found in very small areas, the maximum seasonal trends in some seasons surprisingly concurred with the findings made by Rouault et al. (2009). Showing pronounced significant warming rates exceeding 0.7 °C/decade during autumn in the Southern Agulhas Current and winter in the Agulhas Return Current.

Apart from the seasonal warming trends, and contrary to the long-term annual trends the seasonal cooling trends were statistically significant and particularly evident in the summer and autumn seasons. Coastal upwelling (Schumann et al. 1995; Rouault et al. 2009) and the meandering (McMonigal et al. 2020) of the Agulhas Current might be the reason for the cooling. The meandering of the current cores primarily influences the fluctuation of the temperature field and leads to an increase in offshore temperatures and a decrease near the coast (Schumann et al. 1995). However, these meandering activities have a relatively small impact on temperature transport (Leber et al. 2017; McMonigal et al. 2020).

The small discrepancies in the maximum warming rates reported in this study and the ones reported in previous studies could be due to the temporal scale of the dataset used. For instance, studies which have a longer temporal scale have similar maximum warming rates as this study (e.g., Han and Yan, 2018 (31-year period, ~0.6 ºC/decade); Sweijd and Smit, 2020 (37-year period, 0.512 ºC/decade). Another cause for the inconsistencies in the warming rates could be the limitations of using a coarse spatial resolution satellite data (1º x 1º) which makes

use of an optimal interpolation scheme to close gaps in the data during times of high cloud coverage.

Moreover, the monthly SST anomalies also highlighted decadal variation of warming rates in the Agulhas Current system (Figure 4.7). Enhanced cooling trends dominated the 1982 to 2000 period, while more and stronger warming events were observed in the last two decades, from the 2000 to 2019 period (Figure 4.7). The decadal variations in the intensity of warming trends highlighted by Han and Yan (2018) were also observed in this study (Figure 4.7).

Han and Yan (2018) report that the Agulhas Region has warmed during the 1984 to 2013 period, with great intensity in the last fifteen years (global surface warming slowdown) compared to the acceleration period. According to Han and Yan (2018), the slowdown period spanned from 1998 to 2013, whereas the acceleration period spanned from 1984 to 1998.

The strengthening of the Agulhas Current because of a poleward shift of westerly winds and an increase in trade winds in the South Indian Ocean has been deemed the primary driver of warming in the region (Rouault et al. 2009; Rouault et al. 2010; Wu et al. 2012; Sweijd and Smit, 2020). Observations of the intensification of WBC, including the Agulhas Current, were later confirmed in a recent study by Yang et al. (2016). Through climate models and satellite data, Yang et al. (2016) showed that subtropical western boundary currents, including the Agulhas Current, have been intensifying and warming at an enhanced rate. Another recent study by Beal and Elipot (2016), which used in-situ and satellite data, reveals that there are no signs that the Agulhas Current has intensified, however, intensification of mesoscale eddy activity in the Agulhas Current has been observed. Backeberg et al. (2012) found that an intensification of the south Indian Ocean wind systems resulted in an intensification of the South Equatorial Current, which in turn intensified the eddy dynamics and mesoscale variability in the Agulhas Current system. Additionally, Fadida et al. (2021) suggest that the Agulhas Return Current is shifting poleward although some areas are shifting towards the equator, further supporting the theory that the warming in the Agulhas Current might be induced by the poleward shift of the Current.

When considering the surface current speed trends, it is evident that the findings are generally consistent with the study by Beal and Elipot (2016). According to Beal and Elipot (2016), the Agulhas Current has not experienced a significant intensification process but instead demonstrates heightened levels of mesoscale eddy activity. The results of this study show little strengthening of the Agulhas Current and the visible small areas that show strengthening might be due to an increase in eddy activity in those regions. According to Braby et al. (2016), the presence of eddies both anticyclonic and cyclonic eddies in the Agulhas Current results in a

transfer of momentum, subsequently impacting the average velocity and offshore location of the current. The speed of the Agulhas Current experiences an increase of 0.16 ± 0.17 m s^{-1} when anticyclonic eddies are included, while the inclusion of cyclonic eddies leads to a decrease in speed of 0.13 ± 0.16 m s^{-1}. More research using high-resolution datasets, especially in situ, is needed to investigate these linkages to validate these discoveries that have been made in previous research.

6.3: What are the strongest warming regions within the Agulhas Current?

In agreement with Rouault et al. (2009), Rouault et al. (2010) reported that warming trends in the Agulhas Current vary regionally and increase westward. In this study, the regional variation of the warming trends in the Agulhas Current was observed in the long-term timeseries (Figure 4.3), in the spatial linear trends shown in Figure 4.5, and in the monthly anomalies (Figure 4.7). Rouault et al. (2010), as well as Sweijd and Smit (2020), found the Northern Agulhas Current domain to be generally the least warming (0.25 ºC/decade) domain in the Agulhas Current and their findings are similar to the finding made in this study (0.3 ºC/decade) (Figure 4.5). However, the maximum warming observed in this study is of greater magnitude compared to the findings reported by Rouault et al. (2010).

Rouault et al. (2010) and Sweijd and Smit (2020) observed significant maximum warming trends of up to 0.55 ºC/decade in some small areas of the Southern Agulhas Current, similar to the warming trends (0.55 ºC/decade) observed in this study (Figure 4.5). However, these significant maximum trends in the Southern Agulhas Current were found in areas Sweijd and Smit (2020) defined as hotspot regions, where there is intense warming compared to the surrounding area. Otherwise, general trends in the Southern Agulhas Current were observed at around 0.12 to 0.4 ºC/decade, consistent with the general trends reported by Rouault et al. (2010) and Sweijd and Smit (2020). Moreover, Rouault et al. (2010) observed cooling trends ranging between −0.35 and 0.4 ºC/decade close to the coastline in the Southern Agulhas Current domain due to an increase in upwelling-favourable easterly winds and south-easterly. Similarly, to Rouault et al. (2010), and in agreement with Sweijd and Smit (2020), this study found cooling trends of around -0.35 ºC/decade.

In agreement with Rouault et al. (2009), Rouault et al. (2010), as well as Sweijd and Smit (2020), this study found that some small areas of the Southern Agulhas Current, the Agulhas Retroflection and the Agulhas Return Current are the fastest warming domains in the Agulhas Current, shown by both the annual and the seasonal trends. Similar to Sweijd and Smit (2020) as well as Rouault et al. (2010) who reported warming rates of up to 0.55 ºC/decade, this study

found general warming rates of up to 0.57 ºC/decade in the Agulhas Retroflection and Agulhas Return Current. However, Rouault et al. (2009) reported a higher warming rate of up to 0.7 ºC/decade at the Agulhas Retroflection and Agulhas Return Current, this warming rate was observed only on the seasonal trends in this study, and it appeared in very small areas in the Southern Agulhas Current, Agulhas Retroflection and Agulhas Return Current. The information above shows that the Agulhas Current maximum warming rate has been inconsistent, and according to Elipot and Beal (2018), and Han and Yan (2018), this can be explained by the strong decadal trends connected with atmospheric warming rates, as well as the Agulhas region's position as a significant world heat sink.

In summary, the findings of this study confirm that the Agulhas Current system's strongest warming regions are primarily located in the Southern Agulhas Current, the Agulhas Retroflection, and the Agulhas Return Current. Warming trends in these areas reached up to 0.57 °C/decade, corroborating but slightly exceeding previous research such as Rouault et al. (2009, 2010) and Sweijd and Smit (2020). Interestingly, seasonal trends revealed increased warming rates of up to 0.7 °C/decade in the Southern Agulhas Current, the Agulhas Retroflection, and the Agulhas Return Current, though only in small areas within these domains.

These increased warming rates in specific regions and seasons highlight the Agulhas Current system's nuanced spatial and temporal variability. Given the strategic ecological and climatic significance of Agulhas Current, the findings emphasise the importance of focused scientific research in the region.

6.4: Geostrophic Current Trends

Several studies have assessed the intensification or weakening trends of WBCs including the Agulhas Current by looking at the linear trends of the geostrophic current speed (Chen et al. 2019 (Gulf Stream and Kuroshio Current); Dong et al. 2019 (Gulf Stream); Wang and Wu, 2019 (Kuroshio Current); Wu et al. 2012 (all WBCs); Yang et al. 2016 (all WBCs)). However, previous studies (e.g., Wu et al. 2012; Yang et al. 2016) that have assessed the intensification of the WBCs (including the Agulhas Current) through linear trends calculation did not assess these trends on a regional scale, therefore limited information is available about the spatial variation of linear trends in the Agulhas Current.

This study demonstrated heterogeneous trends for the geostrophic current speed and both geostrophic components in the Agulhas Current. The rate and the pattern of strengthening and weakening varied spatially within domains and between them as well. For instance, the geostrophic current speed trends illustrated a weakened current flow along the Northern and

Southern Agulhas Current coastline, while the current has also shown small areas where it has strengthened on these domains (Figure 4.13). The spatial variation observed in the Southern Agulhas Current domain is consistent with findings made by Jury (2020). Jury (2020) found that the strengthening of the surface current in the Southern Agulhas Current is only along the shelf edge of the eastern Agulhas Bank, not the entire domain.

The Agulhas Retroflection and the Agulhas Return Current domains had the strongest but were mostly dominated by insignificant strengthening and weakening estimates (Figure 4.13). The observed strengthening in the Agulhas Current is somewhat to an extent consistent with the findings of Yang et al. (2016). However, the findings of this study tend to provide more support for the notion that the observed changes in the Agulhas Current system are primarily attributed to heightened eddy activity, rather than strengthening of the overall current (Beal and Elipot, 2016). Beal and Elipot (2016) suggest that the weakening and strengthening observed in the study could mean there have been changes in the eddy kinetic energy (EKE) of the Agulhas Current but not the actual mean flow of the current. According to Beal and Elipot (2016), stronger winds may raise the EKE of boundary currents rather than their mean flow.

According to Yang et al (2016), WBCs are strengthening due to the intensification and poleward shift of near-surface ocean winds. Similar to Yang et al. (2016), Hu et al. (2021) reported that the global intensification of surface winds since the 1990s has contributed to the strengthening of the ocean surface flow. Both studies corroborate a previous study by Wu et al. (2012), which indicated that enhanced warming in WBCs is caused by an intensification and poleward shift of the wind system over the currents. In a study conducted to investigate the intensification of the Kuroshio WBC, Chen et al. (2019) explained how sea surface warming can influence the intensification of surface ocean flow. Chen et al. (2019) found that ocean subduction and advection processes, driven by sea surface warming, can result in uneven warming in certain regions and increase the isopycnal slope across the area, therefore, intensifying the upper layer. Through ocean model experiments, Peng et al. (2022) explain the relationship between changes in SST and surface ocean currents. According to Peng et al. (2022) to some extent, sea surface warming drives the acceleration of surface ocean currents. Peng et al. (2022) suggest that during sea surface warming vertical shear develops and strengthens the currents in the upper surface layer due to density stratification between the upper and bottom layers and because the vertical-integrated volume transfer remains constant, the flow in the layers below weakens.

When considering these results, it is evident that the findings are generally consistent with the hypothesis proposed by Beal and Elipot (2016). According to their hypothesis, the Agulhas Current has not experienced a significant intensification process but instead demonstrates heightened levels of mesoscale eddy activity. This holds particular significance in the context of future climate modelling and risk assessment, as the distinct implications for heat transport, marine ecology, and regional weather patterns may arise from different drivers, namely large-scale intensification, and localised eddy activity. More research using high-resolution datasets will be of utmost importance in validating these discoveries and offering a more comprehensive understanding of the fundamental mechanisms that govern these complicated oceanic conditions.

6.5: Relationship between SST and geostrophic current speed

The spatial (annual and seasonal) and lagged Pearson's correlation analysis highlighted both insignificant and significant relationships between the SST and the geostrophic current speed anomalies on a monthly timescale over the study area (Figure 4.17, Figure 4.18, Figure 4.19).

The findings of this study are consistent with prior research, specifically the studies conducted by Chen et al. (2019) and Peng et al. (2022). These studies similarly observed a positive relationship between anomalies in Sea Surface Temperature (SST) and anomalies in geostrophic current speed. Nevertheless, it is crucial to highlight a significant point of departure, which is that although there is a clear correlation, it does not necessarily indicate a direct causal relationship between the two variables. This study, in particular, did not discover any evidence that supports the enhancement of the Agulhas Current system's overall flow. This notable distinction introduces an additional level of intricacy to our comprehension of oceanic dynamics.

It is important to note, however, that changes in geostrophic current speed in this study are not confused with changes in the overall flow of the Agulhas Current system as the results do not show that. Therefore, while there is a moderate to strong statistically significant relationship between SST anomalies and current speed anomalies, especially in a seasonal context, it does not necessarily translate to a direct influence of these parameters on each other in the Agulhas Current system.

The lag correlation results in Figure 4.19 are interesting. They show immediate and significant relationships between SST and geostrophic current speed anomalies, especially in the Northern and Southern Agulhas Current regions. These immediate correlations may be indicative of short-term processes that affect both SST and current speed at the same time. The Retroflection and Return Current regions showed significant correlations at different lag periods, indicating the

presence of more complex temporal dynamics, possibly linked to larger oceanic or atmospheric systems.

Overall, the intricate relationships between SST anomalies and geostrophic current speed anomalies highlight the Agulhas Current system's complex interplay of factors. The moderate correlations and significant lag relationships point to multifaceted influences, which are likely influenced by a combination of atmospheric, oceanic, and possibly even anthropogenic factors, and require further investigation for a complete understanding.

6.6 Influence of climate modes on SST and geostrophic current speed

According to numerous studies (Beal et al., 2011; Jury, 2015; Elipot and Beal, 2018; Trott et al., 2021) the El Nio-Southern Oscillation (ENSO) is crucial in controlling variations in the world's climate. Previous research has demonstrated the Agulhas Current system's sensitivity to ENSO phenomena, particularly Sea Surface Temperature (SST) anomalies (Rouault et al., 2003; Trott et al., 2021). Trott et al. (2021) have made a significant observation regarding the impact of ENSO peak events on the sea surface temperature (SST) of the Agulhas Current. Their findings indicate a delayed response of approximately 20 to 30 months following these ENSO peak events. The findings of the present study confirm the influence of climate indices in the Agulhas Current especially on SST but there is some inconsistency in the response time to this influence. This study reveals shorter and longer time delays in the response of the ENSO compared to previous research. The response time varies regionally on the Agulhas Current. These findings generate both collaboration and inconsistency when compared to previous research.

One potential rationale for this discrepancy can be ascribed to the methodological division of the Agulhas Current into discrete regions, thereby facilitating a more detailed examination. Moreover, it is worth noting that the temporal range of this study, which extends from 1982 to 2019, exhibits significant differences when compared to the period examined by Trott et al. (2021), which encompasses solely the years 2015 to 2020. The observed variations in lagged response to ENSO events may be attributed to the disparities in methodological approach and time scale.

Regarding the SAM (), prior studies, particularly the work of Malan et al. (2019), have confirmed its impact on alterations in zonal wind patterns over the Agulhas Bank, subsequently leading to effects on sea surface temperatures (SST). Our research, consistent with and further elaborating on these findings, demonstrates that although the correlations are relatively weak, there is a statistically significant influence of the SAM on sea surface temperature (SST)

anomalies at specific time lags. This provides statistical support for the hypothesised influence of SAM, although the magnitude of the correlation remains modest.

The lack of strong statistically significant correlations between current speed and the climate indices suggests that neither ONI nor SAM has a dominant influence on the geostrophic speed of the Agulhas Current over the time scales studied. The minor but statistically significant correlations at longer lags (>40) could be due to more complex underlying mechanisms especially on the Agulhas Return Current, such as inter-basin teleconnections or higher-order ocean-atmosphere interactions, which a univariate lag correlation approach does not capture.

The intricate nature of the observed relationships among ENSO, SAM, and SST anomalies, which exhibit sporadic yet statistically significant weak correlations, implies the presence of multiple-scale influences and the possibility of interference from unexplored variables. The complexities associated with statistical limitations in univariate lag correlation analyses require the adoption of more advanced modelling approaches to account for these complexities. Future research could potentially derive advantages from the utilisation of multi-variable models, which could incorporate additional dynamic variables such as wind stress and upwelling indices. The utilisation of extended time-series data or the implementation of multi-model ensemble strategies can enhance the robustness of the findings.

6. CHAPTER 6: CONCLUSION AND FUTURE RECOMMENDATIONS

In this study, SST and geostrophic current datasets were analysed to find their long-term trends and compare the findings to previous research. The main aim was to investigate the warming trends in the Agulhas Current and determine the strongest warming regions using the NOAA OISST with a higher spatial resolution (1/4^{o}) and longer temporal coverage (1982-2019) compared to datasets used in previous studies (e.g., Rouault et al. 2009 and Rouault et al. 2010). More precisely, this study (1) evaluated if the Agulhas Current is warming as shown by other previous studies.; (2) Whether warming has continued at the same rate compared to the studies done previously. (3) If the Agulhas Retroflection and Agulhas Return Current regions are still the strongest warming regions within the Agulhas Current system, as previously shown; (4) Whether there is a relationship between the geostrophic current speed anomalies and the sea surface temperature anomalies in the Agulhas Current region from 1993 to 2019. And lastly to assess if climate indices (ONI and SAM) influence the SST and geostrophic current speed anomalies in the Agulhas Current.? To achieve the objectives of this study, the least squares regression was used to calculate the trends for both SST and geostrophic current speed including its components. The relationship between the SST and the geostrophic current and the influence of climate indices on SST and geostrophic current speed was assessed using Pearson's Correlation. To determine if the Agulhas Current has been weakened or strengthened between 1993 and 2019, this study also estimated the linear trends using linear least squares regression for the geostrophic current (current speed and both geostrophic components).

According to the quantitative analyses performed on SST in this study, it can be concluded we failed to reject all the null hypotheses. Significant sea surface warming has continued from 1982 to 2019 throughout the Agulhas Current region and the warming trends are comparable to the trends found in previous studies (e.g., Rouault et al. 2009; Rouault et al. 2010; Han and Yan, 2018; Sweijd and Smit, 2020). Although these warming trends are consistent with previous research, the maximum significant warming rates found in this study are slightly different to some of the reported warming rates (Rouault et al. 2009; 0.7 ^{o}C/decade) and (e.g., Rouault et al. 2010; 0.5 ^{o}C/decade). Such variation is probably caused by the use of different datasets with different spatial resolutions or the spatial subsetting done before the statistical analyses in some of the previous studies as well as the different temporal scales of this study compared to other previous studies. Studies that used SST datasets with the same spatial resolution as this study showed very similar or equal maximum warming rates (e.g., Han and Yan, 2018; ~0.6 ^{o}C/decade) and Sweijd and Smit, 2020; 0.57 ^{o}C/decade).

This study also shows that the warming in the Agulhas Current varies spatially and increases westward. The Southern Agulhas Current, Agulhas Retroflection and Agulhas Return Current domains have warmed the strongest in the Agulhas Current and that is consistent with previous findings made by Rouault et al. (2009), Rouault et al. (2010), Han and Yan, (2018), and Sweijd and Smit (2020). Seasonal trends also varied regionally and showed more intense warming in some areas than the annual trends, suggesting a seasonality in the warming trends. Showing pronounced significant warming rates exceeding 0.7 °C/decade during autumn in the Southern Agulhas Current and winter in the Agulhas Return Current, similar to the 0.7 °C/decade reported by Rouault et al. (2009).

Moreover, in agreement with Han and Yan (2018), this study highlighted the decadal variation of warming rates in the Agulhas Current system through SST anomalies. More strong cooling events dominated the 1982 to 2000 period, while more and stronger warming events were observed in the last two decades, from the 2000 to 2019 period.

In terms of the geostrophic current overall flow, no significant trend of strengthening or weakening was observed between 1993 and 2019, though localised trends were noted both annually and seasonally. Over the specified region, the findings show a moderate (annually) to strong (seasonally) positive correlation between SST variations and geostrophic current speed anomalies. This is consistent with recent research, such as studies by Chen et al. (2019) and Peng et al. (2022), which suggest that changes in sea surface temperatures can cause changes in geostrophic current speed. However, based on the overall results, while the correlation is statistically significant, SST may not be directly affecting geostrophic current, and other variables may also play important roles in influencing geostrophic current anomalies. This highlights the importance of multi-variable models and a more comprehensive approach to better understanding the complex relationships between SST, geostrophic currents, and other oceanic and atmospheric variables.

The relationship between climate indices (SAM and ONI), SST, and geostrophic anomalies demonstrates how interconnected the earth's climatic systems are. This study showed a significant influence of the climate indices on environmental parameters in the Agulhas Current, especially SST. However, while statistically significant in some cases, these correlations are negligible, implying that the influence is weak and other local or mesoscale factors may also be at work.

The implications of the WBCs on climate and economics (fishing and shipping) in nearby regions are extensive and well-documented (Rouault et al. 2009). Although catastrophic occurrences

such as large storms connected with the Agulhas Current have occurred on South Africa's east coast, the specific influence of ocean warming regions such as the Agulhas Current on the weather and climate of South Africa has not yet been extensively investigated. Efforts should thus be concentrated on improving our understanding of changes in ocean currents and future sea surface temperatures.

A multi-disciplinary approach incorporating more dynamic variables such as wind stress and upwelling indices is required to gain a more comprehensive understanding of the Agulhas Current's trends. Future research should use high-resolution ocean-atmosphere coupled models and incorporate in-situ data to overcome the limitations caused by dependence on surface-focused satellite data. Given the complex interdependence of ENSO, SAM, SST, and geostrophic currents, a multi-variable model could provide a more nuanced understanding of these interdependencies. Furthermore, efforts should be focused on assessing the effects of these oceanic changes on regional climate and economy, especially given the important roles that Western Boundary Currents (WBCs) play in climatic and economic systems. Understanding whether the observed surface warming extends to deeper ocean layers would provide insights into potential changes in ocean circulation and heat distribution, highlighting the importance of in-situ data in future studies. By filling these knowledge gaps, future research could provide a more comprehensive and nuanced understanding of the Agulhas Current system, contributing to our collective understanding of climate change and its far-reaching effects on oceanic systems and, by extension, global ecosystems.

7. CHAPTER 7: REFERENCES

Backeberg, B.C., Johannessen, J.A., Bertino, L. and Reason, C.J. 2008. The greater Agulhas Current system: An integrated study of its mesoscale variability. *Journal of Operational Oceanography*, 1(1): 29–44.

Backeberg, B.C., Penven, P. and Rouault, M. 2012. Impact of intensified Indian Ocean winds on mesoscale variability in the Agulhas system. *Nature Climate Change*, 2(8): 608–612. http://dx.doi.org/10.1038/nclimate1587.

Beal, L. and Elipot, S. 2016. Broadening not strengthening of the Agulhas Current since the early 1990s. *Nature*, 540(7634).

Beal, L.M., Chereskin, T.K., Lenn, Y.D. and Elipot, S. 2006. The sources and mixing characteristics of the Agulhas Current. *Journal of Physical Oceanography*, 36(11): 2060–2074.

Beal, L.M., Elipot, S., Houk, A. and Leber, G.M. 2015. Capturing the Transport Variability of a Western Boundary Jet: Results from the Agulhas Current Time-Series Experiment (ACT)$^{-1}$. *Journal of Physical Oceanography*, 45(5): 1302–1324. http://dx.doi.org/10.1175/JPO-D-14-.

Beal, L.M., de Ruijter, W.P.M., Biastoch, A., Zahn, R., Cronin, M., Hermes, J., Lutjeharms, J., Quartly, G., Tozuka, T., Baker-Yeboah, S., Bornman, T., Cipollini, P., Dijkstra, H., Hall, I., Park, W., Peeters, F., Penven, P., Ridderinkhof, H. and Zinke, J. 2011. On the role of the Agulhas system in ocean circulation and climate. *Nature*, 472(7344): 429–436.

Beal, L.M., Ruijter, W.P.M. de, Biastoch, A., Zahn, R., de Ruijter, W.P.M., Biastoch, A., Zahn, R., Cronin, M., Hermes, J., Lutjeharms, J., Quartly, G., Tozuka, T., Baker-Yeboah, S., Bornman, T., Cipollini, P., Dijkstra, H., Hall, I., Park, W., Peeters, F., Penven, P., Ridderinkhof, H. and Zinke, J. 2011. On the role of the Agulhas system in ocean circulation and climate. *Nature*, 472(7344): 429–436. http://dx.doi.org/10.1038/nature09983.

Biastoch, A., Böning, C.W., Schwarzkopf, F.U. and Lutjeharms, J.R.E. 2009. Increase in Agulhas leakage due to poleward shift of Southern Hemisphere westerlies. *Nature*, 462(7272): 495–498.

Boebel, O., Rossby, T., Lutjeharms, J., Zenk, W. and Barron, C. 2003. *Path and variability of the Agulhas Return Current*.

Braby, L., Backeberg, B.C., Ansorge, I., Roberts, M.J., Krug, M. and Reason, C.J.C. 2016. Observed eddy dissipation in the Agulhas Current. *Geophysical Research Letters*, 43, pp.8143-8150. doi:10.1002/2016GL069480.

Bryden, H.L., Beal, L.M. and Duncan, L.M. 2005. Structure and Transport of the Agulhas Current and Its Temporal Variability. *Journal of Oceanography*, 61(3): 479–492.

Chen, C., Wang, G., Xie, S.P. and Liu, W. 2019. Why does global warming weaken the gulf stream but intensify the kuroshio? *Journal of Climate*, 32(21): 7437–7451.

Chen, X. and Tung, K.K. 2014. Varying planetary heat sink led to global-warming slowdown and acceleration. *Science*, 345(6199): 897–903.

Christensen, M.S. 1980. Sea-surface temperature charts for southern Africa, south of 26oS. *South African Journal of Science*, 76(12): 541–546.

Ciasto, L.M. and Thompson, D.W.J. 2008. Observations of large-scale ocean–atmosphere interaction in the Southern Hemisphere. *Journal of Climate*, 21(6):1244-1259.

Dong, S., Baringer, M.O. and Goni, G.J. 2019. Slow Down of the Gulf Stream during 1993–2016. *Scientific Reports*, 9(1).

Elipot, S. and Beal, L.M. 2015. Characteristics, energetics, and origins of agulhas current meanders and their limited influence on ring shedding. *Journal of Physical Oceanography*, 45(9): 2294–2314.

Elipot, S. and Beal, L.M. 2018. Observed Agulhas Current sensitivity to interannual and long-term trend atmospheric forcings. *Journal of Climate*, 31(8): 3077–3098.

Fadida, Y., Malan, N., Cronin, M.F. and Hermes, J. 2021. Trends in the Agulhas Return Current. *Deep-Sea Research Part I: Oceanographic Research Papers*, 175(May).

Gong, D. and Wang, S. 1999. Definition of Antarctic Oscillation index. *Geophysical Research Letters*, 26(4):459-462.

Goschen, W.S., Bornman, T.G., Deyzel, S.H.P. and Schumann, E.H. 2015. Coastal upwelling on the far eastern Agulhas Bank associated with large meanders in the Agulhas Current. *Continental Shelf Research*, 101: 34–46. http://dx.doi.org/10.1016/j.csr.2015.04.004.

Han, L. and Yan, X. 2018. Warming in the Agulhas Region during the Global Surface Warming Acceleration and Slowdown. *Scientific Reports*: 1–7. http://dx.doi.org/10.1038/s41598-018-31755-1.

Hogg, R. v, McKean, J.W. and Craig, A.T. 2014. *Introduction to Mathematical Statistics*. 7th Edition. Deirdre Lynch, ed. Pearson Education, Inc.

Hu, S., Lu, X., Li, S., Wang, F., Guan, C., Hu, D., Xin, L. and Ma, J. 2021. Multi-decadal trends in the tropical Pacific western boundary currents retrieved from historical hydrological observations. *Science China Earth Sciences*, 64(4): 600–610.

Hutchinson, K., Ansorge, I., Hermes, J., Beal, L. and Penven, P. 2018. Seasonal Phasing of Agulhas Current Transport Tied to a Baroclinic Adjustment of Near-Field Winds. *Journal of Geophysical Research*, 123(10).

Imbol Nkwinkwa, N.A.S., Rouault, M. and Johannessen, J.A. 2019. Latent Heat Flux in the Agulhas Current. *Remote sensing*, 11(1576).

Jury, M.R. 2020. Marine climate change over the eastern Agulhas Bank of South Africa. *Ocean Science*, 16(6): 1529–1544.

Jury, M., 2015. Passive Suppression of South African Rainfall by the Agulhas Current. *Earth Interactions*, 19(13), pp.1-14. https://journals.ametsoc.org/view/journals/eint/19/13/ei-d-15-0017.1.xml

Krug, M. and Tournadre, J. 2012. Satellite observations of an annual cycle in the Agulhas Current. *Geophysical Research Letters*, 39(15): 1–6.

Krug, M., Tournadre, J. and Dufois, F. 2014. Interactions between the Agulhas Current and the eastern margin of the Agulhas Bank. *Continental Shelf Research*, 81: 67–79.

Leber, G.M. and Beal, L.M. 2014. Evidence that Agulhas Current transport is maintained during a meander. *Journal of Geophysical Research: Oceans*, (119): 3868–3882. http://onlinelibrary.wiley.com/doi/10.1002/jgrc.20353/abstract.

Leber, G.M., Beal, L.M. and Elipot, S. 2017. Wind and current forcing combine to drive strong upwelling in the Agulhas Current. *Journal of Physical Oceanography*, 47(1): 123–134.

Lutjeharms, J.R.E. 2006. *The Agulhas Current*. Springer Berlin Heidelberg.

Lutjeharms, J.R.E. 2007. Three decades of research on the greater Agulhas Current. *Ocean Sci*, 3: 129–147. www.ocean-sci.net/3/129/2007/.

Lutjeharms, J.R.E. and Ansorge, I.J. 2001. The Agulhas Return Current. *Journal of Marine Systems*, 30(1–2): 115–138.

Lutjeharms, J.R.E. and van Ballegooyen, R.C. 1988. Anomalous upstream retroflection in the agulhas current. *Science*, 240(4860).

Lutjeharms, J.R.E., Penven, P. and Roy, C. 2003. Modelling the shear edge eddies of the southern Agulhas Current. *Continental Shelf Research*, 23(11–13): 1099–1115.

Lutjeharms, J.R.E. and Roberts, H.R. 1988. The Natal pulse: an extreme transient on the Agulhas Current. *Journal of Geophysical Research*, 93(C1): 631–645.

Malan, N.C., Durgadoo, J.V., Biastoch, A., Reason, C.J. and Hermes, J.C. 2019. Multidecadal wind variability drives temperature shifts on the Agulhas Bank. *Journal of Geophysical Research*: Oceans, 124, pp.3021-3035. https://doi.org/10.1029/2018JC014614

Marshall, G.J. 2003. Trends in the Southern Annular Mode from observations and reanalyses. *Journal of Climate*, 16:4134-4143.

Marshall, G.J. 2007. Half-century seasonal relationships between the Southern Annular mode and Antarctic temperatures. *International Journal of Climatology*, 27:373-383.

Marshall, G.J. and Speer, K. 2012. Closure of the meridional overturning circulation through Southern Ocean upwelling. *Nature Geoscience*, 5:171-180.

Marshall, G.J. and National Centre for Atmospheric Research Staff (Eds). Last modified 19 March 2018. The Climate Data Guide: Marshall Southern Annular Mode (SAM) Index (Station-based). Available at:

Matano, R.P., Beier, E.J., Strub, P.T. and Tokmakian, R. 2002. Large-scale forcing of the Agulhas variability: The seasonal cycle. *Journal of Physical Oceanography*, 32(4): 1228–1241.

McMonigal, K., Beal, L.M., Elipot, S., Gunn, K.L., Hermes, J., Morris, T. and Houk, A. 2020. The impact of meanders, deepening and broadening, and seasonality on agulhas current temperature variability. *Journal of Physical Oceanography*, 50(12): 3529–3544.

Peng, Q., Xie, S.P., Wang, D., Huang, R.X., Chen, G., Shu, Y., Shi, J.R. and Liu, W. 2022. Surface warming–induced global acceleration of upper ocean currents. *Science Advances*, 8(16): 1–13.

Putrasahan, D.A., Kamenkovich, I., Le Hénaff, M. and Kirtman, B.P. 2017. Importance of ocean mesoscale variability for air-sea interactions in the Gulf of Mexico. *Geophysical Research Letters*, 44: 6352-6362. https://doi.org/10.1002/2017GL072884.

Reason, C.J.C. 2001. Evidence for the Influence of the Agulhas Current on Regional Atmospheric Circulation Patterns. *Journal of Climate*, 14(12): 2769–2778.

Reynolds, R.W. and Marsico, D.C. 1993. An Improved Real-Time Global Sea Surface Temperature Analysis. *Journal of Climate*, 6(1): 114–119. http://journals.ametsoc.org/doi/abs/10.1175/1520-0442(1993)006%3C0114%3AAIRTGS%3E2.0.CO%3B2%0Apapers3://publication/uuid/134602C3-9462-43AD-A4A3-C2DF08A753CF.

Reynolds, R.W., Rayner, N.A., Smith, T.M., Stokes, D.C. and Wang, W. 2002. An improved in-situ and satellite SST analysis for climate. *Journal of Climate*, 15(13): 1609–1625.

Reynolds, R.W., Smith, T.M., Liu, C., Chelton, D.B., Casey, K.S. and Schlax, M.G. 2007. Daily high-resolution-blended analyses for sea surface temperature. *Journal of Climate*, 20(22): 5473–5496.

Rio, M.H., Mulet, S. and Picot, N. 2014. Beyond GOCE for the ocean circulation estimate: Synergetic use of altimetry, gravimetry, and in-situ data provides new insight into geostrophic and Ekman currents. *Geophysical Research Letters*, 41(24).

Rouault, M. and Lutjeharms, J.R.E. 2003. Estimation of sea-surface temperature around southern Africa from satellite-derived microwave observations. *South African Journal of Science*, 99(9–10): 489–494.

Rouault, M., Penven, P. and Pohl, B. 2009. Warming in the Agulhas Current system since the 1980's. *Geophysical Research Letters*, 36(12): 2–6.

Rouault, M., Pohl, B. and Penven, P. 2010. Coastal oceanic climate change and variability from 1982 to 2009 around South Africa. *African Journal of Marine Science*, 32(2): 237–246.

Rouault, M., Reason, C.J.C., Lutjeharms, J.R.E. and Beljaars, A.C.M. 2003. Underestimation of latent and sensible heat fluxes above the Agulhas Current in NCEP and ECMWF analyses. *Journal of Climate*, 16(4): 776–782.

Rouault, M. and Richard, Y. 2005. Intensity and spatial extent of droughts in Southern Africa. *Geophysical Research Letters*, 32:L15702.

Rouault, M.J. and Penven, P. 2011. New perspectives on Natal Pulses from satellite observations. *Journal of Geophysical Research: Oceans*, 116(7): 1–14.

Russo, C.S., Lamont, T., Tutt, G., van den Berg, M., Ansorge, I. and Barlow, R. 2017. Agulhas Current-driven hydrographic variability on the southeast coast of South Africa.

Sarachik, E.S. and Cane, M.A. 2010. *The El Niño-Southern Oscillation Phenomenon*. Cambridge University Press.

Seager, R. and Simpson, I.R. 2016. Western boundary currents and climate change. *Journal of Geophysical Research: Oceans*, 121(9): 7212–7214.

Schouten, M.W., de Ruijter, W.P.M. and van Leeuwen, P.J. 2002. Upstream control of Agulhas Ring shedding. *Journal of Geophysical Research: Oceans*, 107(8).

Schumann, E.H. and Beekman, L.J. 1984. Ocean temperature structures on the agulhas bank. *Transactions of the Royal Society of South Africa*, 45(2): 191–203.

Schumann, E.H., Cohen, A.L. and Jury, M.R. 1995. Coastal sea surface temperature variability along the south coast of South Africa and the relationship to regional and global climate. *Journal of Marine Research*, 53(2): 231–248.

Swart, N.C., Fyfe, J.C., Hawkins, E., Kay, J.E. and Jahn, A. 2015. Influence of internal variability on Arctic sea-ice trends. *Nature Climate Change*, 5(2):86-89.

Sweijd, N.A. and Smit, A.J. 2020. Trends in sea surface temperature and chlorophyll-a in the seven African Large Marine Ecosystems. *Environmental Development*, 36.

Talley, L.D., Pickard, G.L., Emery, W.J. and Swift, J.H. 2011. *Descriptive physical oceanography: An introduction: Sixth edition*.

Thomson, R.E. and Emery, W.J. 2014. *Data analysis in physical oceanography*. Amsterdam: Elsevier Ltd. https://b-ok.cc/book/2382000/0b0594.

Thompson, D.W.J., Solomon, S., Kushner, P.J., England, M.H., Grise, K.M. and Karoly, D.J. 2011. Signatures of the Antarctic ozone hole in Southern Hemisphere surface climate change. *Nature Geoscience*, 4(11):741-749.

Trott, C.B., Subrahmanyam, B. and Washburn, C.E. 2021. Investigating the Response of Temperature and Salinity in the Agulhas Current Region to ENSO Events. *Remote Sensing*, 13, p.1829. https://doi.org/10.3390/rs13091829

Van der Vaart, P.C.F. and De Ruijter, W.P.M. 2001. Stability of western boundary currents with an application to pulse like behavior of the Agulhas current. *American Meteorological Society*, 31(9): 2625–2644.

van Leeuwen, P.J., De Ruijter, W.P.M. and Lutjeharms, J.R.E. 2000. Natal pulses and the formation of Agulhas rings. *Journal of Geophysical Research: Oceans*, 105(C3): 6425–6436.

Wang, X., Giannakis, D. and Slawinska, J. 2017. The Antarctic circumpolar wave and its seasonality: Intrinsic travelling modes and El Niño-Southern Oscillation teleconnections. *International Journal of Climatology*, 39:1026-1040.

Wang, Y.L. and Wu, C.R. 2019. Enhanced warming and intensification of the Kuroshio Extension, 1999-2013. *Remote Sensing*, 11(1): 1–13.

Wilks, D.S. 1995. *Statistical Methods in the Atmospheric Sciences*. Academic Press.

Wu, L., Cai, W., Zhang, L., Nakamura, H., Timmermann, A., Joyce, T., McPhaden, M.J., Alexander, M., Qiu, B., Visbeck, M., Chang, P. and Giese, B. 2012. Enhanced warming over the global subtropical western boundary currents. *Nature Climate Change*, 2(3): 161–166. http://dx.doi.org/10.1038/nclimate1353.

Yamagami, Y., Tozuka, T. and Qiu, B. 2019. Interannual Variability of the Natal Pulse. *Journal of Geophysical Research: Oceans*, 124(12): 9258–9276.

Yang, H., Lohmann, G., Krebs-Kanzow, U., Ionita, M., Shi, X., Sidorenko, D., Gong, X., Chen, X. and Gowan, E.J. 2020. Poleward Shift of the Major Ocean Gyres Detected in a Warming Climate. *Geophysical Research Letters*, 47(5).

Yang, H., Lohmann, G., Wei, W., Dima, M., Ionita, M. and Liu, J. 2016. Intensification and poleward shift of subtropical western boundary currents in a warming climate. *Journal of Geophysical Research: Oceans*, 121(7): 4928–4945.